

國立交通大學

電子工程學系電子研究所碩士班

碩士論文

AAO輔助生成一維氧化鋅奈米陣列之特性研究

Characteristics of 1D ZnO Nanowires Array

Grown by AAO Assistance

研究生：張家瑋

指導教授：曾俊元

中華民國九十五年六月

AAO輔助生成一維氧化鋅奈米陣列之特性研究
**Characteristics of 1D ZnO Nanowires Array grown
by AAO assistance**

研究生：張家瑋

Student: Chia-Wei Chang

指導教授：曾俊元 教授

Advisor: Prof. Tseung-Yuen Tseng

國立交通大學

電子工程學系電子研究所碩士班

碩士論文

A Thesis

Submitted to Department of Electronics Engineering & Institute of
Electronics

College of Electrical and Computer Engineering

National Chiao Tung University

in partial Fulfillment of the Requirements

For the Degree of

Master

in

Electronics Engineering

June 2006

Hsinchu, Taiwan, Republic of China

中華民國九十五年六月

AAO輔助生成一維氧化鋅奈米陣列之特性研究

學生：張家瑋

指導教授：曾俊元 教授

國立交通大學電子工程學系電子研究所碩士班

摘要

本研究以寬能帶(3.37eV)的二六族半導體氧化鋅(ZnO)為主要研究與探討目標；本實驗將重點著眼於一維方向成長的氧化鋅奈米結構，亦即其它兩方向的尺寸限制在100nm以下。另外，陽極氧化鋁(AAO)結構提供許多優異的特性用於奈米研究上。因此，陽極氧化鋁提供可控制的一維方向孔洞陣列將是輔助成長奈米線的絕佳利器。

在本研究中，我們將針對AAO輔助生成一維氧化鋅奈米線陣列的低溫成長方法、化學以及電的特性加以研究探討。此外，我們試圖探討奈米線的幾何尺寸對於場發射特性的影響。在實驗中，我們利用低溫的水熱法成長氧化鋅奈米線，而陽極氧化鋁是由傳統的兩步驟陽極氧化法製備。

事實上，由實驗結果觀察知，奈米線的長寬比與其場發射特性是成正比關係；在實驗中，當奈米線的長寬比提升到53，我們得到優秀的場發射特性($\beta=6100$)。最後，對於實驗結果，我發現一些缺點並且試圖推薦一些修正的可能方法；此外，我們也相信垂直的氧化鋅奈米線陣列在未來平面顯示器應用上將大有可為，且由水熱法提供的低溫製程對於可撓式光電與場發射元件的應用也是一大優勢。

Characteristics of 1D ZnO Nanowires Array grown by AAO assistance

Student: Chia-Wei Chang

Advisor: Tseung-Yuen Tseng

Department of Electronics Engineering and Institute of Electronics

National Chiao Tung University

Abstract

ZnO is a wide band gap semiconductor (3.37eV) with a large exciton binding energy (60meV) at room temperature, and is one of the most important and versatile semiconductor materials. This research is focus on the one dimension nanostructure of ZnO which indicates the two directions were limited by the nano-scale (smaller than 100nm). The Anodic Aluminum Oxide (AAO) structure would provide some properties for nanotechnology study. Therefore, the AAO which could provide controllable one-dimensional pores was an excellent candidate to assistant fabrication of nanowires.

The characteristics of the ZnO nanowires array by AAO assistance are paying attention in low temperature growth method, chemical and electric properties. Furthermore, we investigate influence on field emission by the geometry scale of nanowire. Here we report for ZnO nanowires growth using the hydrothermal method and AAO prepared by conventional two-step anodization.

Actually, we observed the relation between aspect ratio and the field

Characteristics of 1D ZnO Nanowires Array Grown by AAO Assistance

C.W.CHANG

emitting enhancement factor β is in proportion. For example, the β is enhanced to 6100 which shows excellent field emission when the aspect ratio is 53. In summary, we observed some faults and recommended some improvements. Moreover, we believe that ZnO NWs array grow so vertical that it is a good candidate for the future flat panel display applications, and the hydrothermal method provides a low temperature process for fabricating flexible optoelectronic and field emission devices.



誌 謝

回憶，不停地，在時間的流裡製造著；更不停地，在你我心裡反覆放映著。

回憶這些日子，實驗室生活也許將只是生命中的一站，但卻令我成長許多。感謝曾老師俊元教授的指導與教誨，我想在未來旅途中將受益無窮，更感謝老師提供一個良好的環境給我們無後顧之憂的學習與成長；亦感謝佳穎學姊與思毅學長不辭辛勞的帶領與教導，秀玉學姊、群傑學長、志洋學長及昭正學長對於實驗的討論與分析，有了你們的幫助讓實驗能更順利且更有意義；還有一起努力、成長的信賢與秉章，真情流露的相互砥礪，讓生活更添感性；以及可愛的學弟們，冠仲、承佑、鎮宇、重毅、俊勝、俊興、士傑、崧蒔，有你們的協助與參予，使一切更加美好。

兩年的日子，不長，卻在我心裡留下絢爛的色彩，以及心裡滿滿的感謝與回憶； 兩年的日子，轉眼間，邁入尾聲，也許我只是各位曾經協助過我的教授、學長、學弟們人生中的過客，但你們是我生命中獨一無二的貴人，真感謝你們。

最後更感謝，是敬愛的父母親，默默支持與栽培，無怨無悔；也是親愛的女友嵐馨，一路伴我走來，分擔憂愁與喜悅，我想這份成果喜悅亦是屬於你們的。

Contents

Abstract	
Contents.....	I
List of Illustrations	IV
Chapter 1 Introduction	1
Chap. 1.1 Introduction.....	1
Chap. 1.2 ZnO Characteristics and Nanostructures	2
Chap. 1.2.1 ZnO Nanowires	3
Chap. 1.2.2 Synthetic Methods of ZnO Nanowires.....	6
Chap. 1.2.3 Field Emission and PL Characteristics	9
Chap. 1.3 Anodic Aluminum Oxide (AAO) & MASK	13
Chap. 1.4 Capacitance	22
Chapter 2 Experiment Procedure and Details	23
Chap. 2.1 Fabrication of AAO and Mask	23
Chap. 2.1.1 Flow Chart for AAO Fabrication	23
Chap. 2.1.2 Fabrication Procedure of AAO	24
Chap. 2.1.3 Fabrication Procedure of Mask	26

Characteristics of 1D ZnO Nanowires Array Grown by AAO Assistance

Contents

Chap. 2.2 ZnO with AAO	27
Chap. 2.2.1 Flow Chart for ZnO with AAO Fabrication..	27
Chap. 2.2.2 Fabrication ZnO with AAO	28
Chap. 2.3 Capacitance	30
Chap. 2.3.1 Flow Chart of Capacitance.....	30
Chap. 2.3.2 Fabrication of Capacitance.....	31
Chap. 2.4 Measurement Equipment	31
Chap. 2.4.1 Physical Analysis	31
Chap. 2.4.2 Chemical Analysis	33
Chap. 2.4.3 Field Emission Detector	34
Chapter 3 Results and Discussion	35
Chap. 3.1 AAO and Mask	35
Chap. 3.1.1 AAO	35
Chap. 3.1.2 Mask	45
Chap. 3.2 ZnO with AAO	48
Chap. 3.2.1 SEM Analysis.....	48
Chap. 3.2.2 TEM Analysis	63

Characteristics of 1D ZnO Nanowires Array Grown by AAO Assistance

Contents

Chap. 3.2.3 XRD Analysis	66
Chap. 3.2.4 PL Analysis	69
Chap. 3.2.5 Field Emission Analysis.....	70
Chap. 3.3 Capacitance	89
Chapter 4 Conclusions	90
References	92



List of Illustrations

Fig. 1.2-1: (a) It is the fabrication flow of a ZnO NW triode field emission array. (b) the measurement for FE property²¹ 5

Fig. 1.2-2: It illustrates the mechanism of the photoluminescence. 12

Fig. 1.3-1: It illustrates the expansion of aluminum during anodic oxidation. On the left the level of the un-oxidized metal surface is depicted. 15

Fig. 1.3-2: The structure of AAO after anodization. 15

Fig. 1.3-3: Relation between anodic voltage with pore diameter of AAO. 16

Fig. 1.3-4: The process of the partial electric field in the Al₂O₃ surface.. 17

Fig. 1.3-5: 1. SEM micrographs of the bottom view of anodic alumina layers. Anodization was conducted in 0.3 M (1.7 wt %) sulfuric acid at 10 °C at 25 V (a), 0.3 M (2.7 wt %) oxalic acid at 1 °C at 40 V (b), and 10 wt % phosphoric acid at 3 °C at 160 V (c). Pore opening was carried out in 5 wt % phosphoric acid at 30 °C for 30 min. (a) 35 °C for 30 min. (b) and 45 °C for 30 min. (c) The thickness of the oxide films was approximately 120 nm. 18

Fig. 1.3-6: Lower magnification SEM micrographs of porous alumina anodized in sulfuric (a), oxalic (b), or phosphoric acid (c). The anodization conditions are the same as those in FIG- 1.3—5. 19

Fig. 1.3-7: The high order pore array by FIB lithography..... 21

Fig. 1.3-8: The high order pore array by SiC pattern. 21

Fig. 1.4-1: It depicts the cross-section of the nonvolatile memory structure and the measurement setup..... 22

Fig. 2.4-1: It illustrates the field emission measurement system. 34

Fig. 3.1-1: 4N Al sheet annealed at (a) 300(c)350(e)400(g)500°C x 2hrs, it then was fabricated AAO by two-step anodic. The images of right side were after widening treatment (60mins), left ones

were without. (4N Al sheet; applied voltage 50V; space of electros: 7; anodic reaction T: 12°C) 38

Fig. 3.1-2: 4N Al sheet; annealing 400°C x 2hrs; applied voltage 50V; space of electros: 7; reaction T: 12°C 39

Fig. 3.1-3: The brush-liked AAO was fabricated by over widening (widened time 100mins). 40

Fig. 3.1-4: They were fabricated by conventional two-step anodization. (a) SEM image only by fist step anodize (6, 1), (b) Cross section view. (c) SEM image by two-step anodize (6, 1, 3, 1), (d) Cross section view. (4N Al sheet; annealing 400°C x 8hrs; applied voltage 40V; space of electros: 7; reaction T: 28°C)..... 41

Fig. 3.1-5: They were fabricated by multiple step anodization which was more steps then two-step anodize. (a) SEM image by three step anodize (6, 1, 3, 1, 3, 1), (b) Cross section view. (c) SEM image by four step anodize (6, 1, 3, 1, 3, 1, 3, 1), (d) Cross section view. (4N Al sheet; annealing 400°C x 8hrs; applied voltage 40V; space of electros: 7; reaction T: 28°C)..... 42

Fig. 3.1-6: It was cleaned the residuum on the surface by supersonic shock after multiple step anodize. (a) High magnification (100K) SEM image and (b) low magnification (50K) SEM image revealed the uniform pore array. (4N Al sheet; annealing 400°C x 8hrs; applied voltage 40V; space of electros: 7; reaction T: 28°C). 43

Fig. 3.1-7: They were fabricated with the same parameters expect electrolytes. SEM images of the same magnification (100K), (a) was fabricated by 0.3M oxalic and (b) was fabricated by 0.1M H₃PO₄. (4N Al sheet; annealing 400°C x 2hrs; applied voltage 40V; space of electros: 7; reaction T: 28°C)..... 44

Fig. 3.1-8: AAO template (mask) was fabricated by removing bottom layer after removed superfluous Al film with AAO. (a) as-prepared

AAO top view of SEM image. (b) The cross section of AAO after removed superfluous Al film. (c) the cross section view of bottom under widening time of 30 mins, (d) the back view of bottom. (e) another one after widening time of 60 mins, (f) the top view. 46

Fig. 3.1-9: SEM images about back view of AAO with different reaction time combinations which were different widening and different removing bottom time. (a) total time 100 (70+30) mins, (b) 80 (40+40) mins, (c) 60 (0+60)mins. (widening time, removing time)..... 47

Fig. 3.2-1: These AAO were fabricated by two-step anodization (3, 3) on SiO₂/Si-sub. (a), (b) were AAO SEM images without widening treatment, porous of diameter was small then 10nm. (c) (d) were widened in 20 mins, porous of diameter was about 30nm. And (d) (e) were widened in 30 mins, porous of diameter was about 50nm. Thickness of AAO was about 1.2μm. (4N Al /SiO₂/Si; thickness of Al: 1μm; annealing 350°C x 8hrs; applied voltage: 40V; electrolyte: 0.3M oxalic; space of electros: 7; reaction T: 12°C) 52

Fig. 3.2-2: AAO was fabricated by conventional two-step anodization (3, 3) and widening time was 40mins. (a) It revealed the top view of AAO and many residues on surface. (b) cross section view image revealed the AAO thickness was about 1.2μ. (c) The high magnification (150K) image indicated porous diameter was about 60-85nm, thickness of porous well was about 50 nm and thickness of bottom was about 50 nm. The thickness of porous well equaled to thickness of bottom. (4N Al /SiO₂/Si; thickness of Al: 1μm; annealing 350°C x 8hrs; applied voltage: 40V; electrolyte: 0.3M oxalic; space of electros: 7; reaction T: 12°C)

..... 53

Fig. 3.2-3: AAO was fabricated by conventional two-step anodization (3, 12). They were anodized over suitable time (about 3min) at second anodic treatment. (a) it was widened in 50 mins. (b) it was widened in 80 mins, we observed over winding induced porous wall to break and thickness of bottom to thinner. (4N Al /TiN/Si; thickness of Al: 1 μ m; annealing 400 $^{\circ}$ C x 8hrs; applied voltage: 40V; electrolyte: 0.3M oxalic; space of electros: 7; reaction T: 12 $^{\circ}$ C)..... 54

Fig. 3.2-4: (a) AAO was fabricated by conventional two-step anodization (3, 12) and widened in 60 mins. Diameter of pores was about 80nm. (b) It was removed the ZnO residues on AAO surface after pores full of ZnO by hydrothermal method. The SEM image revealed the pores full of ZnO successfully. (4N Al /TiN/Si; thickness of Al: 1.3 μ m; annealing 400 $^{\circ}$ C x 2hrs; applied voltage: 40V; electrolyte: 0.3M oxalic; space of electros: 7; reaction T: 12 $^{\circ}$ C; ZnO hydrothermal in 2hrs at 96 $^{\circ}$ C) 55

Fig. 3.2-5: The AAO full of ZnO was removed AAO in order to form the exposed ZnO NWs. (a). the top view of SEM image revealed island-liked ZnO NWs crowd. (b). the image of cross section view indicated the collapse of ZnO NWs clearly. (4N Al /TiN/Si; thickness of Al: 1.3 μ m; annealing 400 $^{\circ}$ C x 2hrs; applied voltage: 40V; electrolyte: 0.3M oxalic; space of electros: 7; reaction T: 12 $^{\circ}$ C; ZnO hydrothermal in 2hrs at 95 $^{\circ}$ C)..... 56

Fig. 3.2-6: AAO was fabricated by conventional two-step anodization. The special treatment was supersonic shake to remove residues on surface after widening. (a) Top view. (b)Cross-section view and (c) was high magnification (250K) image of the bottom area. (4N Al /TiN/Si; thickness of Al: 1 μ m; annealing 400 $^{\circ}$ C x 8hrs;

applied voltage: 40V; electrolyte: 0.3M oxalic; space of electros:
7; reaction T: 12°C) 57

Fig. 3.2-7: AAO was fabricated by two-step anodization. The top-view
SEM images were the same magnification, (a) employed 5N Al
source and (b) employed 4N Al source. We could clearly
observe the improvement of reduced impurities on the surface
due to high concentration of Al film. 58

Fig. 3.2-8: SEM images of cross section(a),top view(b)(c) Temperature not
high enough to assist ZnO migrated into pores, so we observed
the ZnO covered the surface and would not full into the
porous.(b) 30 mins at 80°C ,(c) 1hr at 80°C . The inset in (a) was
the high magnification SEM image. 59

Fig. 3.2-9: SEM images of cross-section view (a)(b)(c) were different
applied voltage to anodize according to 30V, 40V, 50V. (d), (e),
and (f) were reveled different widening time form the sample of
(c), and the widening time was 10 mins, 20 mins, 40 mins,
respectively. (5N Al /TiN/Si; thickness of Al: 850nm; annealing
400°C x 2hrs; electrolyte: 0.3M oxalic; space of electros: 7;
reaction T: 12°C)..... 60

Fig. 3.2-10: (a), (c) are the SEM images of top view, and (b), (d) are SEM
images of cross-section view. (a), (b) are fabricated by
convectional two-step anodization.(1, 3.5) (c), (d) are widened
in 60 mins, the diameter become about 80 nm from 10 nm. (5N
Al /TiN/Si; thickness of Al: 500nm; annealing 400°C x 2hrs;
applied voltage: 50V; electrolyte: 0.3M oxalic; space of electros:
7; reaction T: 12°C) 61

Fig. 3.2-11: They are SEM images of cross-section view, (a) is the original
structure, diameter: 20-30nm, length: 1800nm. And (b), (c), (d)
reveal the broken area after field emission measurement. (5N Al
VIII

/TiN/Si; thickness of Al: 1500nm; annealing 400°C x 2hrs; applied voltage: 50V; electrolyte: 0.3M oxalic; space of electros: 7; reaction T: 12°C; widening time 20) 62

Fig. 3.2-12: The TEM cross-section image of AAO full of ZnO prepared by FIB; ; the porous diameter is about 80nm after 40mins widening treatment; the structure is AAO/SiO₂/Si-sub..... 64

Fig. 3.2-13: (a) TEM image of ZnO NW prepared by supersonic shake treatment; (b) SAED of ZnO NWs.(c) EDS of ZnO NWs..... 65

Fig. 3.2-14: It reveals XRD patterns of Al film with different annealing treatment on TiN/Si-sub., and compares with (a) different annealing time and temperature, (b) RTA. 67

Fig. 3.2-15: It reveals XRD patterns of AAO full of ZnO on SiO₂/Si-sub., and compares with (a) annealing (400°C 2hr) and (b)without annealing..... 68

Fig. 3.2-16: It reveals the with Xe lamp as an excitation source (320 nm) at room-temperature..... 69

Fig. 3.2-17: Field emitting J-E curve and $\ln(J/E^2)-1/E$ curve..... 71

Fig. 3.2-18: It illustrates operation region of field emission. 71

Fig. 3.2-19: The SEM images reveals the morphology of sample B2. It was AAO full of ZnO by hydrothermal in 2.5 hrs at 95°C 72

Fig. 3.2-20: It shows field emission J-E curve and F-N plot of sample B2. The table shows the detail data..... 73

Fig. 3.2-21: It shows field emission J-E curve and F-N plot of sample B2 under a 30W lamp. The table shows the detail data. It indicates the photo-enhanced field emission characteristic..... 74

Fig. 3.2-22: The SEM images reveals the morphology of sample C1. It was AAO full of ZnO by hydrothermal in 2.5 hrs at 95°C and removed the surplus ZnO on the AAO surface. And length/diameter is 500-600/70-80nm..... 75

Fig. 3.2-23: It shows field emission J-E curve and F-N plot of sample C2.
The table shows the detail data..... 76

Fig. 3.2-24: It shows field emission J-E curve and F-N plot of sample C2
which was improved by annealing (with 400°C at 2hrs). The
table shows the detail data. 77

Fig. 3.2-25: It shows field emission J-E curve and F-N plot of sample
ASS6.4. The table shows the detail data. And length/diameter is
1600/70-80nm..... 81

Fig. 3.2-26: It shows field emission J-E curves of different aspect ratio and
fixed the diameter. 82

Fig. 3.2-27: (a) Turn on field versus NW length, and (b) FE-β versus
Different NW length..... 83

Fig. 3.2-28: Active region for Different NW length (fixed
diameter=80nm).Length (um):ASS1.4=0.5, ASS11.3=1,
ASS6.4=1.6, Cb=0.6, ASS5.1=1.2..... 84

Fig. 3.2-29: Active region for Different NW length fixed the diameter. . 85

Fig. 3.2-30: FE for Different NW diameter fixed length (L=500nm).
Diameter (nm): ASS1.4 = 80, ASS1.2 = 30. 86

Fig. 3.2-31: FE for Different NW diameter fixed length (L=1600nm).
Diameter (nm): ASS6.4 = 80; ASS6.2 = 30 87

Fig. 3.2-32: FE-β versus Different aspect ratio. 88

Fig. 3.3-1: SEM images of cross-section view (a), top-view(b)(c). (d) was
illustration of capacitance measurement. (a) reveals the AAO
full ZnO. (b) reveals few ZnO residues on the surface. The
partial circle in the image (c)was the top electrode..... 89

Chapter 1 Introduction

Chap. 1.1 Introduction

Recently, the nanotechnology have been extensively researched, which contains many kinds of different dimensional nanostructures. For example, there are one dimensional (1D) nanostructure, such as nano-tubes^{1,2,3}, nano-wires⁴ and nano-rods^{5,6,7}; two dimensional (2D) nanostructure, such as nano-sheets^{8,9}, nano-planes and nano-discs; three dimensional (3D) nanostructure, such as nano-dots^{10,11}. The above-mentioned are great importance in studying the physical and chemical properties of nano-materials or constructing functional nano-scale devices, which have been investigated in the potential applications of photonic, electro-optical and electronic device. For example, some applications of different kinds of nanostructures were extensively studied, including to nanodot for nonvolatile memory (nano-crystal memory device, IBM, 1995), nanosheet for solar cell, nanowire for field emission¹² and photofluorescent device, etc.

About the studies of one dimensional (1D) nanostructure were quite popular, since the first discovery of carbon nanotubes (CNTs) that were fabricated in 1991¹³. Considerable effort of CNTs has been devoted to the synthesis and characterization of nanoscale. Because of their attractive physical properties enable them to play a major role in nanoscale electronic and nanoscale devices, large studied about CNTs was published. Moreover, many materials were researched to replace carbon in order to improve some insufficient effects of CNTs. So, expect for carbon, a novel material,

ZnO, was attractive and utilized for nanostructure.

The subject was focused on the characteristic and fabrication of 1D ZnO nanostructure. The particulars will be discussed at following sections.

Chap. 1.2 ZnO Characteristics and Nanostructures

ZnO is a wide band gap semiconductor (3.37eV) with a large exciton binding energy (60meV) at room temperature, and is one of the most important and versatile semiconductor materials. Previous studies were investigated into its optical and electric properties¹⁴, as well as its ferromagnetic, transparency, photoconductivity, piezoelectric, field emission¹², and light-emitting properties. Further, ZnO has attracted much attention since possible applications in phosphors, transparent conducting films for solar cells, ultra-violet (UV) laser devices¹⁵ and flat panel displays were suggested^{16,17,18}.

Since the first report of ultraviolet lasing from ZnO nanowires¹⁹, nanostructure of ZnO has stimulated intensive research. Indeed, ZnO nanostructures are interesting to study not only the property of UV lasing emission in nanowire form, but also because a wide variety of morphologies have been prepared. Some kinds of the ZnO nanostructures contain nanowire, nanorod, nanosheet, nanoribbon, nanotube, nanoplate, tetrapod, and flower-liked²⁰ structures. Indeed, based on the nano-scale structure on interface, those applications of morphological properties will exceed normal expectations and behave prominent effect.

Furthermore, the ZnO nanowires are believed to be a viable candidate which compare to CNTs for field emission device, due to its excellent thermal and chemical stability. So, about the prominent properties and the synthetic methods of ZnO nanowires we are interested will be discussed in next sections.

Chap. 1.2.1 ZnO Nanowires

To come back to the subject, the focus is the 1D ZnO nanowires. The nanowire array is the major structure to investigate; contrary, the signal nanowire was no more attraction as nanowire array, and the main causes were fabricated hardly and applied restrictedly.

To continue mention of Chap. 1.2 , the applications of the ZnO nanowires were focused on the properties of photoluminescence and field-emission (the mechanisms would be discussed at Chap. 1.2.3), due to its excellent thermal and chemical stability. There are some qualitative and specific factors for measurement and analysis objectively. About factors of metrical, there are work function and square resistor, etc; about factors of morphology is such as aspect ratio, number density and surface roughness.

We will cit some instants and illustrate some applications at following contents:

1. nanowires array

In particular, exploration of the materials for flat panel displays has been a hot topic for the last few decades. So, current trends in

nanotechnology and nanomaterials play an important role in the potential applications. Then, high aspect ratio one-dimensional (1D) nanostructures, such as nanotubes, nanowires and nanobelts, have been extensively studied with a view to use in vacuum microelectronic devices, including field emission displays (FEDs), electron sources, microwave devices and high power rf amplifiers, because of the advantage of the low turn-on electric field and high electron emission efficiency¹².

Recently, ZnO nanowire emitters have been reported to exhibit good emission properties with high stability, low threshold electric field, high emission current density, good emission stability and durability. The ZnO NWs have been synthesized by various procedures (we will discuss in next section); however, the main challenge in fabricating the nanowire based FED devices is the high synthesis temperature which retards the integration processes for FED device structures. A hydrothermal method would offer a superior route for FED fabrication because of the catalyst-free growth, low cost, low reaction temperature, large area and uniform production, environment friendliness and process compatibility with VLSI. As above advantages, the hydrothermal method for low temperature was applied in our works.

2. Field emission triode^{21,22}

Basing on nanowire array, the ZnO NW triode shows good and controllable emission properties with the turn-on anode electric field, threshold anode electric field and field enhancement factor (β), respectively. The main cause is the gat structure was applied, and the gat which was applied suitable gat voltage could enhance emission current

density higher at the same turn-on electric field which compared with one without applying gat structure.

However, the main advantages for the nanowire based field emission device (FED) are a large area display, high uniformity, high productivity, high brightness, low cost, low power consumption and reliability. From this point of view, triode-type FED devices with low driving voltage, high resolution and controllable electron emission characteristics are candidates for constituting a new generation of FED devices. Fig. 1.2-1 illustrates the fabrication flow of a ZnO NW triode field emission array.

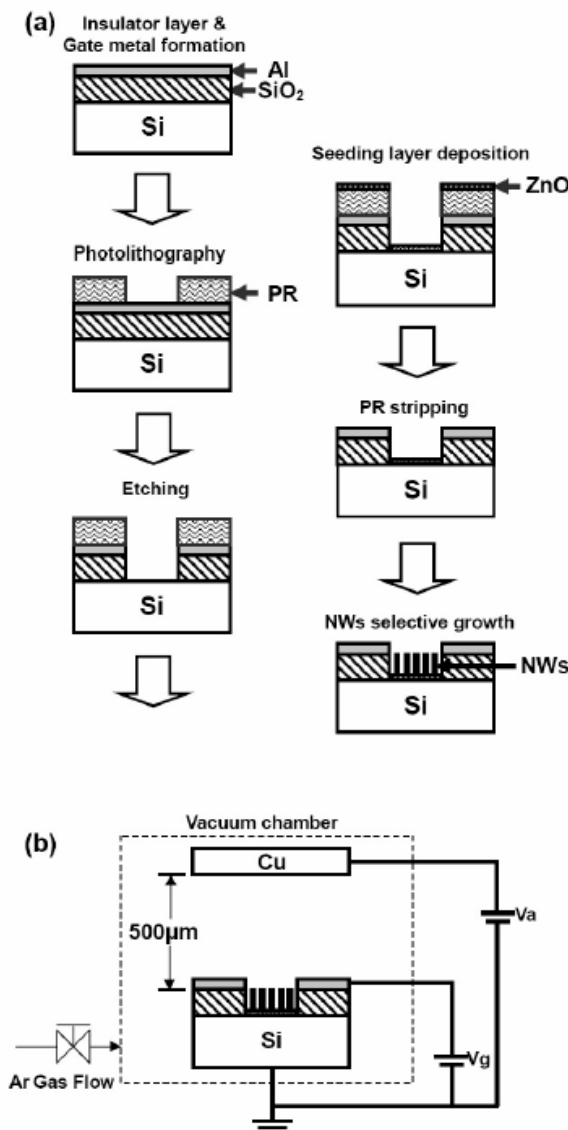


Fig. 1.2-1: (a) It is the fabrication flow of a ZnO NW triode field emission array. (b) the measurement for FE property²¹.

3. Doped ZnO nanowires¹⁸

We can study the variation and effect on the photoluminescence and field-emission properties by doping the different elements into ZnO nanowire. Farther, we can modulate those characteristic to satisfy with application actuality. For example, Norton and co-workers have reported that the $P_{0.02}Mg_{0.1}Zn_{0.90}$ film showed stable p-type behavior by adding Mg and P together—doping with Mg to increase the band gap and P to introduce the acceptor level^{23,24}.

Moreover, such suitable doped NWs exhibit better field-emission properties including the lower threshold electric field, lower resistance in series, and higher emission current density, in comparison with undoped NWs. The improved field-emission characteristic is attributed to the changes in surface state of the nanostructure at both threshold voltage and F-N field-emission regions. Furthermore, the modulated band gap can be obtained with suitable doping, which may also be able to be applied for the future enanohomojunction optoelectronic and field-emission devices.

Chap. 1.2.2 Synthetic Methods of ZnO Nanowires

Synthesis methods of ZnO nanostructures can be achieved by various techniques, for example, including as vapor-liquid-solid (VLS) growth¹², metal-organic vapor phase epitaxy (MOVPE) procedures, physical deposition process²⁵, electro-chemical deposition method^{7,26}, template enhancement method^{5,6}, hydrothermal method^{20, 21, 27, 28}, etc. Those

Characteristics of 1D ZnO Nanowires Array Grown by AAO Assistance

C-W Chang

synthesis techniques employed some general semiconductor process machinery equipments, classed like as chemical vapor deposition (CVD), physical vapor deposition (PVD), electrical gun evaporation, thermal evaporation, high temperature chamber, etc. Those synthesis techniques look like similar for results. But, there were some different advantages and handicaps during some procedures. We focused on those handicaps which were fatal; some handicaps of physical property can not be overcome and endured for some applications, which for some materials, such as polymer substrates, will be melted due to high temperature treatment.

Consequently, one of the most serious handicaps to fabricate the nanowire is the high synthesis temperature, which will restrict the selection of substrate materials, even affect integration procedures. Thus, the main challenge in fabricating the NW based FED devices is the high synthesis temperature which retards the integration processes for FED device structures.

Particularity, the hydrothermal method offers a superior route for FED fabrication because of the catalyst-free growth, low cost, low reaction temperature, large area and uniform production, environment friendliness and process compatibility with VLSI.

Farther, following discussion was about the comparison of VLS with hydrothermal method, and listed the difference in their detail process and certain limits.

First, the main deficiency in VLS process was the high synthesis temperature (750-950°C). And, the synthesis temperature of hydrothermal

method was low than 100°C . However, the high temperature would provide well aligned array and excellent structure oppositely, such as high quality and high aspect ratio.

Another notable difference of VLS with hydrothermal method was the catalyst. For example, the VLS employ Cu (copper) or Au (gold)^{12,25} as catalyst for growth ZnO. And, the intrinsic properties of catalyst, such as surface morphology and large different of lattice parameter with reaction elements, would cause to variation different of product. Following the example¹², the surface of the Cu catalyst film has many ordered square and hexagonal Cu island structures and the lattice parameter of Cu ($a=3.215 \text{ \AA}$) is close to that of the ZnO ($a=3.253 \text{ \AA}$). Consequently, the ZnO nanowires can vertically grow from Cu catalyst layer on the Si substrate with VLS, rather than grow from Au catalyst layer. However, the hydrothermal method was always catalyst-free. Generally, the VLS process was complex than hydrothermal method in many particulars, such as flow ratio of carrier gas would obviously effect the product of VLS process.

However, we identify the VLS process was more complex than hydrothermal method. But, we also can not disregard the advances of VLS process. We could select suitably and search the balance according to our applications.

Following would list in Tab.1.2-1 about the comparison between VLS process and hydrothermal method.

Characteristics of 1D ZnO Nanowires Array Grown by AAO Assistance

C-W Chang

Method	synthesis temperature	catalyst	procedure	quality of product	compatibility with VLSI
VLS	higher	requisite	More complex	excellent	no
Hydrothermal	lower	no	simple	acceptable	yes

Tab. 1.2-1: It shows details of comparison between VLS process and hydrothermal method.

Chap. 1.2.3 Field Emission and PL Characteristics

© Field emission

In brief words, the field emission is a point discharge phenomenon. It was easily occurred at a long and sharp rod liked needle. When we applied a negative voltage on it, the tip would exhibit a large electric field then other parts naturally. If the applied field is large enough, the potential barrier would narrow and an appreciable number of electrons at the Fermi level can tunnel through. We set a grounded probe or plant in a suitable distance between with the tip to receive would emit electrons from the tip. So we could constitute measurement equipment illustrated at Fig- 2.4-1, and we could measure the current I (a current passed by probe or plant) and calculate the current density (J) that was I divided by A (area of the probe or plant).

However, this point discharge phenomenon we observed was not sure

of field emission; we must check some properties to fit some conditions of the field emission mechanism. We could demonstrate by utilizing those discharge properties fitted the Fowler-Nordheim (FN) equation. The simple mode was that making sure the curve which was the relationship between J and E (applied voltage divided by the emission distance) to fit the F-N relationship. the FN relationship is as follows:

※Fowler-Nordheim (FN) equation:

$$J = (A\beta^2 E^2 / \Phi) \exp(-B\Phi^{3/2} / \beta E)$$

$$A = 1.56 \times 10^{-10} \text{ (AV}^{-2} \text{eV)}; \quad B = 6.83 \times 10^3 \text{ (VeV}^{-3/2} \mu\text{m}^{-1})$$

Where J is the current density, E is the applied field, Φ is the work function of the ZnO (4.45 eV), β is the field enhancement factor, and A, B are constants, $A = 1.56 \times 10^{-10} \text{ (AV}^{-2} \text{eV)}$ and $B = 6.83 \times 10^3 \text{ (V eV}^{-3/2} \mu\text{m}^{-1})$.

※The field emitting enhancement factor, β :

$$m = B\Phi^{3/2} d / \beta; \quad m = \text{slop} \rightarrow \beta = B\Phi^{3/2} / m$$

where the value of β can be calculated from the slope of the F–N plot. The calculated β value would determine the field emission was good or not. Thus, large β value represented a well field emission mechanism; contrariwise small β value meant a poor field emission mechanism. And the β value was positive. In other word, by the above-mentioned, it is well known that the β value depends only on the geometry, structure, tip size and number of emitters on the substrate.

© Photoluminescence (PL)

The photoluminescence analysis was a simple physical mechanism which was illustrated in Fig. 1.2-2. In brief statement, about the mechanism of photoluminescence was an energy transport. Generally, the excitation source was some kinds of lamps which could emit different wave length. Different lamp which was filled of different gas would manage to provide a limited range of wave length. For example, we could employ two different kinds of lamps to provide a wide range of wave length. As we know, different metrical absorb particular wave length to provide energy for electron. If electron obtained enough energy, it would be transition from low energy level to high energy level; then, it would release energy when it transit to low energy level. The energy could be released by two type of light: one was excitation, another was emission. And, if the released light was classified according to wave length, it could class as fluorescence and luminescence.

To take a point of ZnO NW array, a photoluminescence analyzer with Xe lamp as an excitation source (~320 nm) was used for optical studies at room temperature. The major photoluminescence peak was the ultraviolet (U.V.) emission which was due to band-edge emission of ZnO, and it could detect different peak. In many studies, those peaks at special wave lengths for ZnO were reported to be caused by the Zn vacancy, oxygen deficiency, deep level, or singly ionized oxygen vacancies, etc. In other words, those

defects of product would cause different energy states excited in the band-gap. So, those minor peaks would suggest that the produce excited defects.

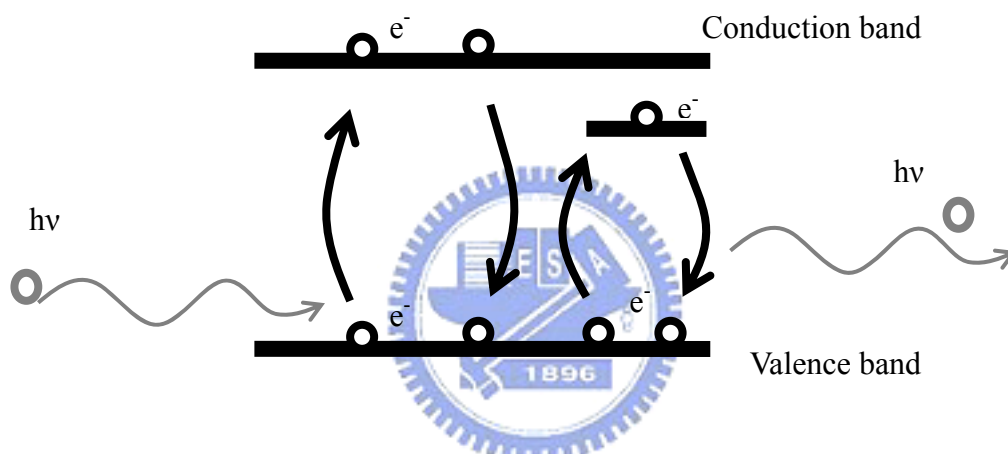


Fig. 1.2-2: It illustrates the mechanism of the photoluminescence.

Chap. 1.3 Anodic Aluminum Oxide (AAO) & MASK

◎ Anodic Aluminum Oxide (AAO)

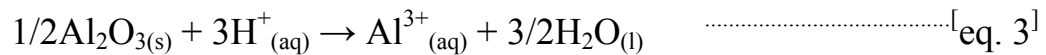
The Anodic Aluminum Oxide (AAO) structure would provide some properties for nanotechnology study, which including high ordered density of pores, controllable diameter and length of pores, large area and high uniform, stable chemical property of product, etc. As the result, recently, the AAO applications in nano-scale were studied extensively. Because of the one-dimensional nano-materials exhibit interesting properties, the AAO which could provide controllable one-dimensional pores was an excellent candidate to assistant fabrication.

Generally, the AAO structure was fabricated by a conventional two-step method. From the previous literature²⁹, the two-step was classed as 1. as-prepared pore formation and 2. stable porous growth.

The interaction mechanisms were illustrated at Fig. 1.3-1. Pores grow perpendicular to the surface with the equilibrium of field-enhanced oxide dissolution at the oxide/electrolyte interface and oxide growth at the metal/oxide interface. While the latter is due to the migration of oxygen containing ions (O^{2-}/OH^-) from the electrolyte through the oxide layer at the pore bottom, Al^{3+} ions which simultaneously drift through the oxide layer are ejected into the solution at the oxide/electrolyte interface. The fact that Al^{3+} ions are lost to the electrolyte has been shown to be a prerequisite for porous oxide growth, whereas Al^{3+} ions which reach the oxide/electrolyte interface contribute to oxide formation in the case of barrier oxide growth. A possible origin of forces between neighboring

pores is therefore the mechanical stress which is associated with the expansion during oxide formation at the metal/oxide interface. Since the oxidation takes place at the entire pore bottom simultaneously, the material can only expand in the vertical direction, so that the existing pore walls are pushed upwards. Under usual experimental conditions the expansion of aluminum during oxidation leads to less than twice the original volume, since Al ions are mobile in the oxide under the electric field, so partly the oxidized aluminum does not contribute to oxide formation. In experiments, we could observe the relative thickness of the porous alumina layer compared to the consumed aluminum was found to vary with applied voltage and electrolyte concentration.

Following list showed the main chemical reactions of AAO:



The AAO cross-section structure after conventional fabrication was illustrated at Fig. 1.3-2. We could control the porous diameters by utilizing chemical etching to widen the pore.

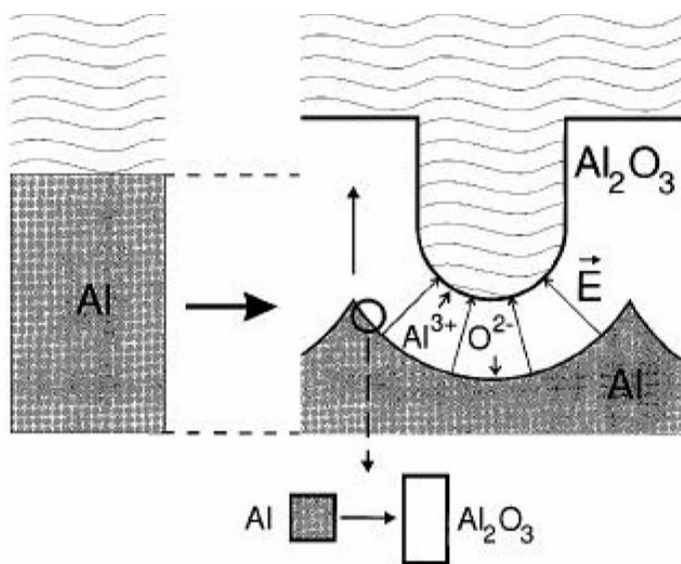


Fig. 1.3-1: It illustrates the expansion of aluminum during anodic oxidation. On the left the level of the un-oxidized metal surface is depicted.

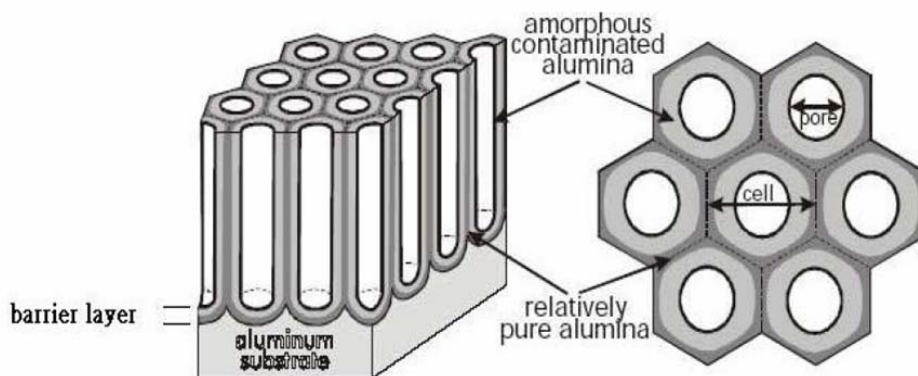


Fig. 1.3-2: The structure of AAO after anodization.

The Fig. 1.3-3 revealed direct proportion between anodic voltage with porous diameter of AAO; when the applied voltage was increase, the porous diameter would increase, and no matter what kinds of electrolyte. The main cause was the applied voltage formed a field-enhance porous reaction. By the way, we obtain different porous diameter at the same applied voltage in different electrolyte.

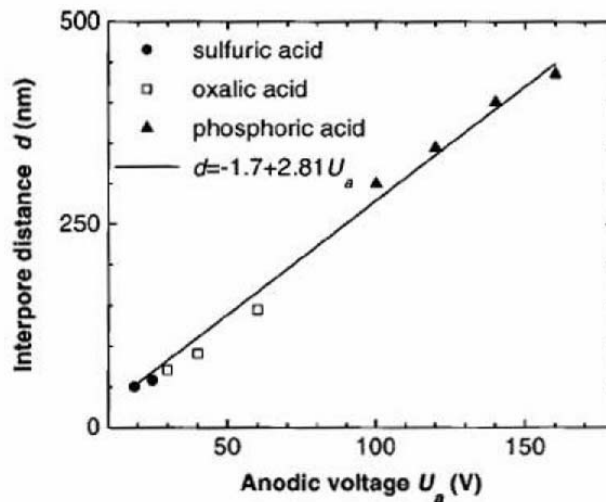


Fig. 1.3-3: Relation between anodic voltage with pore diameter of AAO³⁰.

The mechanism details of as-prepare pores were shown in the Fig. 1.3-4. The partial electric field would become more concentration in the Al_2O_3 surface when the applied voltage was increased gradually. Those partial area would higher reaction ratio (the field-enhance oxide dissolution at the oxide/electrolyte interface and oxide growth at the metal/oxide interface) then neighbor area, and those area would form the as-prepare pores. Fig. 1.3-1 revealed the interactive mechanism of AAO.

Characteristics of 1D ZnO Nanowires Array Grown by AAO Assistance

C-W Chang

The Al^{3+} and O^{2-} were combined to form Al_2O_3 in the surface. Simultaneously, it would dissolve in the electrolyte due to that the as-prepare pores areas had higher concentrative voltage and higher reaction ratio (those complex ion interactions were discussed at above content). Further, we obtained the Al surface formed the vertical porous array after the second anodic step.

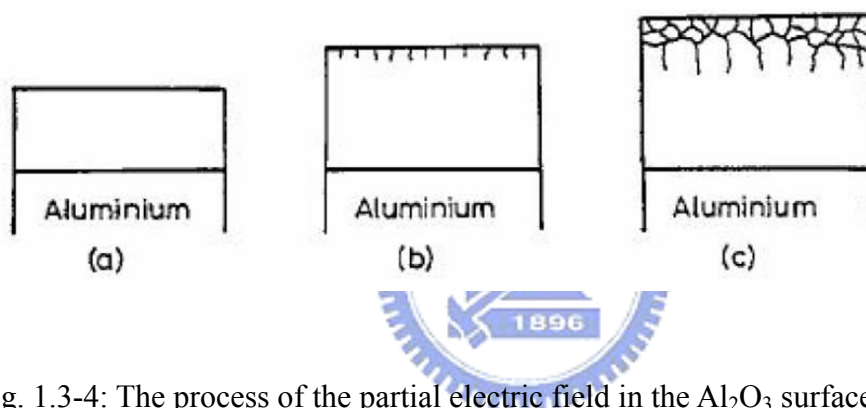


Fig. 1.3-4: The process of the partial electric field in the Al_2O_3 surface.

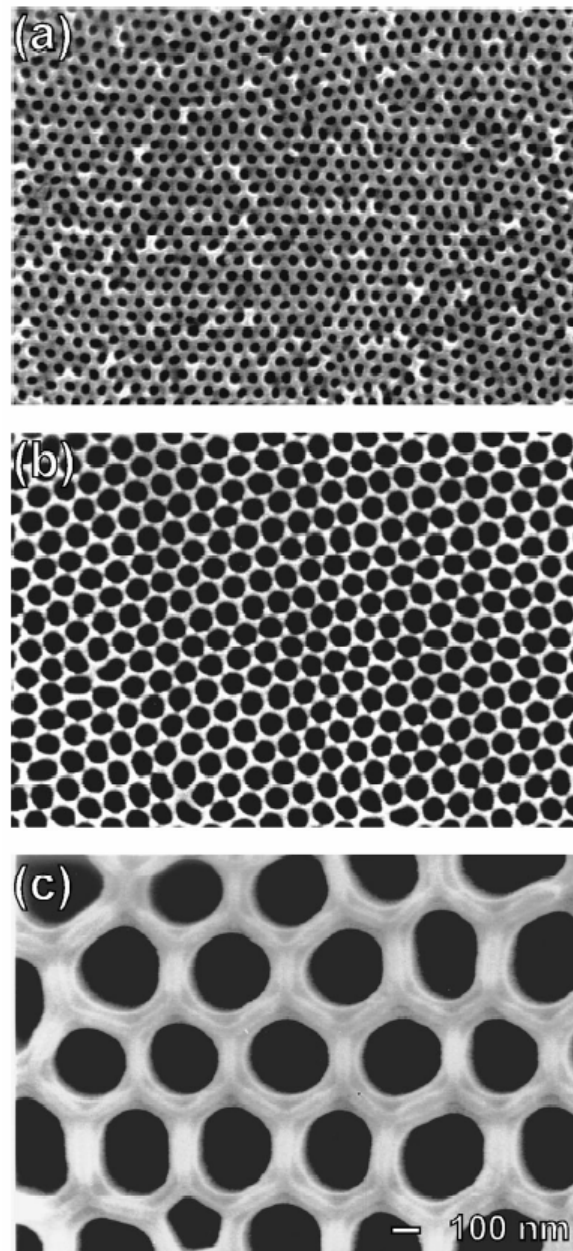


Fig. 1.3-5: 1. SEM micrographs of the bottom view of anodic alumina layers. Anodization was conducted in 0.3 M (1.7 wt %) sulfuric acid at 10 °C at 25 V (a), 0.3 M (2.7 wt %) oxalic acid at 1 °C at 40 V (b), and 10 wt % phosphoric acid at 3 °C at 160 V (c). Pore opening was carried out in 5 wt % phosphoric acid at 30 °C for 30 min. (a) 35 °C for 30 min. (b) and 45 °C for 30 min. (c) The thickness of the oxide films was approximately 120 nm.³¹

Characteristics of 1D ZnO Nanowires Array Grown by AAO Assistance

C-W Chang

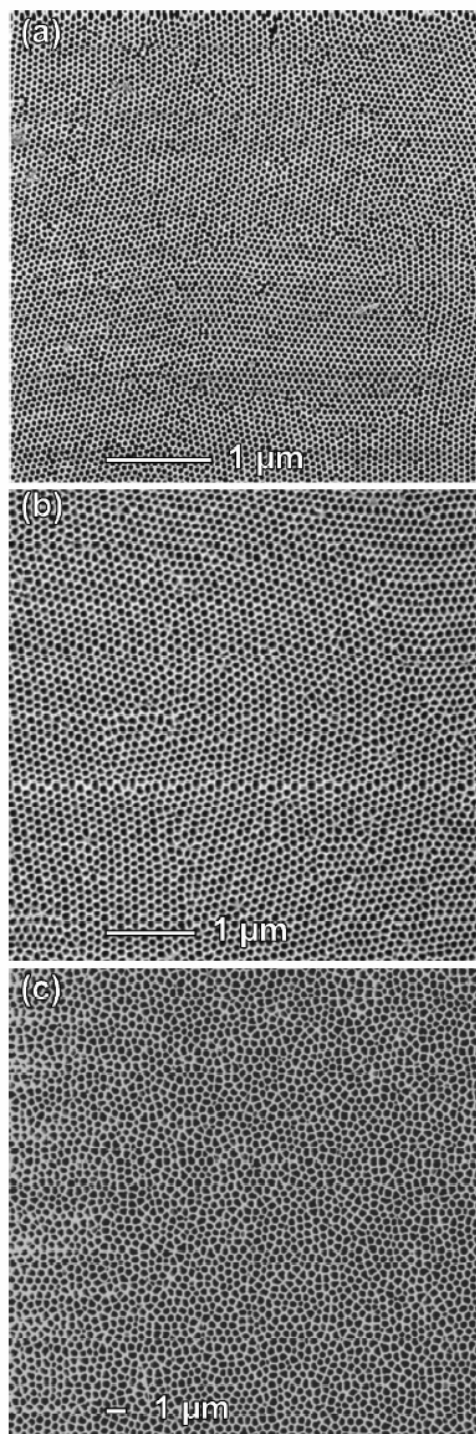


Fig. 1.3-6: Lower magnification SEM micrographs of porous alumina anodized in sulfuric (a), oxalic (b), or phosphoric acid (c). The anodization conditions are the same as those in Fig. 1.3-5.

◎ MASK

After the two step process, the main structure was AAO on Al sheet or substrate. The mask was fabricated by etching treatment for removing the film under AAO. Removing the redundant Al sheet and barrier layer was by the different selectivity of etching treatments. We would obtain a nano-channel array look like meshed thin film. It could be employed as mask to fabricate nanotube or nanowire if we widened the porous diameter to achieve suitable scale.

However, the as-prepared pore would determine the further porous properties; however, the as-prepared pore would defined by first anodic procedure, electrolyte, and experiment condition. Hence, some methods were reported in order to improve this question. For example, we could utilize FIB lithography or SiC hard mask to parent the required nano-scale porous array. Those methods were illustrated at Fig. 1.3-8. Although it could achieve the high ordered pore, the process became more complex.

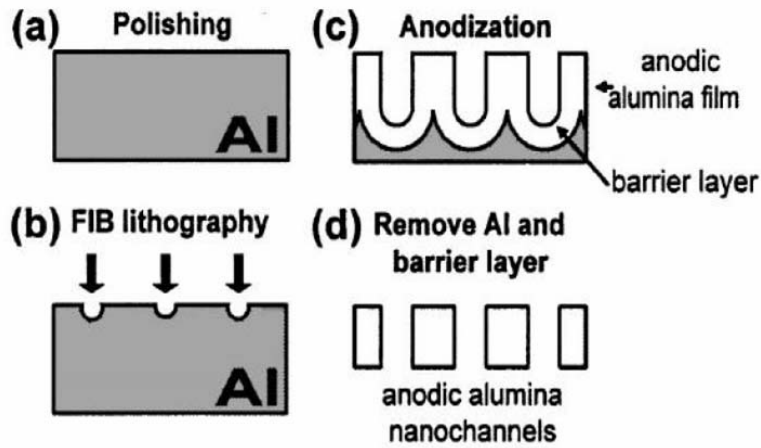


Fig. 1.3-7: The high order pore array by FIB lithography.

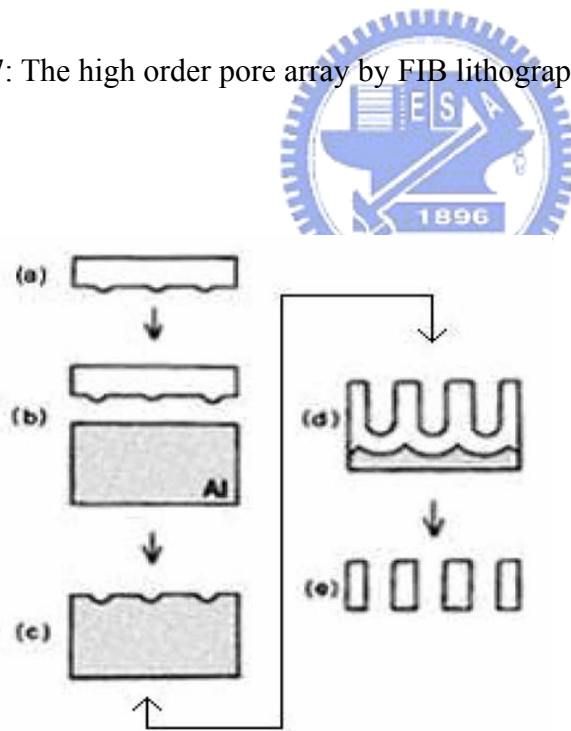


Fig. 1.3-8: The high order pore array by SiC pattern.

Chap. 1.4 Capacitance

Based on the AAO porous template, one material was deposited on it as electrode. The dielectric was the compound of one metrical with alumina. To control the quality of nano-scale structure was a challenge. It always had large current leakage due to the not well crystalline of alumina.

If we focused on the high interface of AAO, the major point was the contact of material and the porous anodic alumina films, it would exist a large contact surface between material and alumina in the pores. The interface would provide some kinds states. The quality of the interface states would dominate the electric behavior. And the best quality might be employed to applications of memory. In the previous report^{32, 33}: cadmium sulfide (CdS) nanowires of 10nm diameter, electrodeposited in porous anodic alumina films, exhibit an electronic bi-stability that can be harnessed for nonvolatile memory. The current–voltage characteristics of the wires show two stable conductance states that are well separated and long lived. The structure was illustration in Fig. 1.4-1.

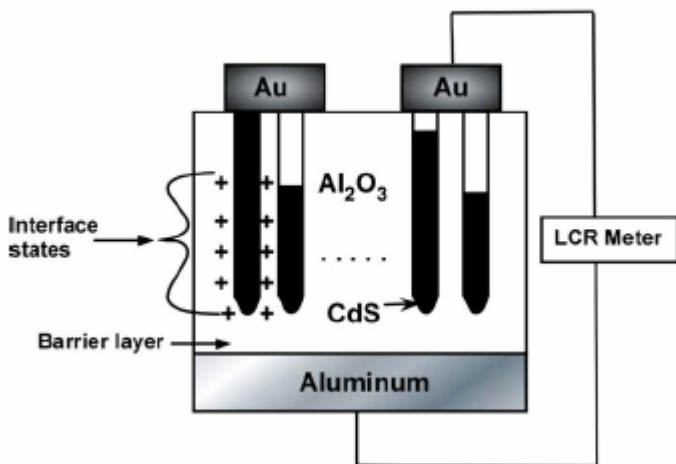
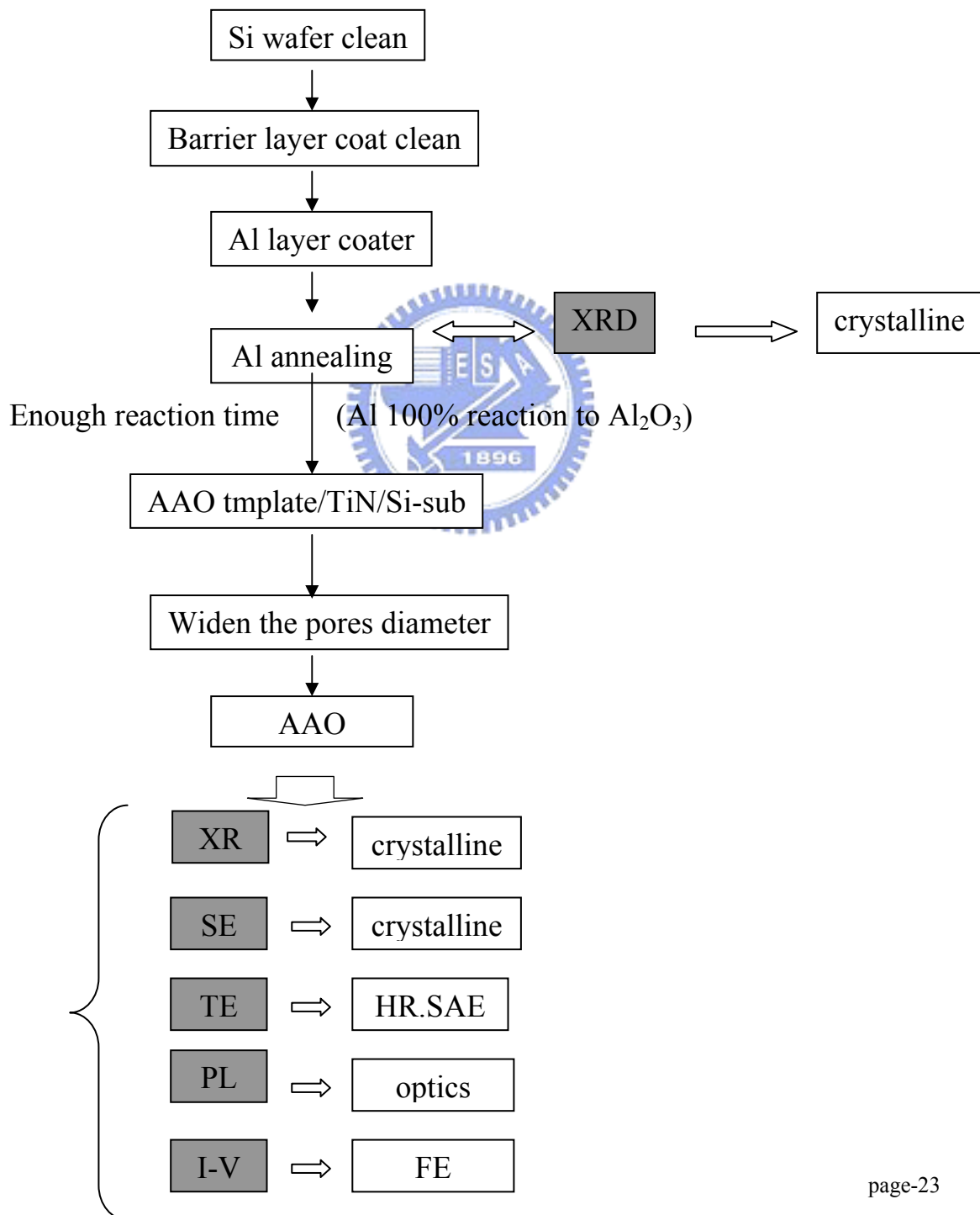


Fig. 1.4-1: It depicts the cross-section of the nonvolatile memory structure and the measurement setup.

Chapter 2 Experiment Procedure and Details

Chap. 2.1 Fabrication of AAO and Mask

Chap. 2.1.1 Flow Chart for AAO Fabrication



Chap. 2.1.2 Fabrication Procedure of AAO

As-prepared procedure was RCA clean for p-type Si-substrate (100). For barrier the follow-up thermal treatment, we employed TiN thin film as barrier layer, and deposited it on Si substrate by DC sputter in N₂ atmosphere, and in vacuum chamber (1×10^{-6} Torr). Moreover, the barrier layer provided with conductivity to play a role of sub-electrode. For the prepared AAO template, Al thin film of required thickness was first deposited on the Si wafer by thermal evaporation in vacuum chamber ($< 5 \times 10^{-7}$ Torr). The purity of Al source was 5N (99.999%) ingots of Al. annealing the Al thin film on TiN/Si-sub at 350-500°C was in order to release mechanical stress and enhance the crystallization quality. As we knew, the porous morphology of AAO depended on the quality of Al.

The two step anodic procedure, which has been reported in detail elsewhere, was employed to prepare high order porous channel arrays of AAO. Following, the major procedure would list simply. First anodic treatment was carried out in a 0.3M oxalic solution(H₂C₂O₄) at 12°C and applied a constant polarization voltage for a few time. The produce was a thin nano-porous AAO in the top surface. Then, we removed the thin nano-porous film by wet chemical etching with a mixed solution of H₃PO₄ and CrO₃ at 60°C, and therefore the surface on the Al film was exhibited a relatively ordered indent pattern. The indent pattern was the as-prepared porous pattern and determined the surface morphology of AAO channel array further. The second anodic treatment was performed for a reaction time under the same constant polarization voltage as fist step one. Then, the product was the initial sample after clean process by DI water.

Characteristics of 1D ZnO Nanowires Array Grown by AAO Assistance

C-W Chang

However, the existing porous diameter was not wide enough. The pore diameter of the AAO template was widened in a 5% H_3PO_4 solution for a widened time.

The mechanism of two step anodic procedure was displayed at ch1-3, and the surface morphology and initial porous diameter were mainly determined by applied polarization voltage and electrolyte. Among of every electrolyte of AAO which were reported in previous literature, the reaction was carried out and based on acid solution, including chromic acid (CrO_3), sulfuric acid (H_2SO_4), oxalic acid ($\text{H}_2\text{C}_2\text{O}_4$), boric acid (H_3BO_3), or phosphoric acid (H_3PO_4). Those acid solutions were controlled to effective reaction by different solution concentration and reaction temperature. Actually, we achieved the porous length and diameter that we ordered by controlled the reaction time and widened time, when we fixed the parameter such as applied polarization voltage, space of electrodes, reaction temperature and electrolyte. The structure of result was AAO template on barrier layer of TiN and substrate of Si (AAO/TiN/Si).

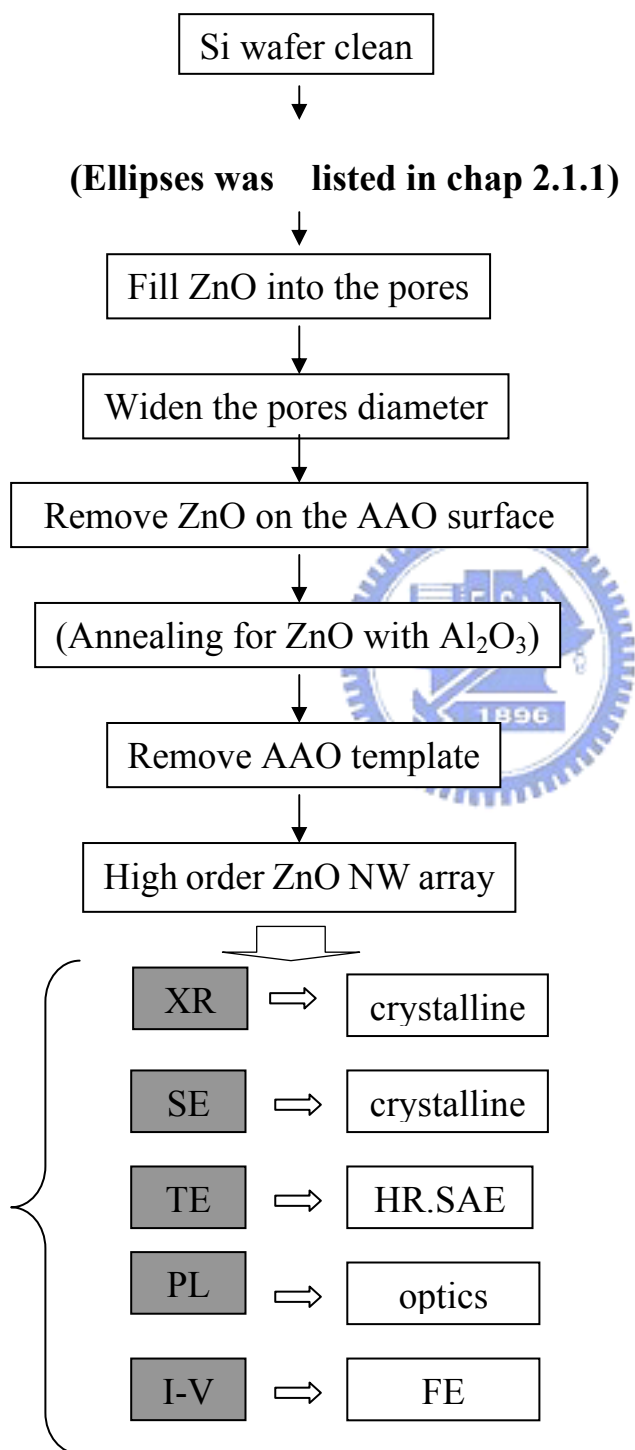
Chap. 2.1.3 Fabrication Procedure of Mask

For the preparation of the AAO mask, an Al sheet of about several mm in thickness was employed and replaced the Al thin film on TiN/Si-sub in the above process. The Al sheet was passed through the same process flow as fabrication procedure of AAO, such as annealing, two step anodic treatment, and widened treatment. The structure of result was AAO on Al sheet, and we must remove the unnecessary Al sheet first. Further, we removed the bottom (barrier layer) of AAO according to chemical etching in H_3PO_4 for removed time. At least, the product was the AAO mask without bottom.



Chap. 2.2 ZnO with AAO

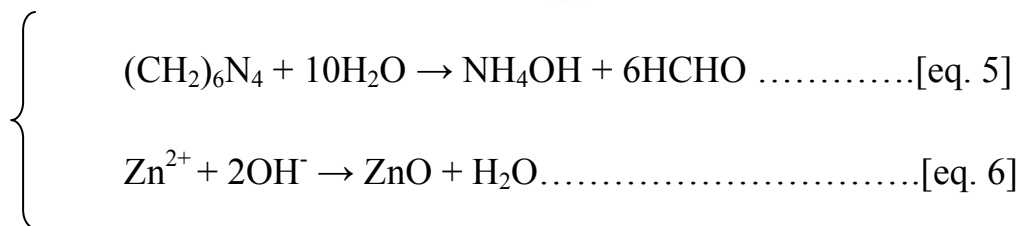
Chap. 2.2.1 Flow Chart for ZnO with AAO Fabrication



Chap. 2.2.2 Fabrication ZnO with AAO

As the references of ch1-2-2, there were some main methods that could synthesis ZnO. Through by considering and testing, we choose the hydrothermal method from others. At present, one of the most serious points to fabrication was the synthesis temperature. The physical limit of material was too high temperature to apply to integration procedures. In other points, we had to consider other factors, including as experiment cost, migration ration of reactant on nano-scale porous, interaction between reactants, experiment environment, restricts of every kinds of machines, etc.

Following list showed the main chemical reactions of ZnO hydrothermal method in aqueous solution:



Above reactions could take place at relatively low temperature of between 75°C and 95°C. By the way, many details of the hydrothermal procedures were studied and reported, such as optimum reaction PH, effect on NW morphology by different concentrations of solutes, etc.

In our experiment, we employ some experiment parameters²⁰ in order to obtain quality ZnO crystalline. The structure (AAO/TiN/Si) was put

Characteristics of 1D ZnO Nanowires Array Grown by AAO Assistance

C-W Chang

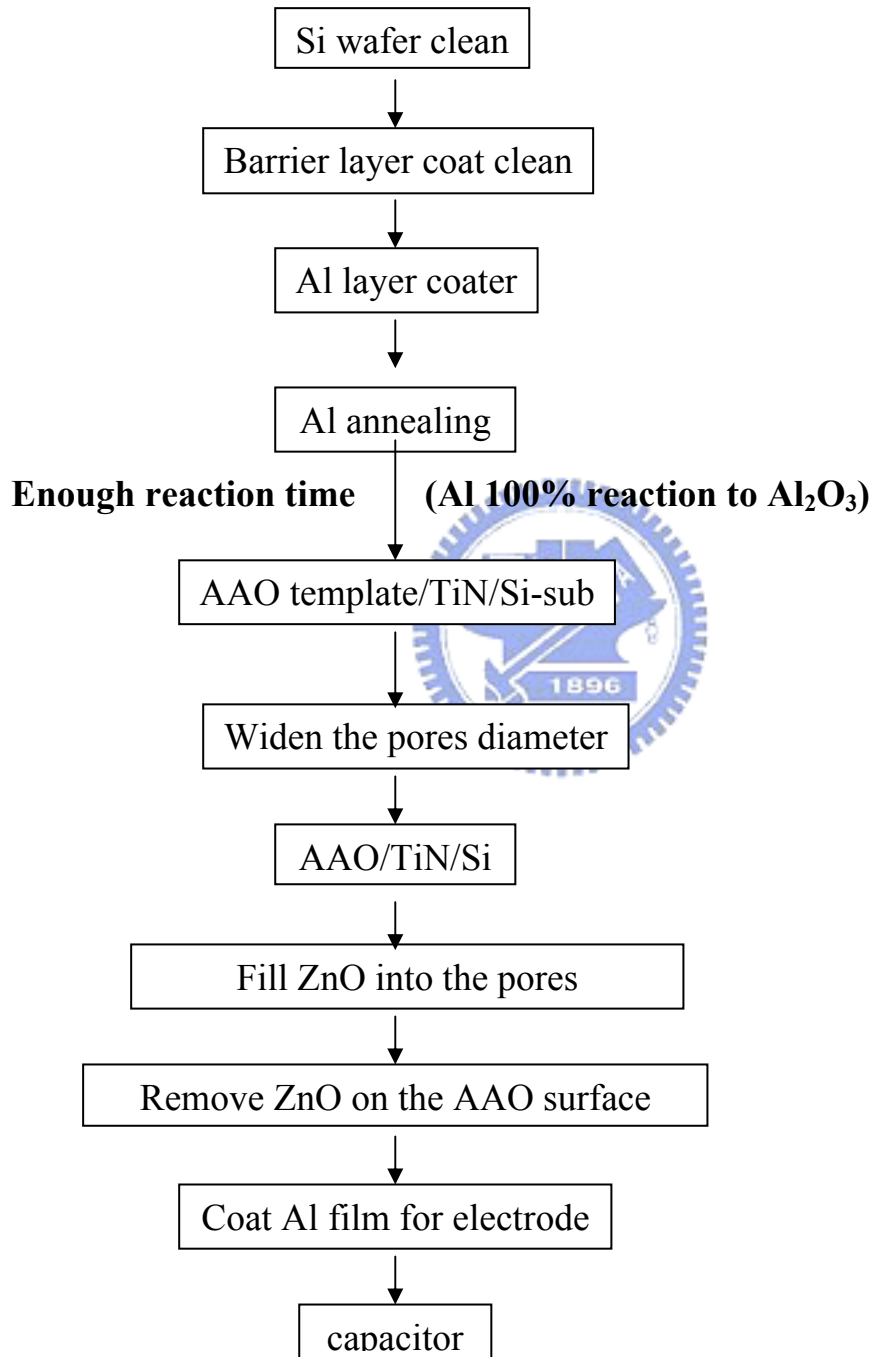
into sealed vessel, which contain an aqueous solution (Milli Q, 18.2MΩcm) of zinc nitrate hexahydrate ($\text{Zn}(\text{NO}_3)_2 \cdot 6\text{H}_2\text{O}$, 0.01M) and diethylenetriamine (HMTA, $\text{C}_6\text{H}_{12}\text{N}_4$, 0.01M) for ZnO NWs hydrothermally grown at $\sim 95^\circ\text{C}$ for 1hr~2.5hrs.

After the hydrothermal procedure, the pores of AAO were full of ZnO. The surface and cross-section morphology was observed by field emission scanning electron microscopy (FE-SEM). It appeared the flower-liked ZnO on the top surface, and we removed the park by chemical etching in HNO_3 solution. Then, we etched the AAO and retained ZnO which were in the AAO pores by different selectivity. It would form a high ordered ZnO array from above processes. Further, we measured and discussed the physical and chemical properties.



Chap. 2.3 Capacitance

Chap. 2.3.1 Flow Chart of Capacitance



Chap. 2.3.2 Fabrication of Capacitance

As the flow chat, we defined the electrodes when the ZnO was full on AAO and removed superfluous ones. We forecasted it could provide a large capacitance. This was a simple capacitance structure in nano-scale and provided large surface area to increase capacitance.

Chap. 2.4 Measurement Equipment

The materials and electricity analysis indicated that the several kinds characteristics of the ZnO NWs. Through these analyses, the crystalline, lattice structure, defects of crystalline, chemical composition, morphology, field emission and capacitance could be understood easily.

Chap. 2.4.1 Physical Analysis

Typically, the XRD (X-ray diffraction) method determines the crystal structure and the information of the lattice arrangements. Generally, the theta two-theta method was employed to analysis the intensities of the diffraction peaks. Through the specific peak was sharp or width, it indicated the grain size and the crystal structure. Then, the Full-Width-Half-Maximum (FWHM) indicated that the crystalline and lattice parameter.

The FE-SEM (field emission scanning electron microscopy) relied on the higher accelerate voltage than thermal SEM which offered good resolution to analyze the geometry. Through the accurate focus ability

from the FE-SEM, the morphology of the nanowires was easily measured and calculated their aspect ration.

The HR-TEM (high resolution transmission electron microscopy) had the well transmission ability that could offer many detail information for the selected area to observe. It could indicate the lattice structure, micro region composition, and high resolution images of surface morphology. The information which observed by the HR-TEM listed as following:

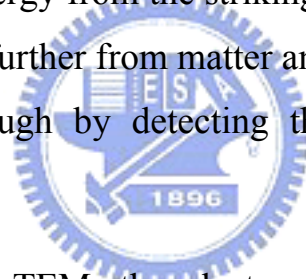
- (a) Bright view images: the images revealed the morphology directly.
- (b) Dark view images: the images indicated fewer defects such as line defect or lattice mismatch which hid in bright view images.
- (c) High resolution lattice images: the clear lattice fringes would indicate the atom arrangement and help to calculate the d-spacing along the c-axis if it was a quality crystalline.
- (d) Selected area electron diffraction (SAED) patterns: the possible d-spacings would be calculated by diffraction rules form SAED patterns. After compare the lattice parameter, the crystalline of ZnO NWs is easily to identify and discuss which process made.

For TEM, the major challenge was the sample preparation, which could prepare by some methods, such as thin sheet sample by FIB (Focus Ion Beam), nanotube or nanowire by supersonic shake methods, etc.

Chap. 2.4.2 Chemical Analysis

The fundamental analyses were used to precisely judge the composition and what kinds of elements of the ZnO NWs.

The XPS (X-ray Photoelectron Spectroscopy) or ESCA (Electron Spectroscopy for Chemical Analysis) were the key tools in surface analyses, mainly because of the two features: Quantitative analysis and Information on the chemical nature and state of the detected elements. By absorbing a photon, an atom gains an energy amount equal to $h\nu$. It released an electron to regain its original stable energy state. The released electron retains all the energy from the striking photon. It can then escape from the atom, and even further from matter and kinetic energy. We could judge the elements through by detecting the energy of the released electrons.



While using the HR-TEM, the electron diffraction spectra (EDS) detected the elements which the ZnO NWs composed. The spectra were very sensitive that help to simply analyze the atomic weight percentage of each element due to the small focus electron beam and high accelerate voltage.

About the photoluminescence (PL) spectrum, the mechanism was discussed at ch1-2-3. Through by detecting the energy of the released electrons, we could infer the defects of crystalline.

The morphology of the ZnO nanowires was analyzed by field emission scanning electron microscopy (FE-SEM, Hitachi S-4700I, Japan) and high resolution transmission electron microscopy (HRTEM, Philips

tecani-20). The chemical composition of the ZnO nanowires was characterized by Auger electron microprobe (AES, VG Scientific Microlab 350, UK).

Chap. 2.4.3 Field Emission Detector

A Keithley 237 source-measure unit was used for measuring the current–voltage ($I - V$) and field emission characteristics. Field emission measurements were carried out in a vacuum chamber with a pressure of 5×10^{-6} Torr at room temperature. The measurement equipment was illustrated in FIG-2.4-1.

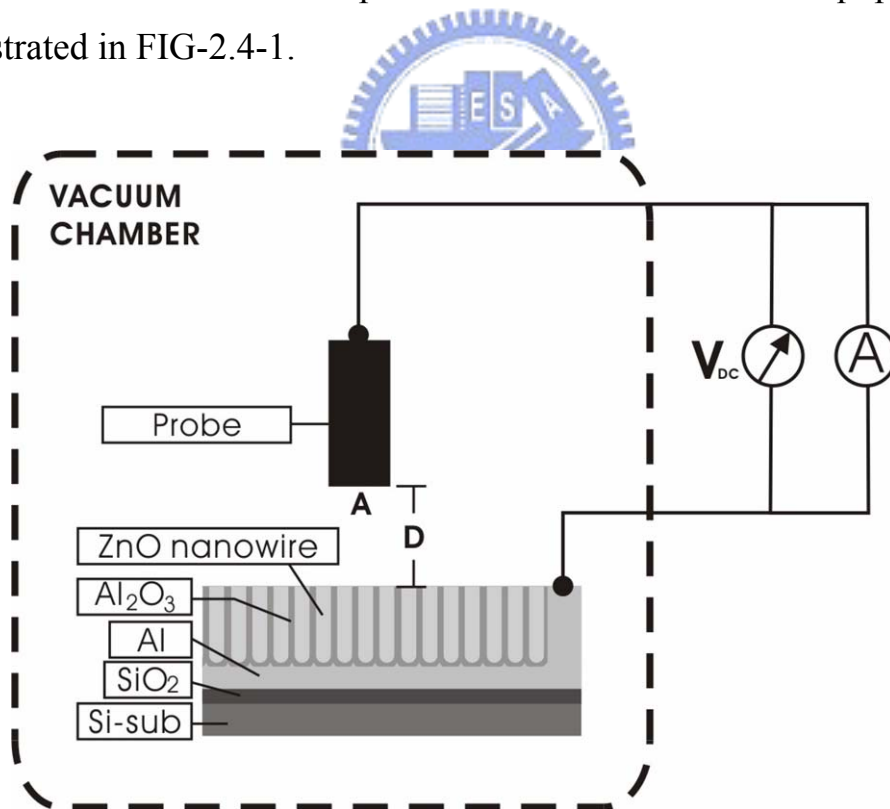


Fig. 2.4-1: It illustrates the field emission measurement system.

Chapter 3 Results and Discussion

Chap. 3.1 AAO and Mask

Chap. 3.1.1 AAO

As introduction of AAO at Chap. 1.3, we should take notices on some factors in order to prepare a standard which conformed to our requirements. Those key points were classed as and the process details of anodization.

First, the factors of aluminous intrinsic quality were purity and crystallization enough or not. The purity was depended on the Al sheet or ingot for evaporation. For Al sheet, we employed the high purity as well as we can. However, it was still not good enough to form AAO due to problems about crystalline of Al. We should enhance the crystalline quality by annealing. The factors in annealing aspect were such as atmosphere, length of time, temperature. As lots of reports, we knew intuitively that higher temperature, under inert gas atmosphere, and longer time would improve batter crystalline quality. Exactly, the re-crystallization of Al caused of the suitable annealing. We considered the melting point of Al, environment friendliness, and process integration, so we employed suitable parameters including annealing temperature: 300~500°C, time: 2-8hrs, in Ar atmosphere.

Second, we focused on the parameters of anodic process including different kinds of electrolyte, reaction temperature, applied polarization voltage, reaction time, widening time, removed time, supersonic shake time, and concentration about above every kinds of chemical solutions. As

previous studies, we employed suitable parameters, list as following: Al sheet or Al/TiN/Si-sub, applied voltage: 30, 40, 50V, space of electros: 7 units, anodic reaction T: 12°C. The reaction time and widening time were depended on geometry scale we required; for example, we observed the porous length of 1μm by total reaction time of 6 min in our two-step anodization and the diameter of 80nm by widening time of 40 mins in our recipes. However, AAO was fabricated by improved recipes. For example, the supersonic shake procedure removed the fracture on the AAO surface; if conventional two-step anodization replaced by multiple-step anodization, we avoided supersonic shake procedure and obtained satisfied products.

Following would show some images of measurement and discuss with those data.

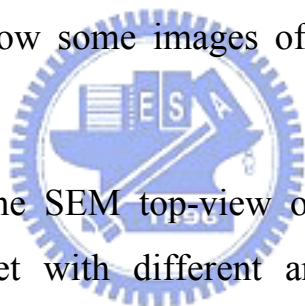


Fig. 3.1-1 depicts the SEM top-view of AAO array morphology formed by 4Nⁱ Al sheet with different annealing temperature. We observed the porous array along a direction in all images and the different phenomenon by the same widening recipe. It appears the intrinsic quality of Al is the major cause, and we suggest the distance is formed by the machine stretch. It can be solved by chemical polish or machine polish.

Fig. 3.1-2 shows the relation of widened time and AAO morphology. We can confirm that the widening time with porous diameter in proportion.

ⁱ 4N means concentration of 99.99%, and 5N means 99.999%, 5N5 means 99.9995%, to reason by analogy.

Characteristics of 1D ZnO Nanowires Array Grown by AAO Assistance

C-W Chang

The over widening time was applied; the AAO became brush-liked AAO (Fig. 3.1-3) which was composed by fracture pores on the AAO surface. The structure has been studied³⁴.

Fig. 3.1-4 and Fig. 3.1-5 reveal AAO structures fabricated by multiple step anodization. We observed the more fracture pores on the AAO surface by more step anodization. We observed further the ideal AAO pores array under the fracture pores film in Fig. 3.1-5(a), (c). Fig. 3.1-6 reveals the result of AAO array after supersonic shake procedure. The result equaled to AAO after widening and supersonic shake procedure. We obtained the satisfied AAO array, and the MASK based on the structure.

Fig. 3.1-7 indicates the AAO structures fabricated with the same parameters expect electrolytes. (a) was fabricated by 0.3M oxalic and (b) was fabricated by 0.1M H₃PO₄, and both without widening treatment. We demonstrate the porous diameter depends on the kind of electrolytes.

Characteristics of 1D ZnO Nanowires Array Grown by AAO Assistance

C-W Chang

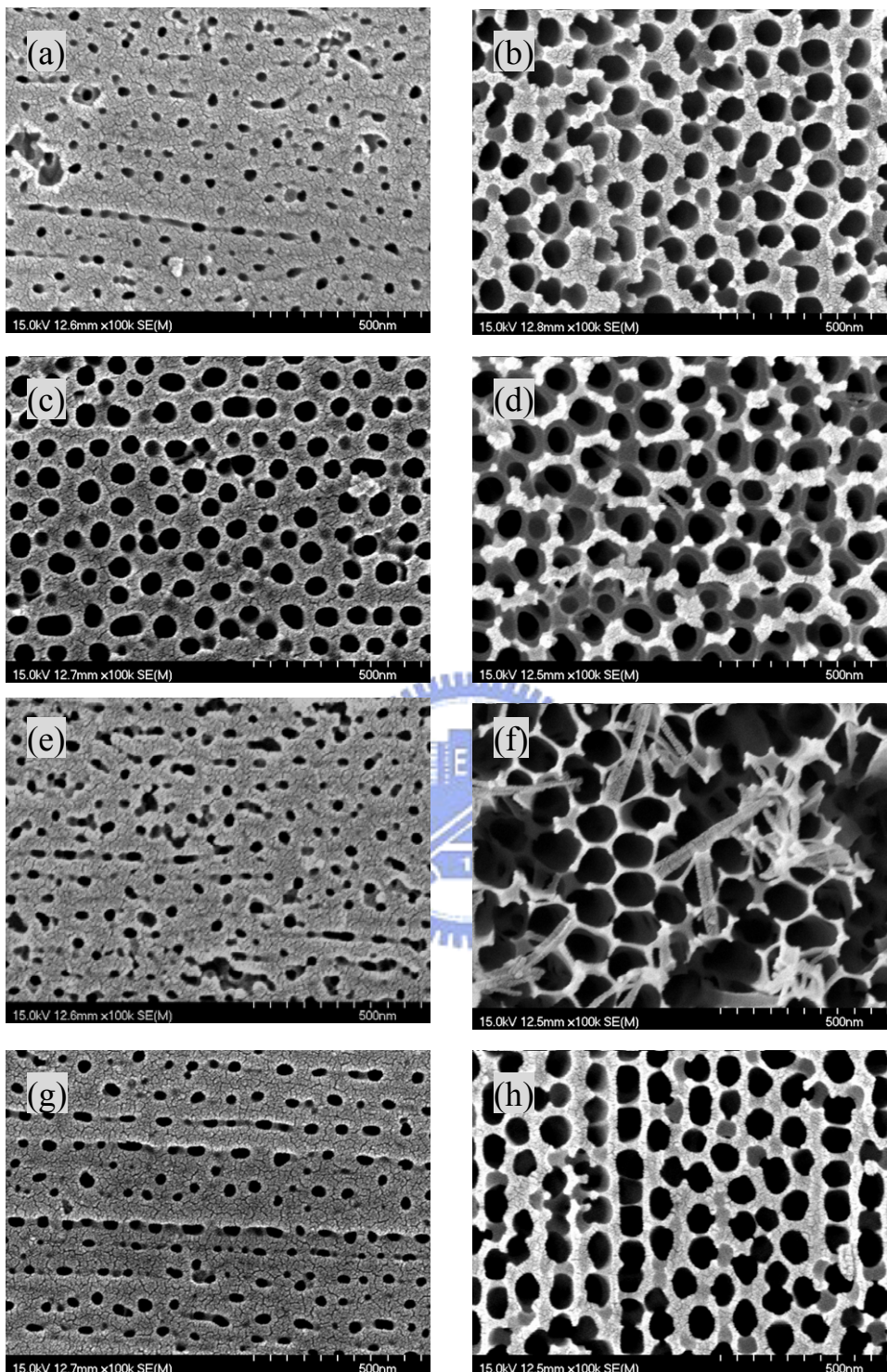


Fig. 3.1-1: 4N Al sheet annealed at (a) 300(c)350(e)400(g)500°C x 2hrs, it then was fabricated AAO by two-step anodic. The images of right side were after widening treatment (60mins), left ones were without. (4N Al sheet; applied voltage 50V; space of electros: 7; anodic reaction T: 12°C)

Characteristics of 1D ZnO Nanowires Array Grown by AAO Assistance

C-W Chang

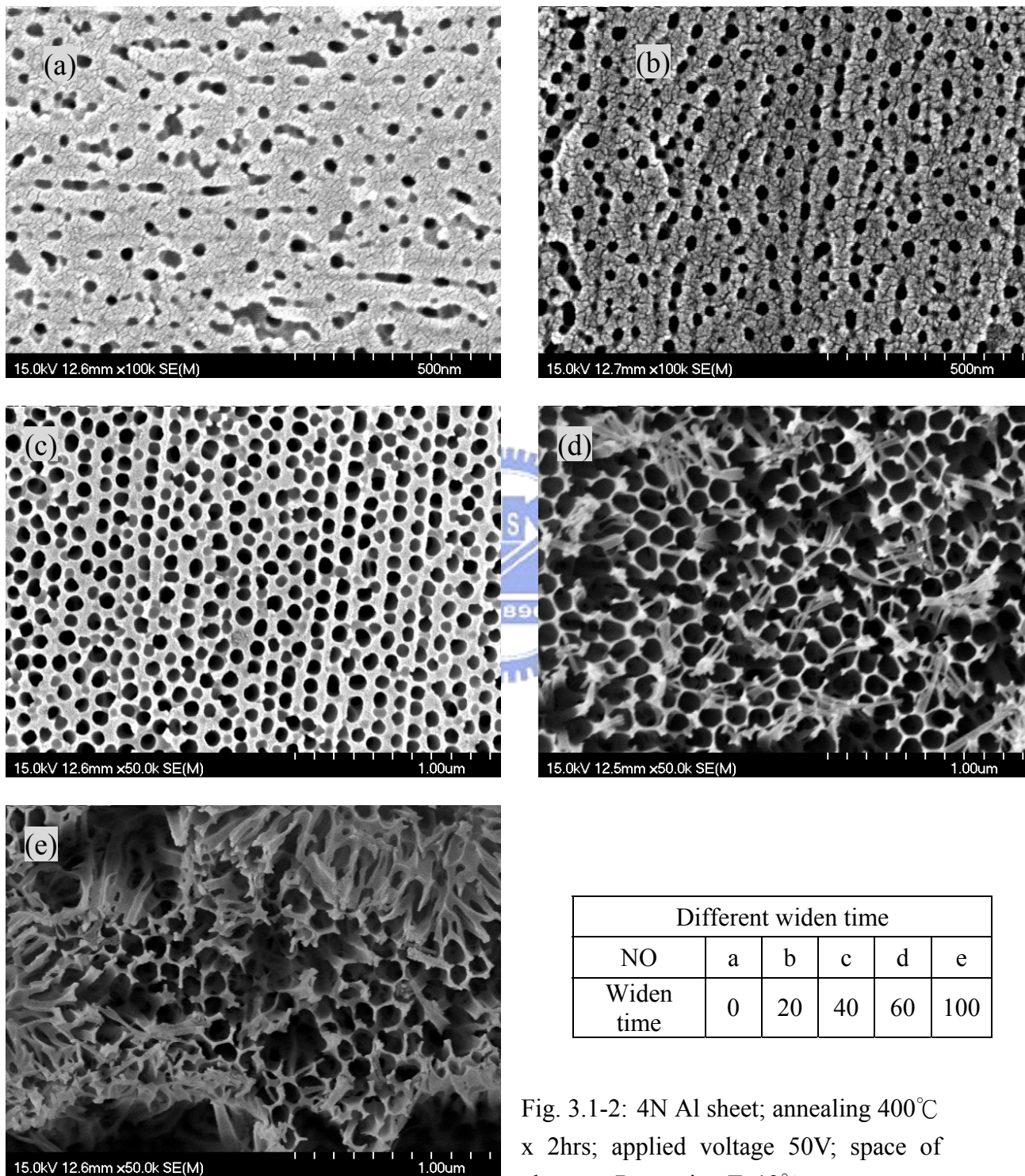


Fig. 3.1-2: 4N Al sheet; annealing 400°C x 2hrs; applied voltage 50V; space of electros: 7; reaction T: 12°C

Characteristics of 1D ZnO Nanowires Array Grown by AAO Assistance

C-W Chang

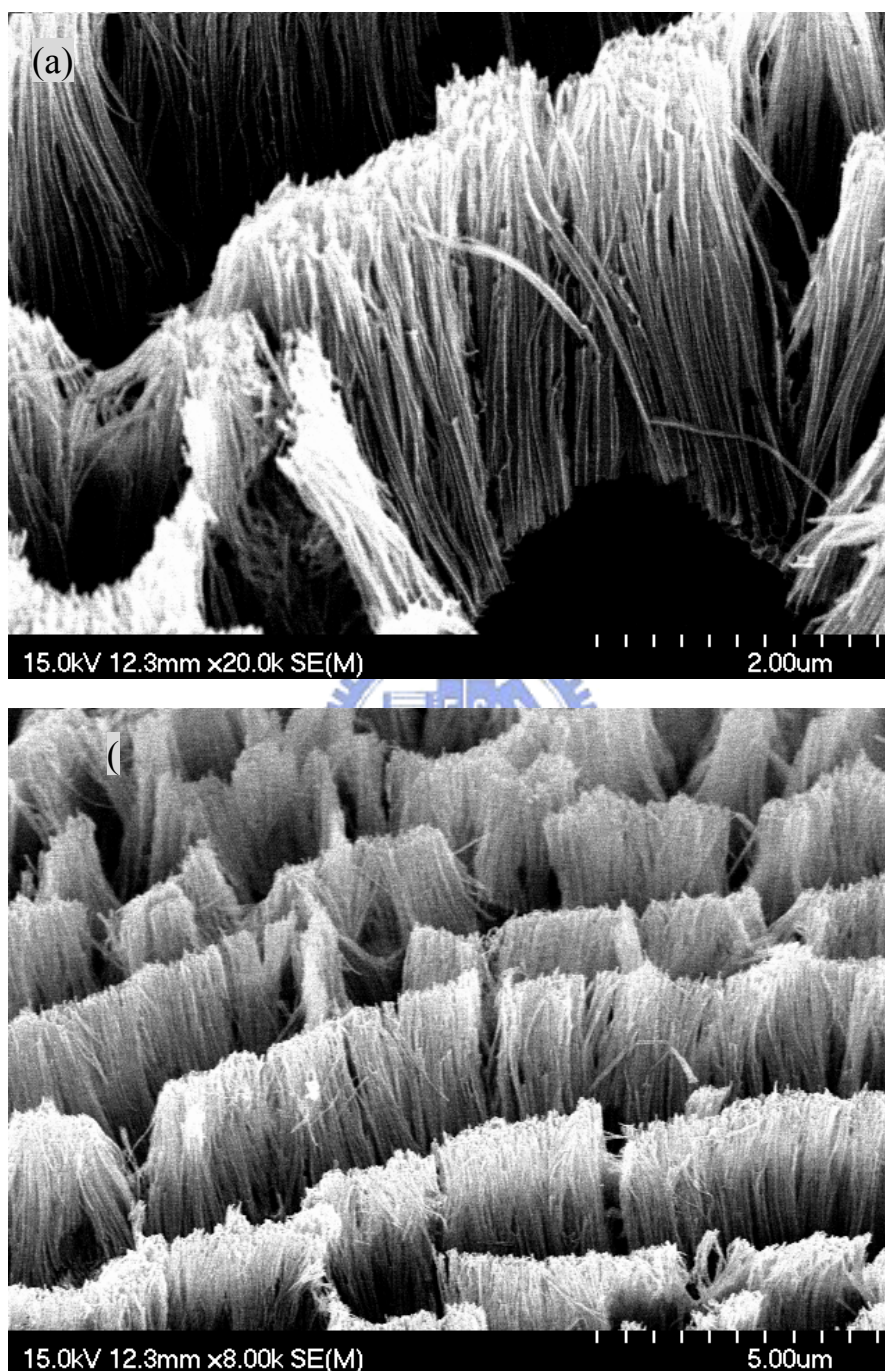


Fig. 3.1-3: The brush-like AAO was fabricated by over widening (widened time 100mins).

Characteristics of 1D ZnO Nanowires Array Grown by AAO Assistance

C-W Chang

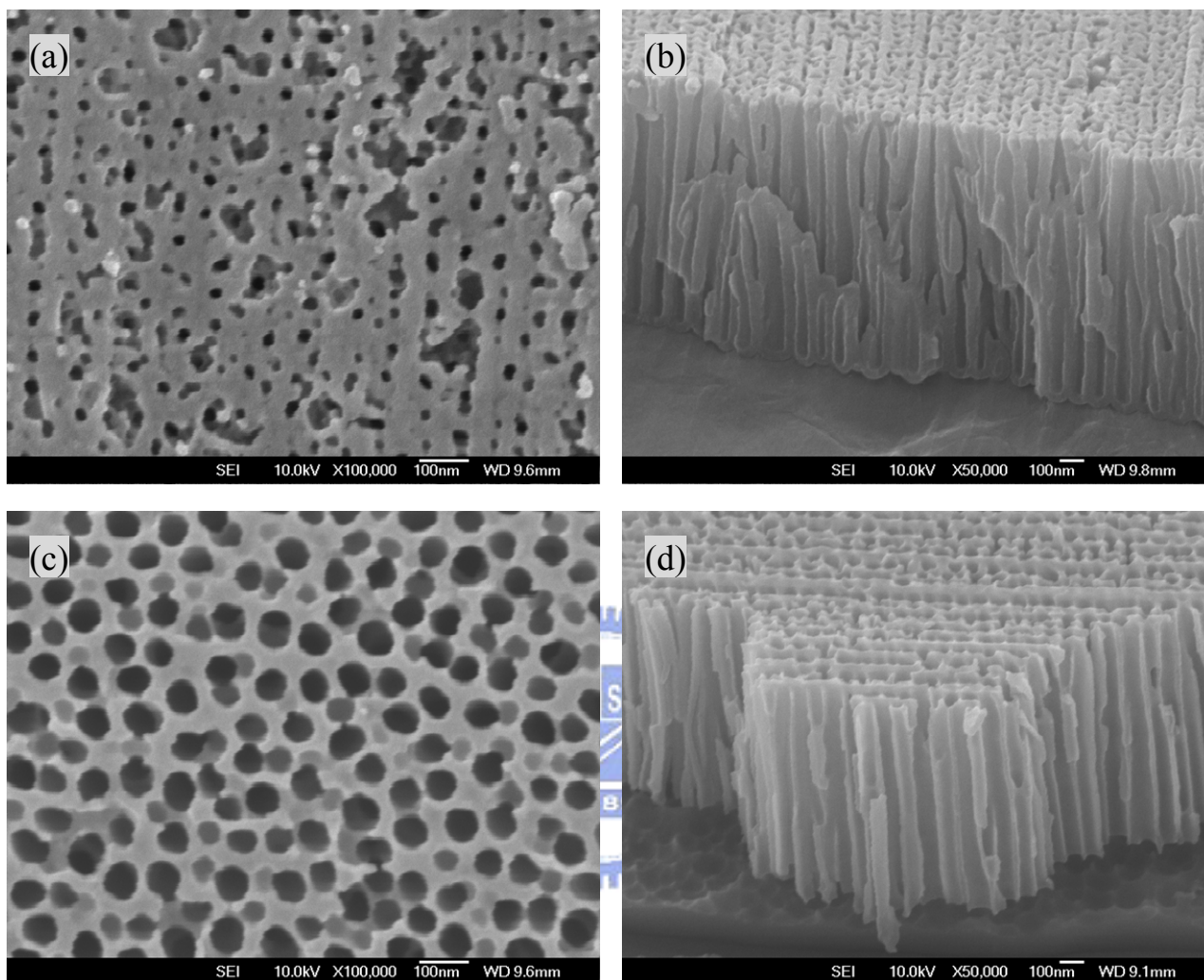


Fig. 3.1-4: They were fabricated by conventional two-step anodization. (a) SEM image only by first step anodize (6, 1), (b) Cross section view. (c) SEM image by two-step anodize (6, 1, 3, 1), (d) Cross section view. (4N Al sheet; annealing 400°C x 8hrs; applied voltage 40V; space of electros: 7; reaction T: 28°C)

Characteristics of 1D ZnO Nanowires Array Grown by AAO Assistance

C-W Chang

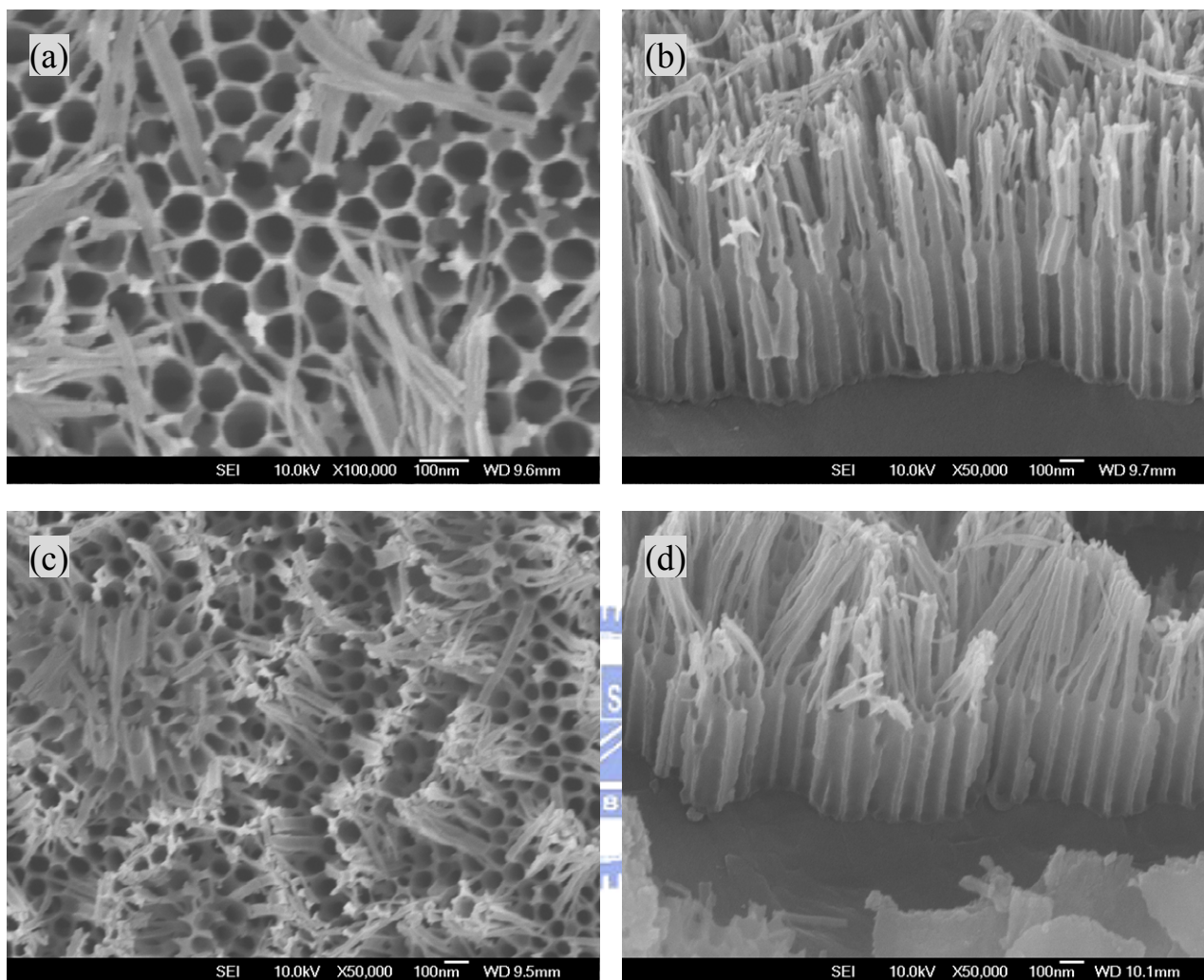


Fig. 3.1-5: They were fabricated by multiple step anodization which was more steps than two-step anodize. (a) SEM image by three step anodize (6, 1, 3, 1, 3, 1), (b) Cross section view. (c) SEM image by four step anodize (6, 1, 3, 1, 3, 1, 3, 1), (d) Cross section view. (4N Al sheet; annealing 400°C x 8hrs; applied voltage 40V; space of electros: 7; reaction T: 28°C)

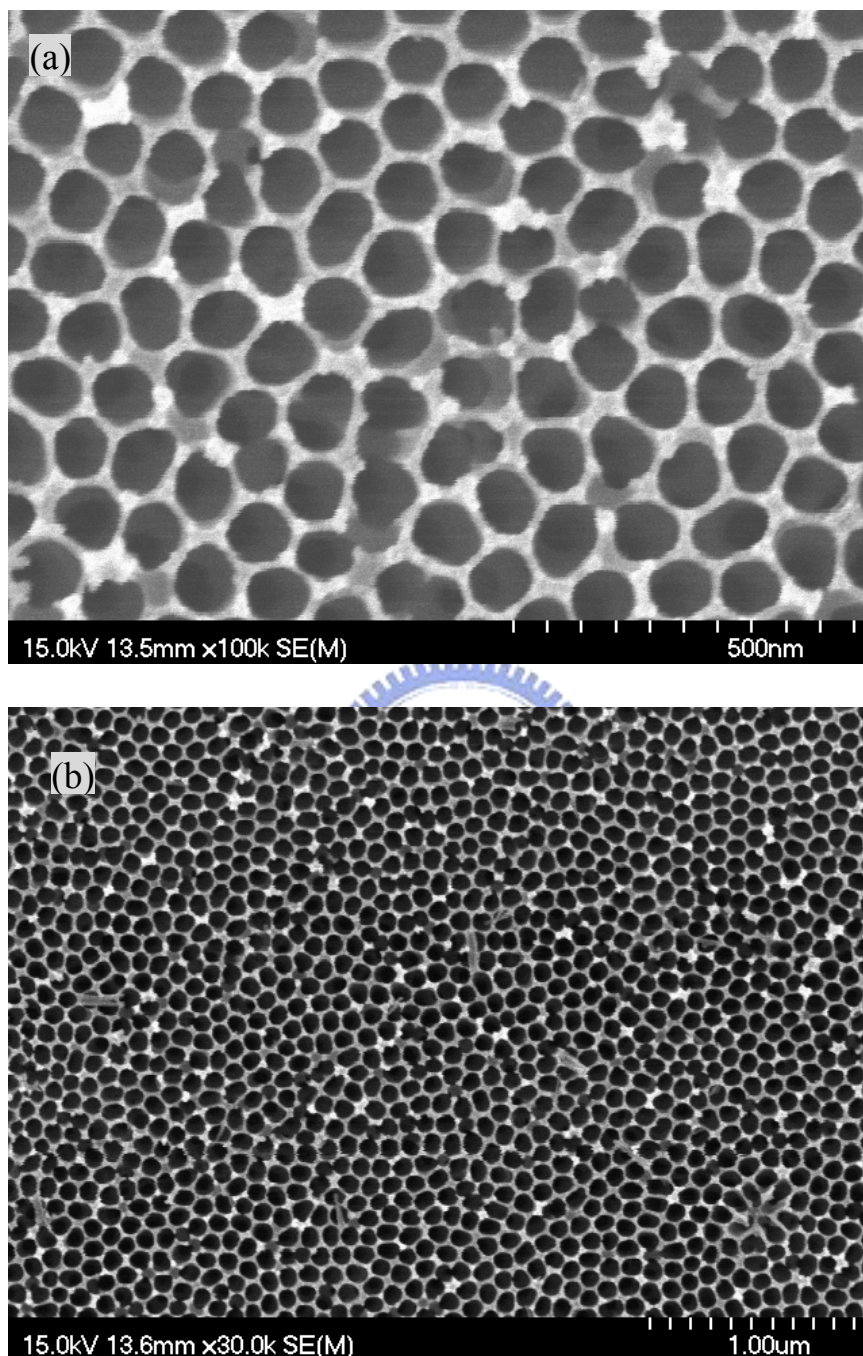


Fig. 3.1-6: It was cleaned the residuum on the surface by supersonic shock after multiple step anodize. (a) High magnification (100K) SEM image and (b) low magnification (50K) SEM image revealed the uniform pore array. (4N Al sheet; annealing 400°C x 8hrs; applied voltage 40V; space of electros: 7; reaction T: 28°C)

Characteristics of 1D ZnO Nanowires Array Grown by AAO Assistance

C-W Chang

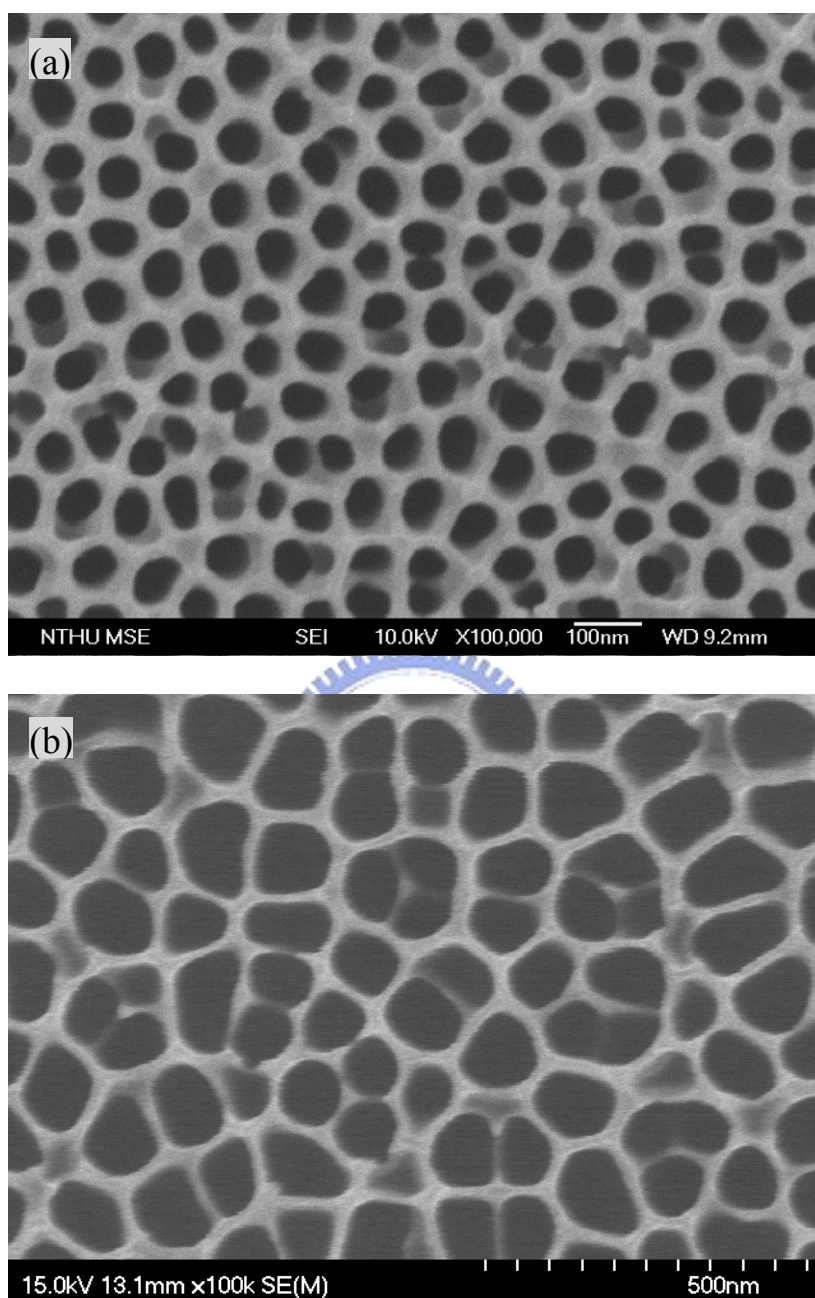


Fig. 3.1-7: They were fabricated with the same parameters except electrolytes. SEM images of the same magnification (100K), (a) was fabricated by 0.3M oxalic and (b) was fabricated by 0.1M H_3PO_4 . (4N Al sheet; annealing 400°C x 2hrs; applied voltage 40V; space of electros: 7; reaction T: 28°C)

Chap. 3.1.2 Mask

Based on the AAO structure, we obtained the MASK by removed the barrier (bottom) layer. The key point was on the recipe of removing bottom and widening.

Fig. 3.1-8 shows the SEM images of MASK, including top-view, back-view, and cross-section view. When removing time was increased, we observed that the thickness of bottom was thinner and the porous wall was thinner simultaneously.

Large area (more than 1cm^2) mask would be fabricated by the suitable time combinations with widening and different removing bottom time (Fig. 3.1-9 (c)). Otherwise, we observed partial porous bottom were removed and partial ones were remained (Fig. 3.1-9 (a), (b)), although the (a) and (b) carried out by more reaction time than (a). Based on the isotropic chemical etching, it seems be controlled by the reaction ratio due to contact surface. And the uniformity of the top surface is a problem, it maybe roughness caused of fringe-liked residues of AAO.

Characteristics of 1D ZnO Nanowires Array Grown by AAO Assistance

C-W Chang

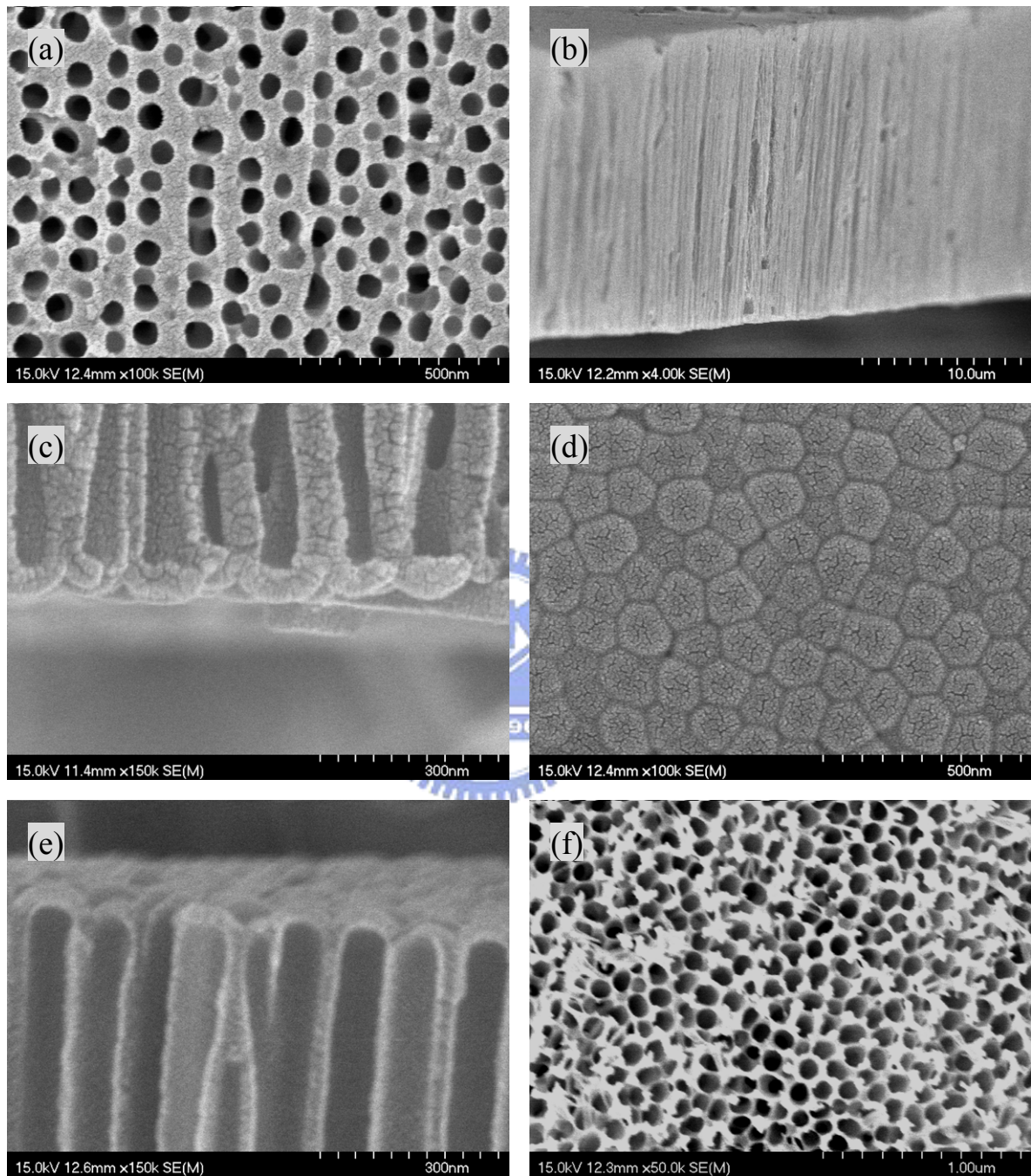


Fig. 3.1-8: AAO template (mask) was fabricated by removing bottom layer after removed superfluous Al film with AAO. (a) as-prepared AAO top view of SEM image. (b) The cross section of AAO after removed superfluous Al film. (c) the cross section view of bottom under widening time of 30 mins, (d) the back view of bottom. (e) another one after widening time of 60 mins, (f) the top view.

Characteristics of 1D ZnO Nanowires Array Grown by AAO Assistance

C-W Chang

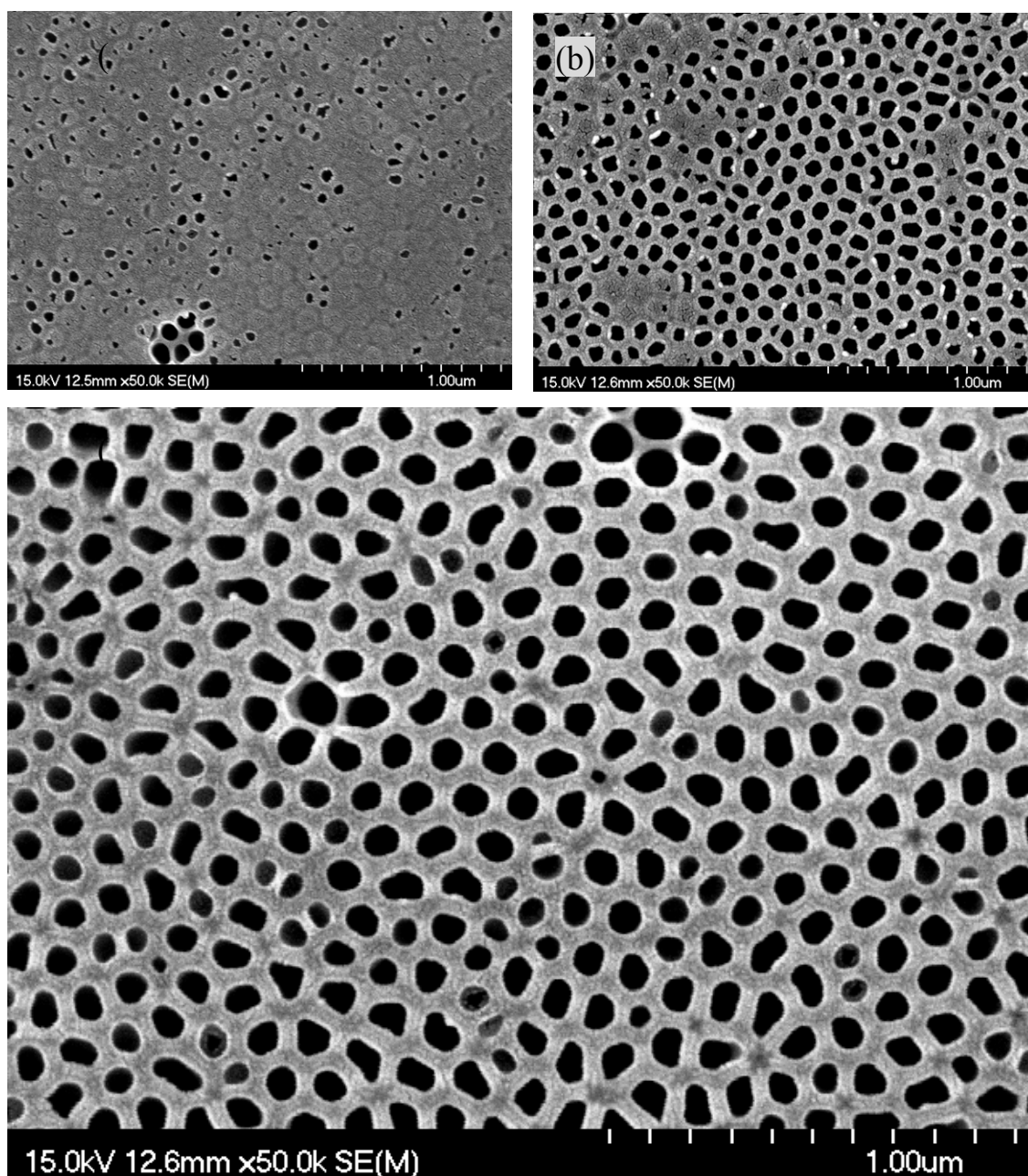


Fig. 3.1-9: SEM images about back view of AAO with different reaction time combinations which were different widening and different removing bottom time. (a) total time 100 (70+30) mins, (b) 80 (40+40) mins, (c) 60 (0+60)mins. (widening time, removing time)

Chap. 3.2 ZnO with AAO

Based on the recipe of fabrication AAO on Al sheet, we fabricated on Al/TiN/Si-sub in order to integrate into VLS and increase the applications. Following, the section lists results and discussions including SEM, PL, XRD, TEM, FE measurements.

Chap. 3.2.1 SEM Analysis

Fig. 3.2-1 shows the relation of widened time and AAO morphology. We can confirm that the widening time with porous diameter in proportion according to fabricated once on Al sheet. So we control the widening time to achieve the required aspect ration. However, because of the Al film formed by 4N Al ingot, we observed residues on the surface and effect on porous direction. We suggest the residues formed by impurities precipitated after annealing treatment.

Fig. 3.2-2 reveals the top view of AAO and many residues remain on surface because of the quality Al film was no good enough. And (c) is the high magnification (150K) image indicates porous diameter was about 60-85nm, thickness of porous well was about 50 nm and thickness of bottom was about 50 nm. The thickness of porous well equaled to thickness of bottom. The details of structure was AAO/Al/TiN/Si-sub, the Al film was the remainder which was not reaction to AAO. The bottom layer still exists, and it will be a obstacle for application of field emission.

Fig. 3.2-3 reveals the bottom layer becomes thinner after over reaction treatment. Relatively, the pores become fracture. We suggest that Si and Ti would tend to form silicide after 400°C annealing, maybe the Al and Ti formed alloy, too. So, we observed a layer existed under the AAO after over suitable second anodic time.

Fig. 3.2-4 reveals clearly the cross-section view of pores full of ZnO successfully, (a): AAO was fabricated by conventional two-step anodization (3, 12) and widened in 60 mins. Diameter of pores was about 80nm, (b): It was removed the ZnO residues on AAO surface after pores full of ZnO by hydrothermal method. Then we removed the AAO by chemical etching in HNO₃ solution. It is showed at Fig. 3.2-5 (a) is the top view of SEM image reveals island-liked ZnO NWs crowd. (b) is the image of cross section view indicates the collapse of ZnO NWs clearly. We observed some broke NWs which stood on the TiN layer vertically, and the other ones which were intact structure were merge together.

Fig. 3.2-6 reveals SEM images of that AAO was fabricated by conventional two-step anodization. The special treatment was supersonic shake to remove residues on surface after widening. We observed the better structure than Fig. 3.2-2, but the porous length was shorter as a result to sacrifice a little AAO film when the supersonic shake treatment.

As the Fig. 3.2-7, it reveals the different surface morphology of Al film which was evaporated by 4N and 5N Al ingot respectively. We observed lots of impurities on the AAO surface formed by 4N Al source, and another was clean and uniform. Further, the high purity of Al film would provide higher uniform, ordered, vertical pores for applications.

If the reaction temperature of hydrothermal method is too low, we observed those ions could not successfully migrate into pores. Fig. 3.2-8 indicates clearly that the ZnO crystallized at top of pores when the reaction temperature was 80°C. The causes maybe include the morphology of AAO and the geometry of pores except the reaction temperature; we suggest the reaction temperature is the principal cause.

Fig. 3.2-9 and Fig. 3.2-10 reveal the morphology of AAO formed by 5N Al film. At

Fig. 3.2-9, (a), (b), (c) reveal different applied voltage to anodize according to 30V, 40V, 50V. (d), (e), and (f) reveal different widening time from the sample of (c), and the widening time was 10 mins, 20 mins, 40 mins, respectively. We can understand that the applied voltage only

Characteristics of 1D ZnO Nanowires Array Grown by AAO Assistance

C-W Chang

dominate the growth ration of AAO and do not affect the scale of porous diameter.

Fig. 3.2-11 reveals the image which the sample after field emission measurement. (a) is the original structure, diameter: 20-30nm, length: 1800nm. And (b), (c), (d) reveal the broken area after field emission measurement.



Characteristics of 1D ZnO Nanowires Array Grown by AAO Assistance

C-W Chang

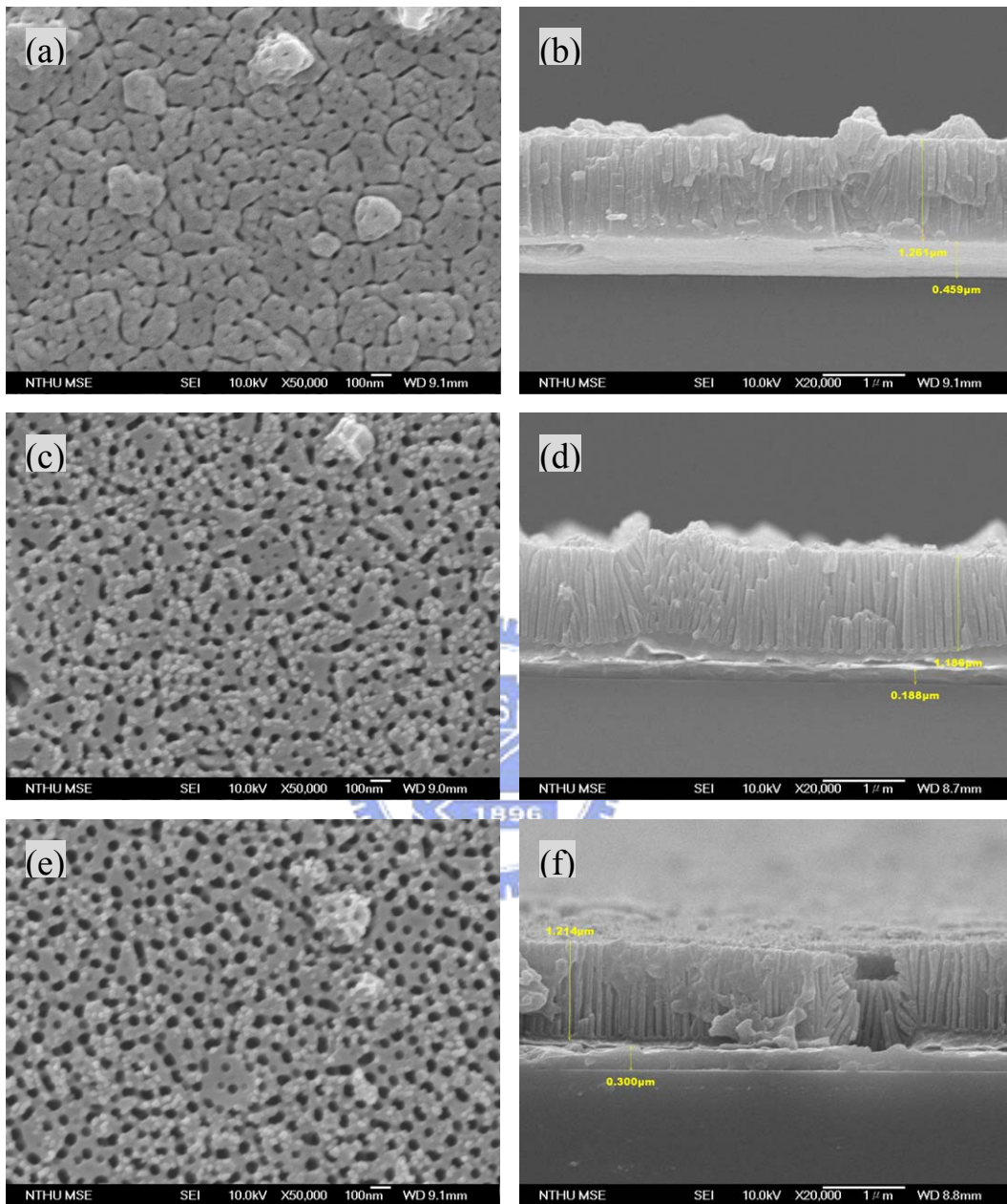


Fig. 3.2-1: These AAO were fabricated by two-step anodization (3, 3) on SiO_2/Si -sub. (a), (b) were AAO SEM images without widening treatment, porous of diameter was small then 10nm. (c) (d) were widened in 20 mins, porous of diameter was about 30nm. And (d) (e) were widened in 30 mins, porous of diameter was about 50nm. Thickness of AAO was about 1.2 μm . (4N Al / SiO_2/Si ; thickness of Al: 1 μm ; annealing 350 $^\circ\text{C}$ x 8hrs; applied voltage: 40V; electrolyte: 0.3M oxalic; space of electros: 7; reaction T: 12 $^\circ\text{C}$)

Characteristics of 1D ZnO Nanowires Array Grown by AAO Assistance

C-W Chang

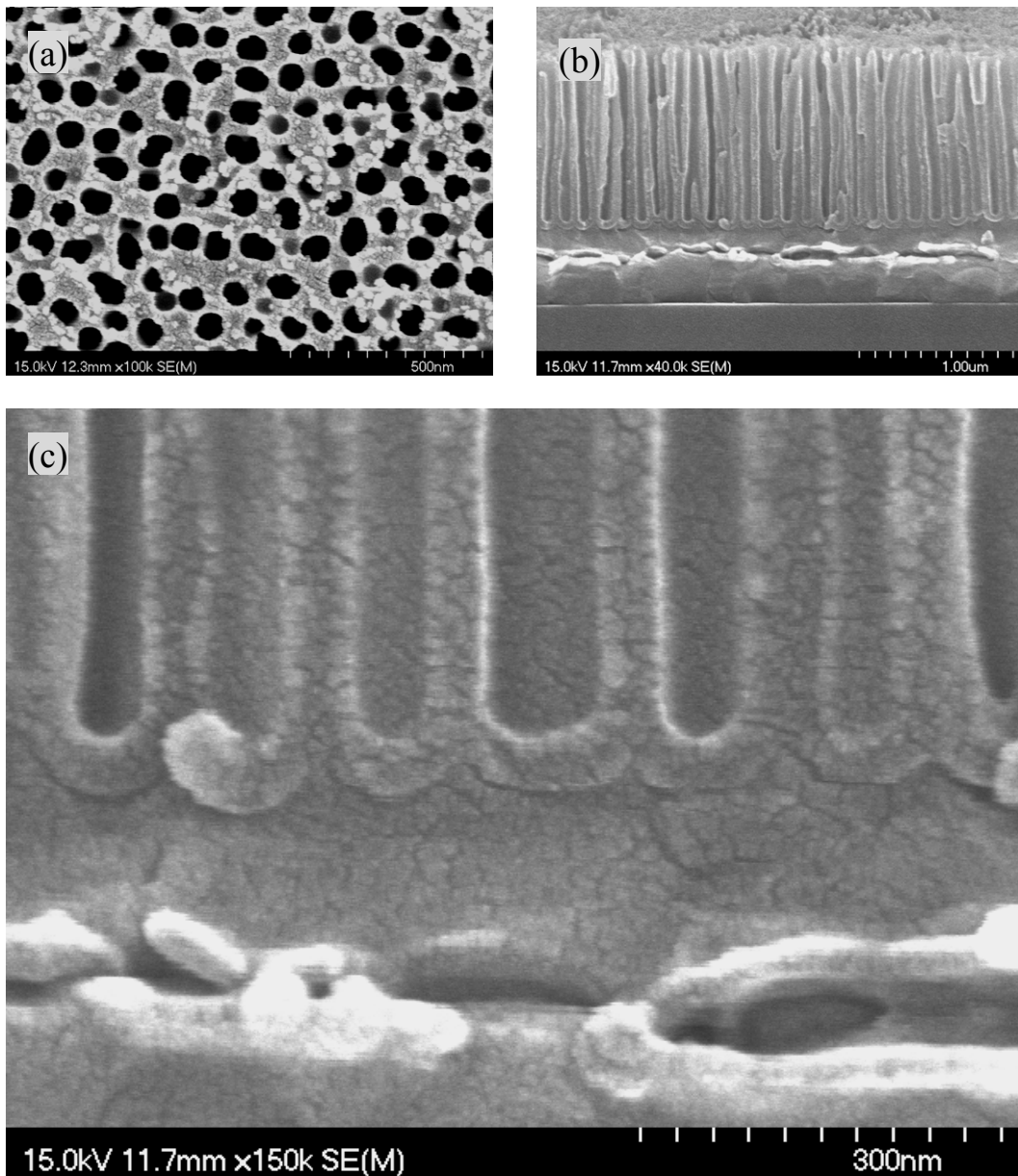


Fig. 3.2-2: AAO was fabricated by conventional two-step anodization (3, 3) and widening time was 40mins. (a) It revealed the top view of AAO and many residues on surface. (b) cross section view image revealed the AAO thickness was about 1.2μ . (c) The high magnification (150K) image indicated porous diameter was about 60-85nm, thickness of porous well was about 50 nm and thickness of bottom was about 50 nm. The thickness of porous well equaled to thickness of bottom. (4N Al/SiO₂/Si; thickness of Al: 1μm; annealing 350°C x 8hrs; applied voltage: 40V; electrolyte: 0.3M oxalic; space of electros: 7; reaction T: 12°C)

Characteristics of 1D ZnO Nanowires Array Grown by AAO Assistance

C-W Chang

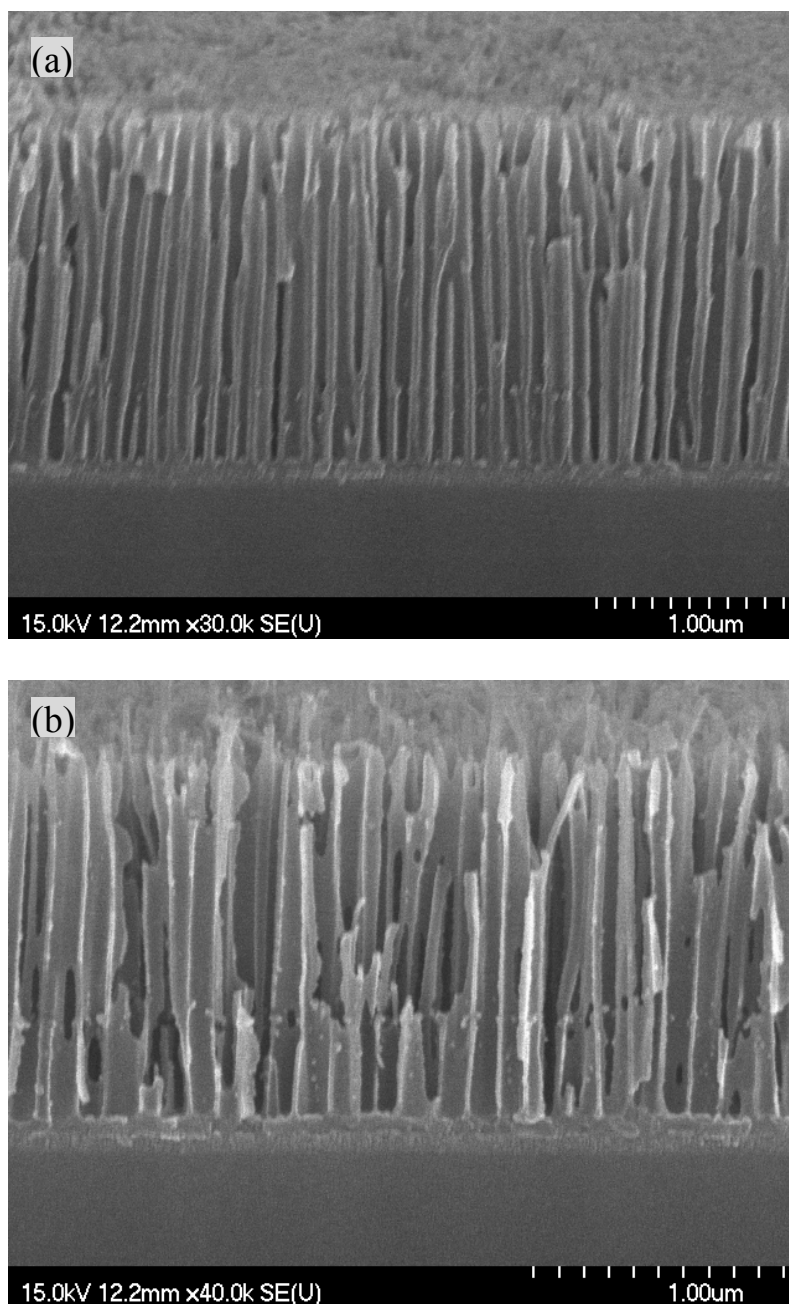


Fig. 3.2-3: AAO was fabricated by conventional two-step anodization (3, 12). They were anodized over suitable time (about 3min) at second anodic treatment. (a) it was widened in 50 mins. (b) it was widened in 80 mins, we observed over winding induced porous wall to break and thickness of bottom to thinner. (4N Al /TiN/Si; thickness of Al: 1 μ m; annealing 400 $^{\circ}$ C x 8hrs; applied voltage: 40V; electrolyte: 0.3M oxalic; space of electros: 7; reaction T: 12 $^{\circ}$ C)

Characteristics of 1D ZnO Nanowires Array Grown by AAO Assistance

C-W Chang

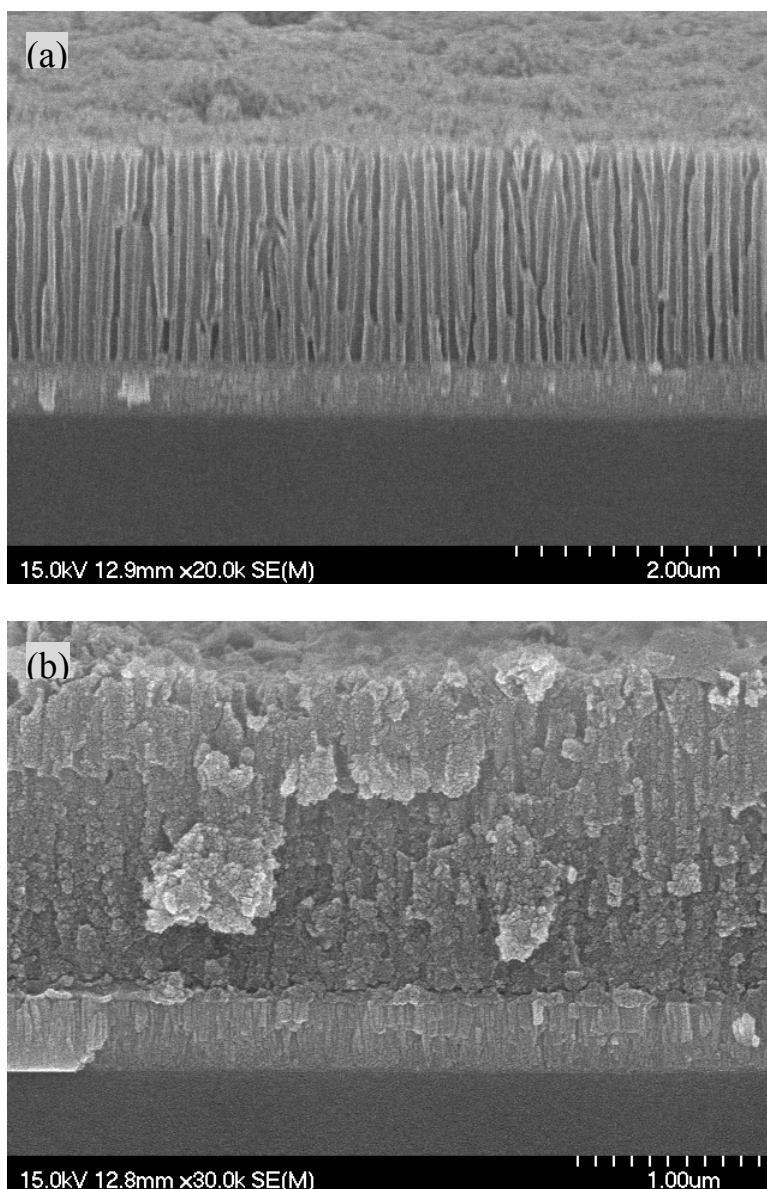


Fig. 3.2-4: (a) AAO was fabricated by conventional two-step anodization (3, 12) and widened in 60 mins. Diameter of pores was about 80nm. (b) It was removed the ZnO residues on AAO surface after pores full of ZnO by hydrothermal method. The SEM image revealed the pores full of ZnO successfully. (4N Al /TiN/Si; thickness of Al: 1.3 μ m; annealing 400 $^{\circ}$ C x 2hrs; applied voltage: 40V; electrolyte: 0.3M oxalic; space of electros: 7; reaction T: 12 $^{\circ}$ C; ZnO hydrothermal in 2hrs at 96 $^{\circ}$ C)

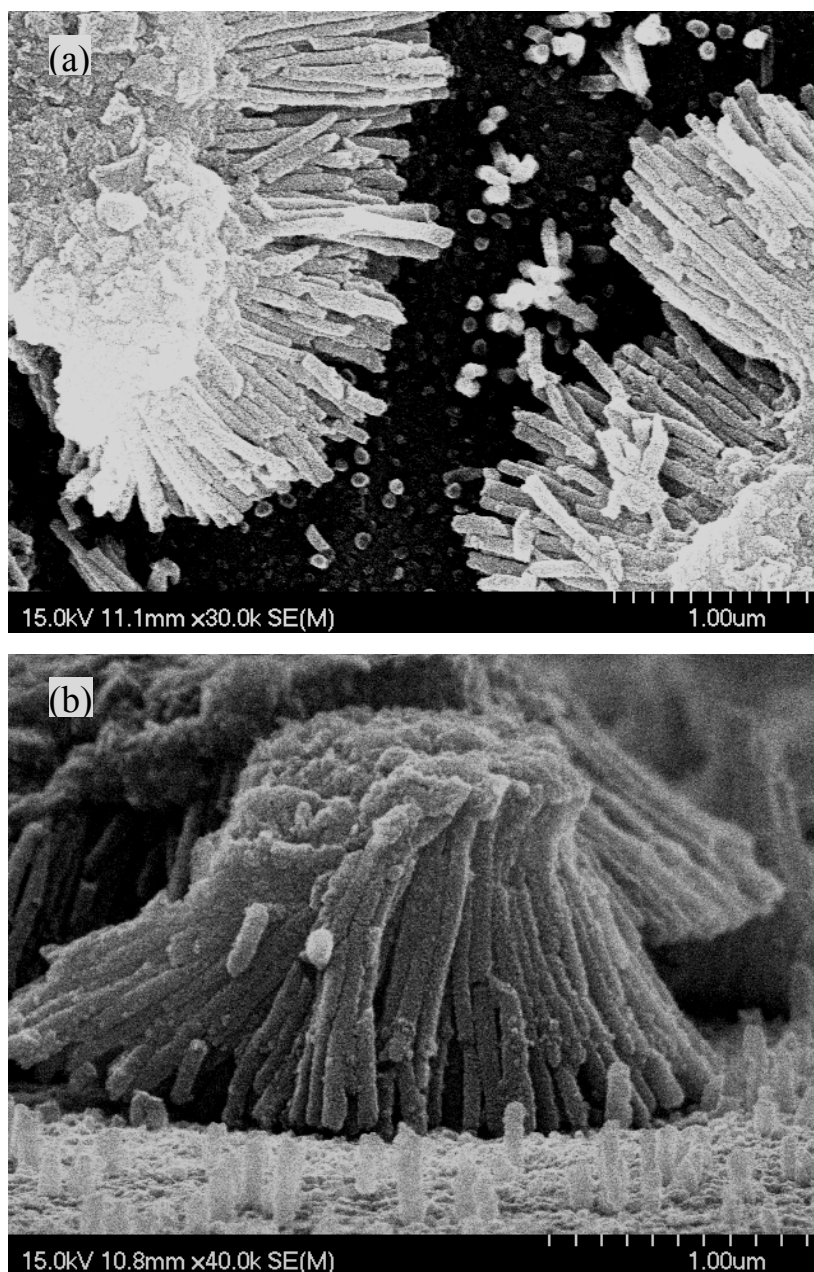


Fig. 3.2-5: The AAO full of ZnO was removed AAO in order to form the exposed ZnO NWs. (a). the top view of SEM image revealed island-liked ZnO NWs crowd. (b). the image of cross section view indicated the collapse of ZnO NWs clearly. (4N Al /TiN/Si; thickness of Al: 1.3 μ m; annealing 400 $^{\circ}$ C x 2hrs; applied voltage: 40V; electrolyte: 0.3M oxalic; space of electros: 7; reaction T: 12 $^{\circ}$ C ; ZnO hydrothermal in 2hrs at 95 $^{\circ}$ C)

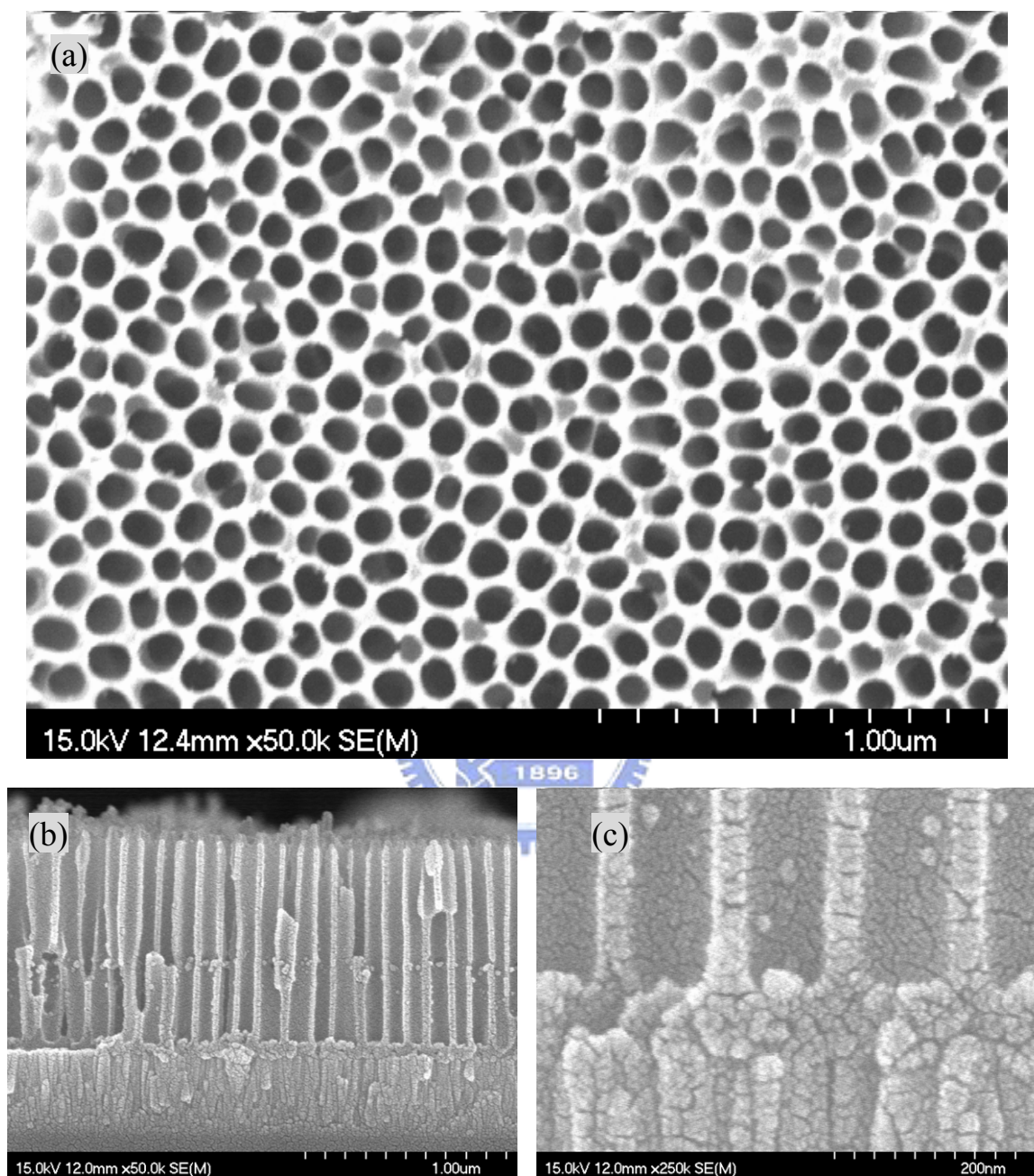


Fig. 3.2-6: AAO was fabricated by conventional two-step anodization. The special treatment was supersonic shake to remove residues on surface after widening. (a) Top view. (b) Cross-section view and (c) was high magnification (250K) image of the bottom area. (4N Al /TiN/Si; thickness of Al: 1 μ m; annealing 400 $^{\circ}$ C x 8hrs; applied voltage: 40V; electrolyte: 0.3M oxalic; space of electros: 7; reaction T: 12 $^{\circ}$ C)

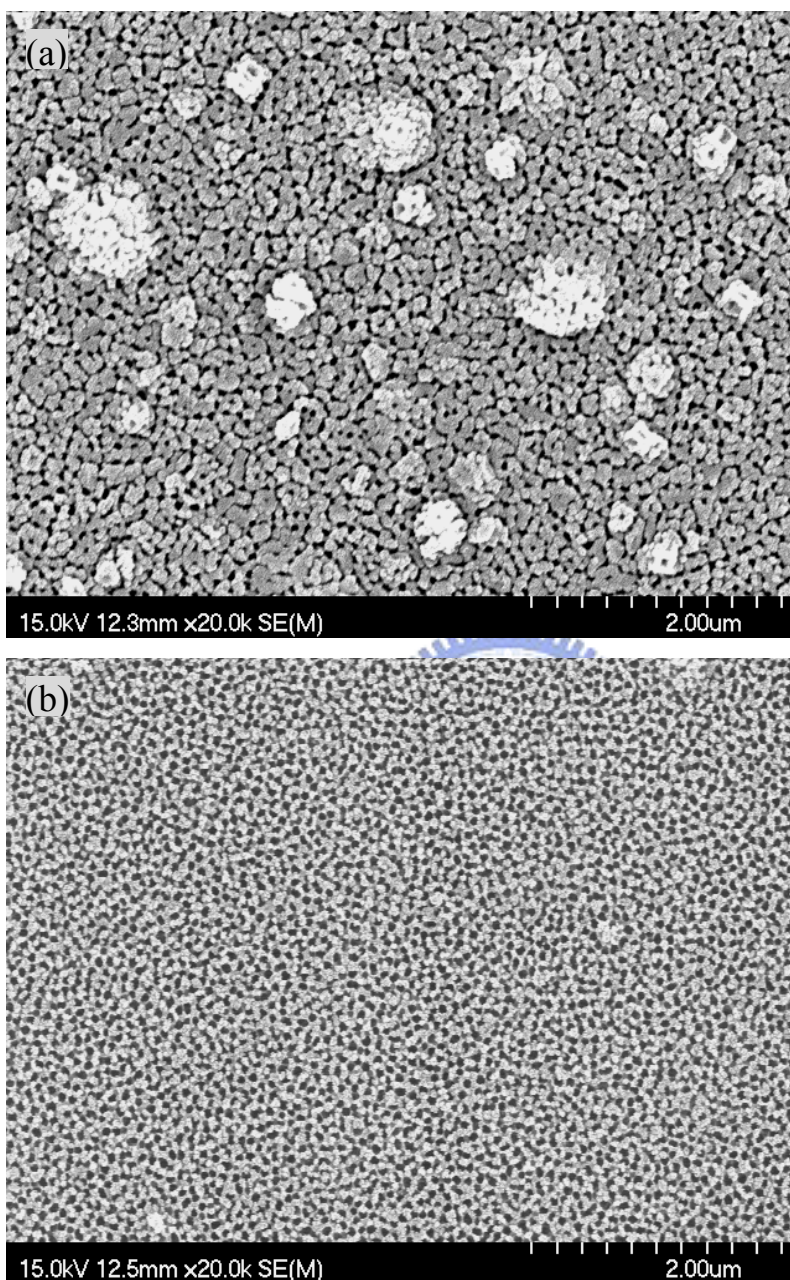


Fig. 3.2-7: AAO was fabricated by two-step anodization. The top-view SEM images were the same magnification, (a) employed 5N Al source and (b) employed 4N Al source. We could clearly observe the improvement of reduced impurities on the surface due to high concentration of Al film.

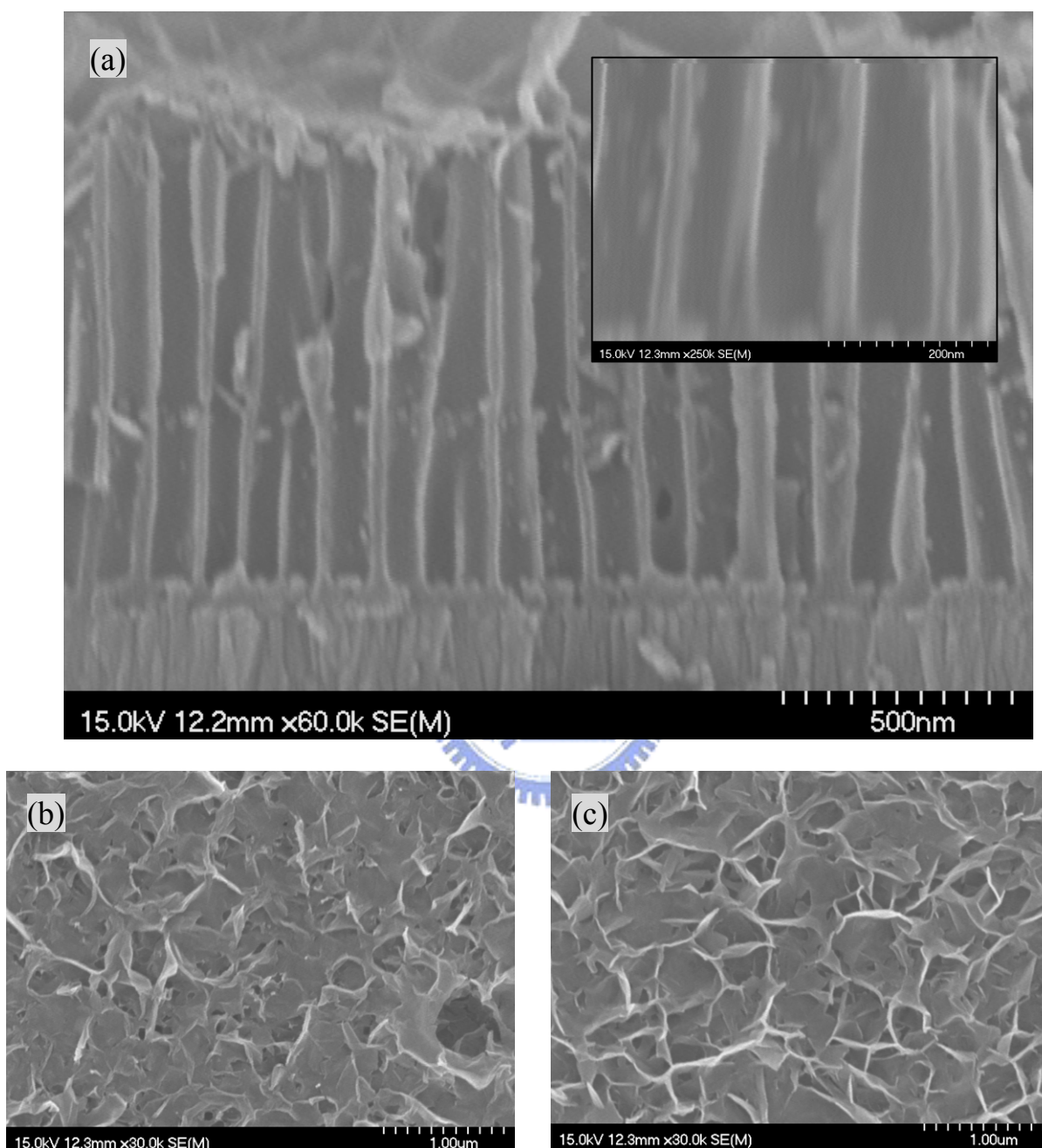


Fig. 3.2-8: SEM images of cross section(a),top view(b)(c) Temperature not high enough to assist ZnO migrated into pores, so we observed the ZnO covered the surface and would not full into the porous.(b) 30 mins at 80°C ,(c) 1hr at 80°C . The inset in (a) was the high magnification SEM image.

Characteristics of 1D ZnO Nanowires Array Grown by AAO Assistance

C-W Chang

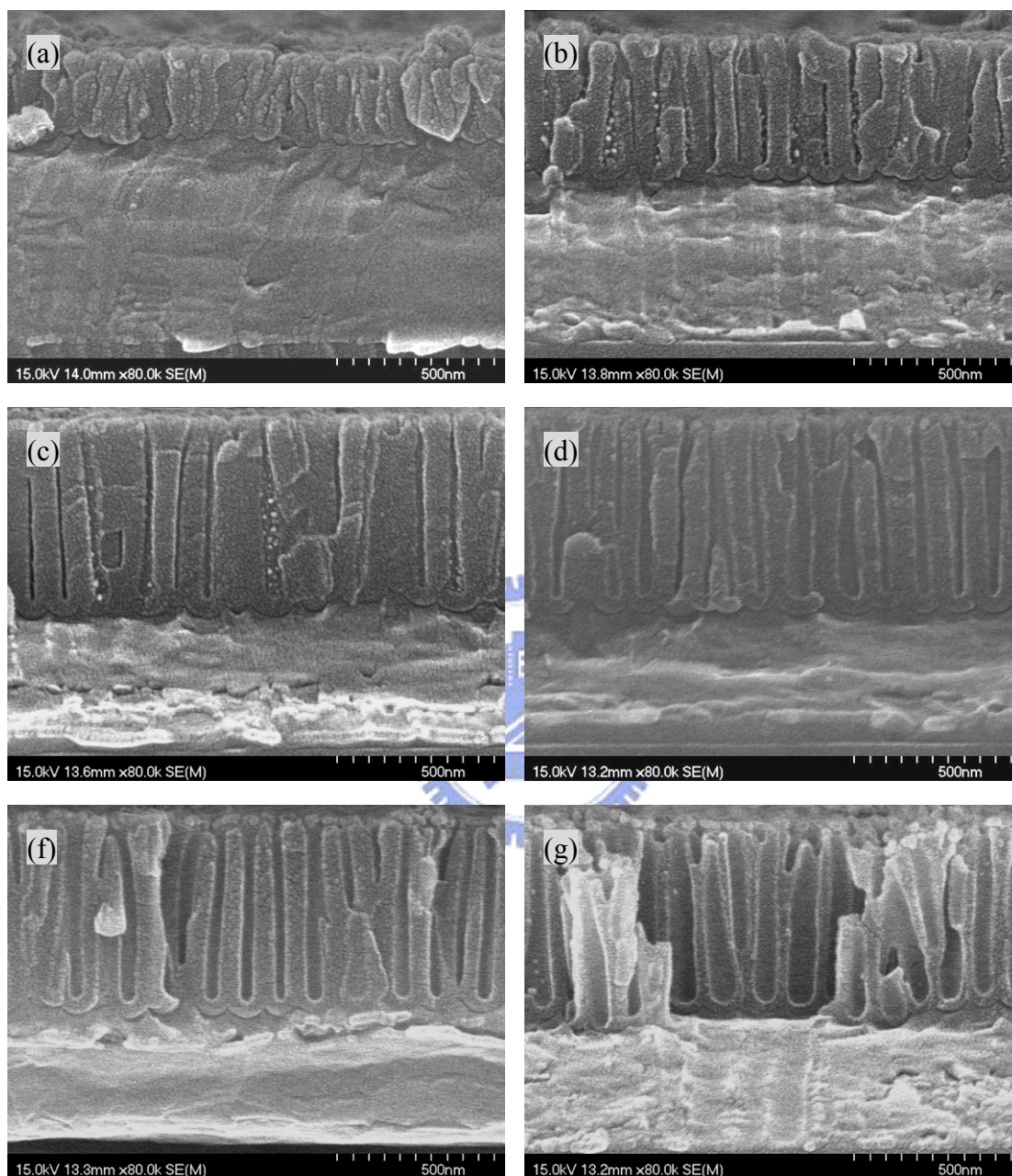


Fig. 3.2-9: SEM images of cross-section view (a)(b)(c) were different applied voltage to anodize according to 30V, 40V, 50V. (d), (e), and (f) were revealed different widening time form the sample of (c), and the widening time was 10 mins, 20 mins, 40 mins, respectively. (5N Al /TiN/Si; thickness of Al: 850nm; annealing 400°C x 2hrs; electrolyte: 0.3M oxalic; space of electros: 7; reaction T: 12°C).

Characteristics of 1D ZnO Nanowires Array Grown by AAO Assistance

C-W Chang

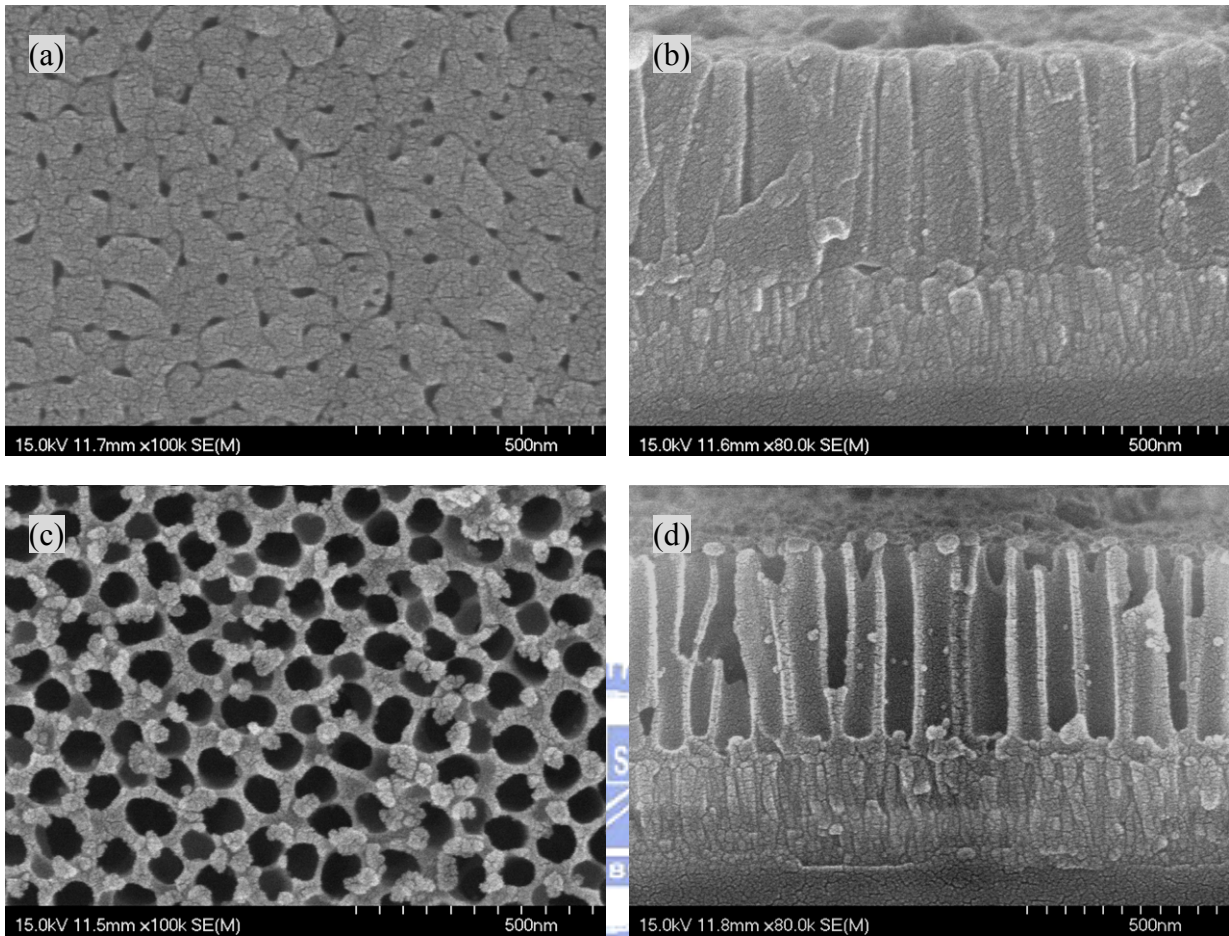


Fig. 3.2-10: (a), (c) are the SEM images of top view, and (b), (d) are SEM images of cross-section view. (a), (b) are fabricated by convectional two-step anodization.(1, 3.5) (c), (d) are widened in 60 mins, the diameter become about 80 nm from 10 nm. (5N Al /TiN/Si; thickness of Al: 500nm; annealing 400°C x 2hrs; applied voltage: 50V; electrolyte: 0.3M oxalic; space of electros: 7; reaction T: 12°C)

Characteristics of 1D ZnO Nanowires Array Grown by AAO Assistance

C-W Chang

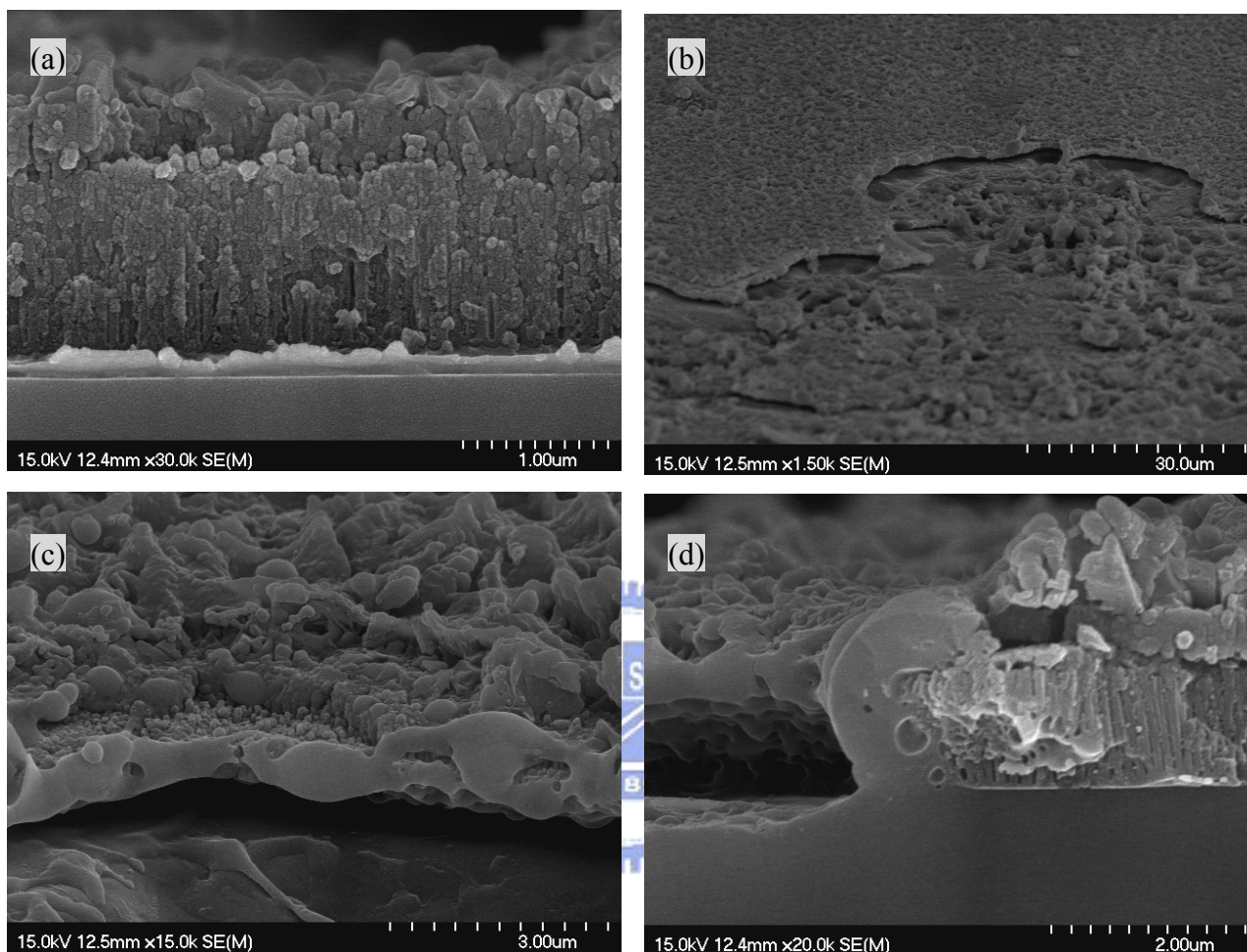


Fig. 3.2-11: They are SEM images of cross-section view, (a) is the original structure, diameter: 20-30nm, length: 1800nm. And (b), (c), (d) reveal the broken area after field emission measurement. (5N Al/TiN/Si; thickness of Al: 1500nm; annealing 400°C x 2hrs; applied voltage: 50V; electrolyte: 0.3M oxalic; space of electros: 7; reaction T: 12°C; widening time 20)

Chap. 3.2.2 TEM Analysis

About the analysis of TEM, we show data at following. Moreover, we prepared the sample for TEM by FIB (focus ion beam) and supersonic shake method.

Fig. 3.2-12 reveals the high resolution image about the cross-section view of AAO full of ZnO. Fig. 3.2-13 reveals: (a) the TEM image of ZnO NW by supersonic shake treatment; (b) the SAED of ZnO NW. (c) the EDS of ZnO NW.

We observe the SAED pattern which seems the type of crystallization mixes with amorphous and poly. We suggest the crystalline of ZnO maybe a poly type, and the amorphous signal from AAO according to the Al_2O_3 of AAO is amorphous type. The result is expectable due to the structure of ZnO NW, prepared by supersonic shake treatment, was a ZnO wire covered with a Al_2O_3 film, the EDS shows the concentration of Zn is lower.

TEM images

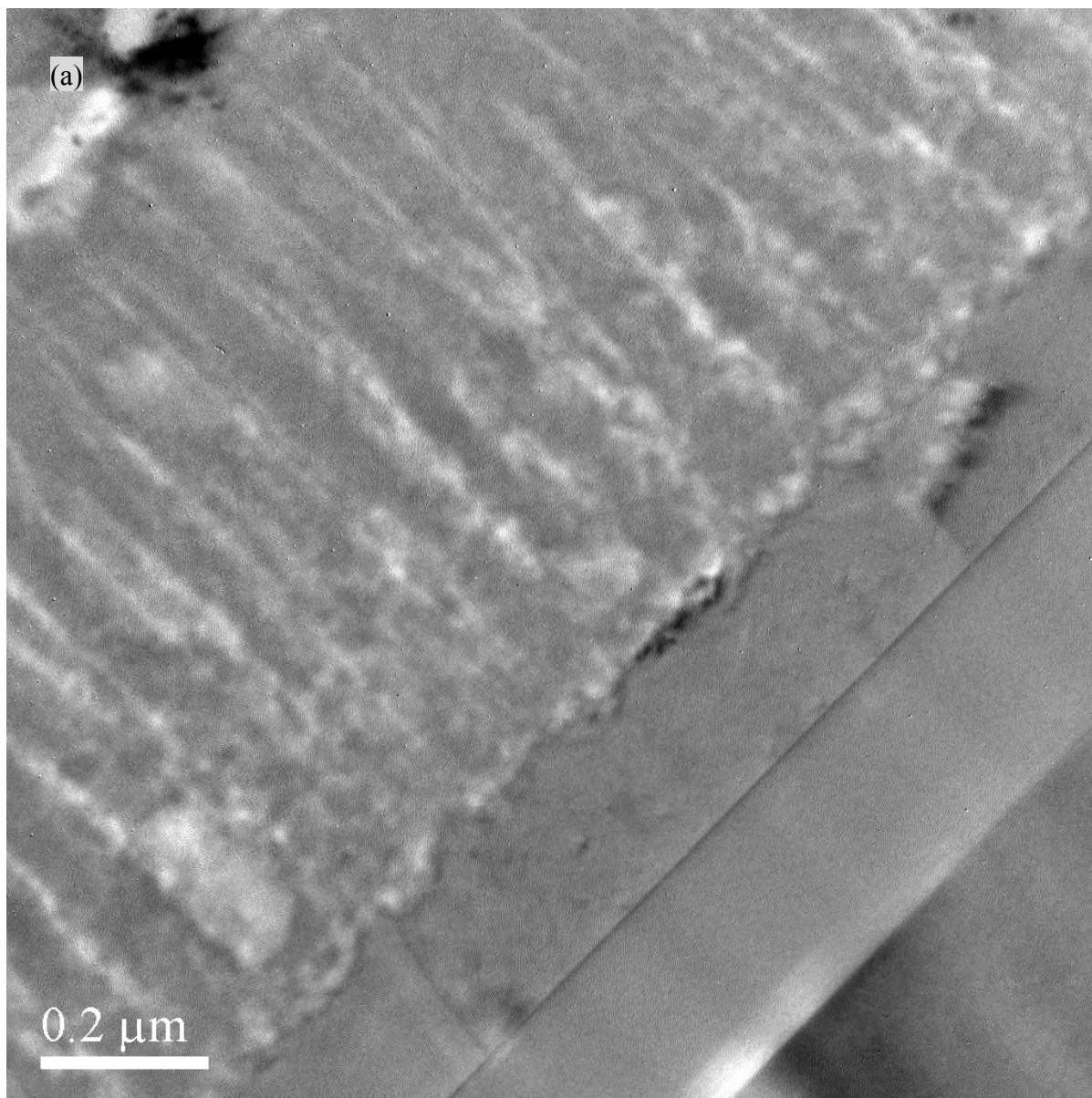


Fig. 3.2-12: The TEM cross-section image of AAO full of ZnO prepared by FIB; ; the porous diameter is about 80nm after 40mins widening treatment; the structure is AAO/SiO₂/Si-sub.

Characteristics of 1D ZnO Nanowires Array Grown by AAO Assistance

C-W Chang

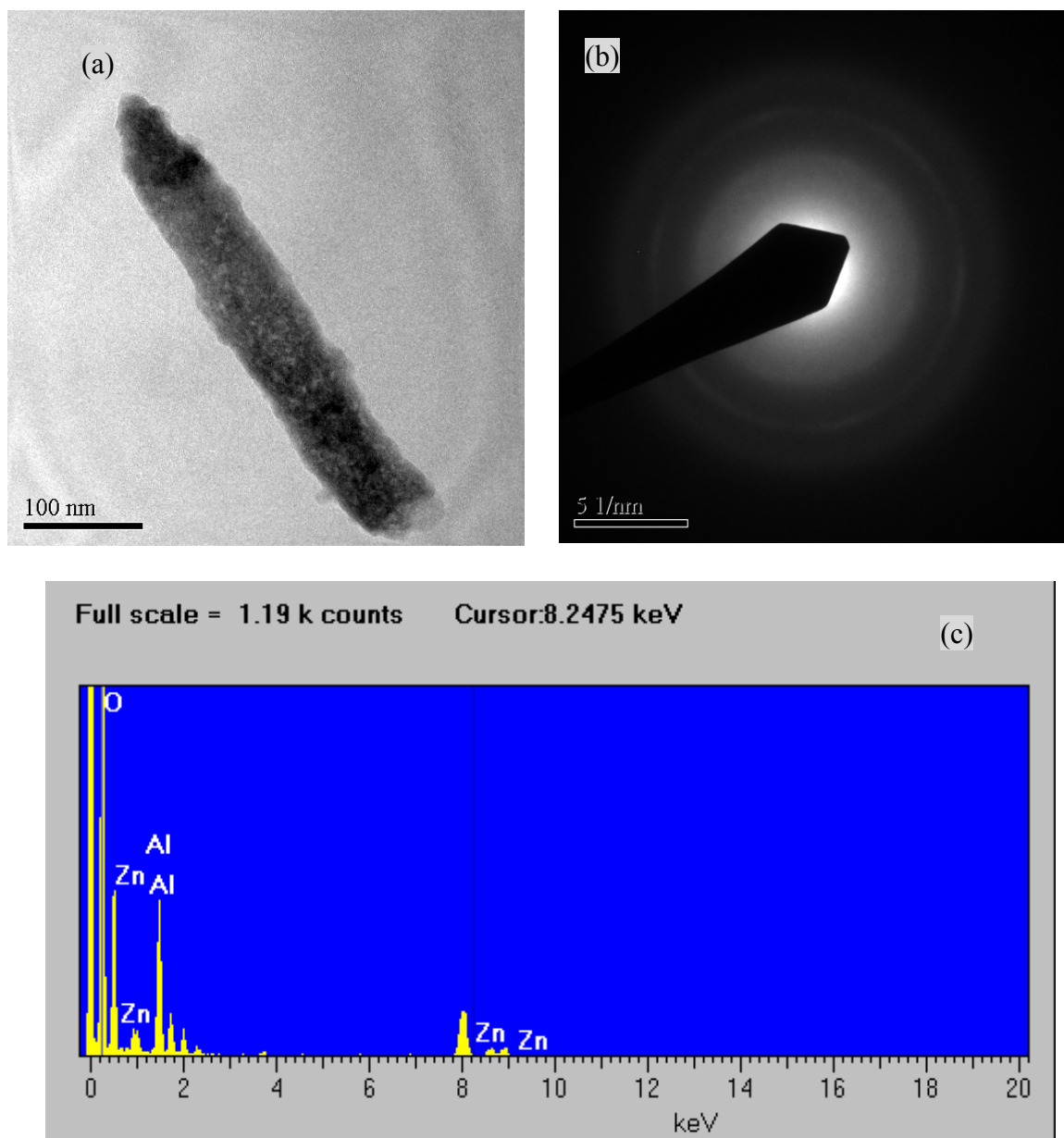


Fig. 3.2-13: (a) TEM image of ZnO NW prepared by supersonic shake treatment; (b) SAED of ZnO NWs.(c) EDS of ZnO NWs.

Chap. 3.2.3 XRD Analysis

The crystal structure and phase of the NWs were determined by X-ray diffraction (XRD, MAC Science, MXP18, and Japan). Fig. 3.2-14 depicts the XRD patterns of Al thin film under different annealing treatment on TiN/Si-sub, it compares with (a) different annealing time and temperature, (b) RTA, respectively. The major annealing treatment was at 300~500 °C for 1~8 hrs in the Ar atmosphere, and cool down to room temperature in chamber naturally. Another one was rapid thermally annealed (RTA) at 400 or 500 °C for 3 min in the Ar atmosphere. We observe the peak of TiN disappeared due to the higher T and longer time annealing or RTA. It seems to imply that TiN was composed with Al or the quality of TiN deposited by sputter was not good. Actually, we observed interface (between Al film and TiN) adhesion after RTA treatment was inferior to ones after long time annealing. Consequently, we elected some suitable parameter for annealing which annealing was carried out at 400 °C for 2hrs, and replaced barrier layer of TiN with SiO₂ layer.

At Fig. 3.2-15, those XRD patterns of AAO full of ZnO on SiO₂/Si-sub indicate the different crystalline of sample with annealing or not. The XRD peak at around 33° is caused by the ZnO crystal, and the main peaks indexed as (002) of the wurtzite structure. The better crystalline of ZnO would exhibit better FE properties according to annealing treatment.

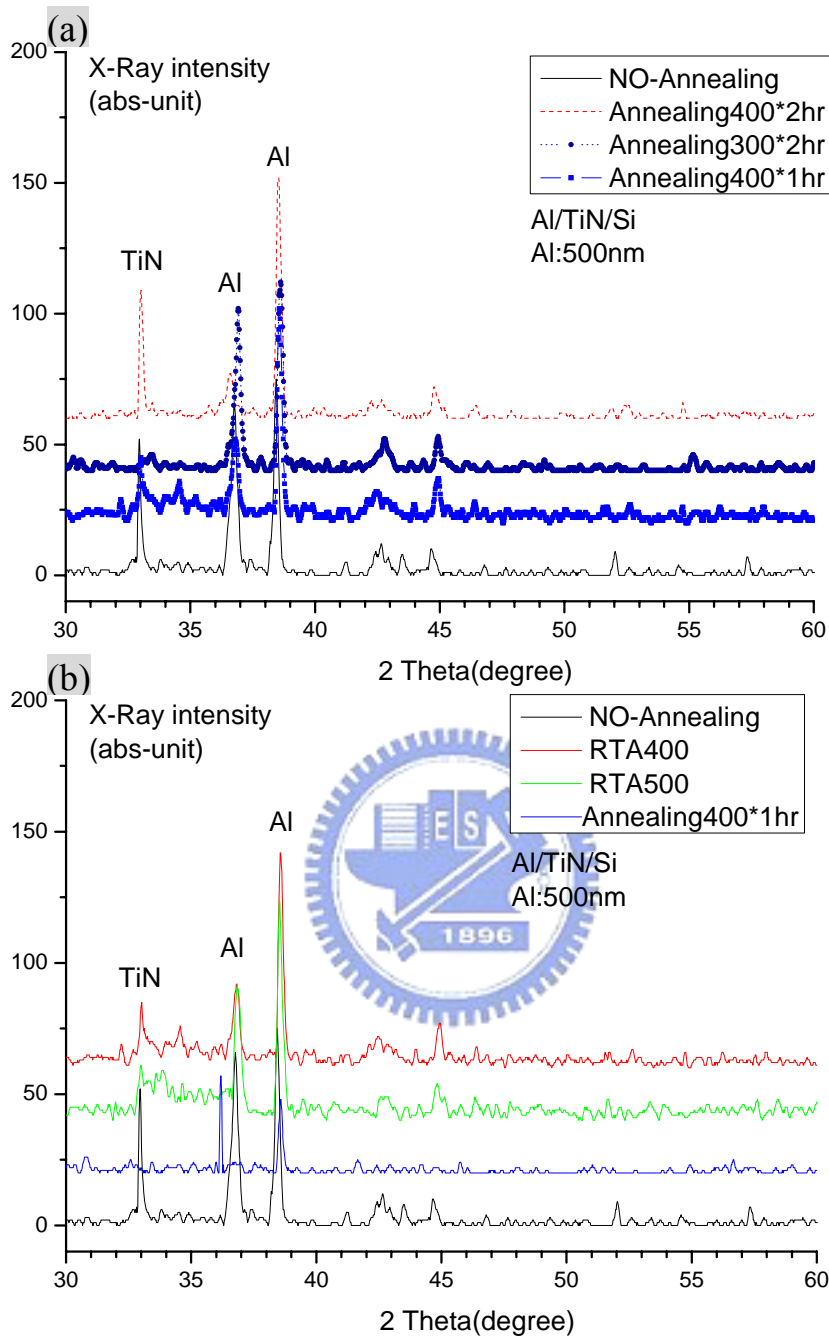


Fig. 3.2-14: It reveals XRD patterns of Al film with different annealing treatment on TiN/Si-sub., and compares with (a) different annealing time and temperature, (b) RTA.

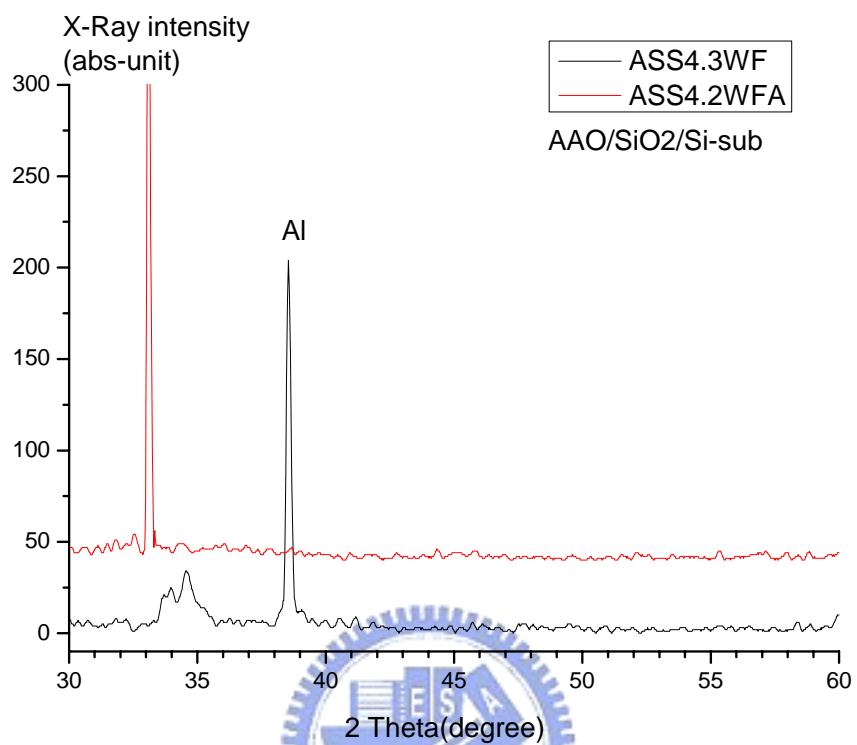


Fig. 3.2-15: It reveals XRD patterns of AAO full of ZnO on SiO₂/Si-sub., and compares with (a) annealing (400°C 2hr) and (b) without annealing.

Chap. 3.2.4 PL Analysis

A photoluminescence analyzer (PL, Hitachi F-4500, Japan) with Xe lamp as an excitation source (320 nm) was used for optical studies at room temperature. From the reaction equations (Chap. 2.2.2), the Zn^{2+} ions are sufficient in this solution, but the OH^- ions are finite in the solution because hexamethylenetetramine (HMTA) slowly releases OH^- . Thus, oxygen is expected to be lacking in the NWs fabricated by the hydrothermal method. This phenomenon also results in the deep-level³⁵ and singly ionized oxygen vacancies³⁶ luminescence at 495 and 520 nm as shown in Fig. 3.2-16.

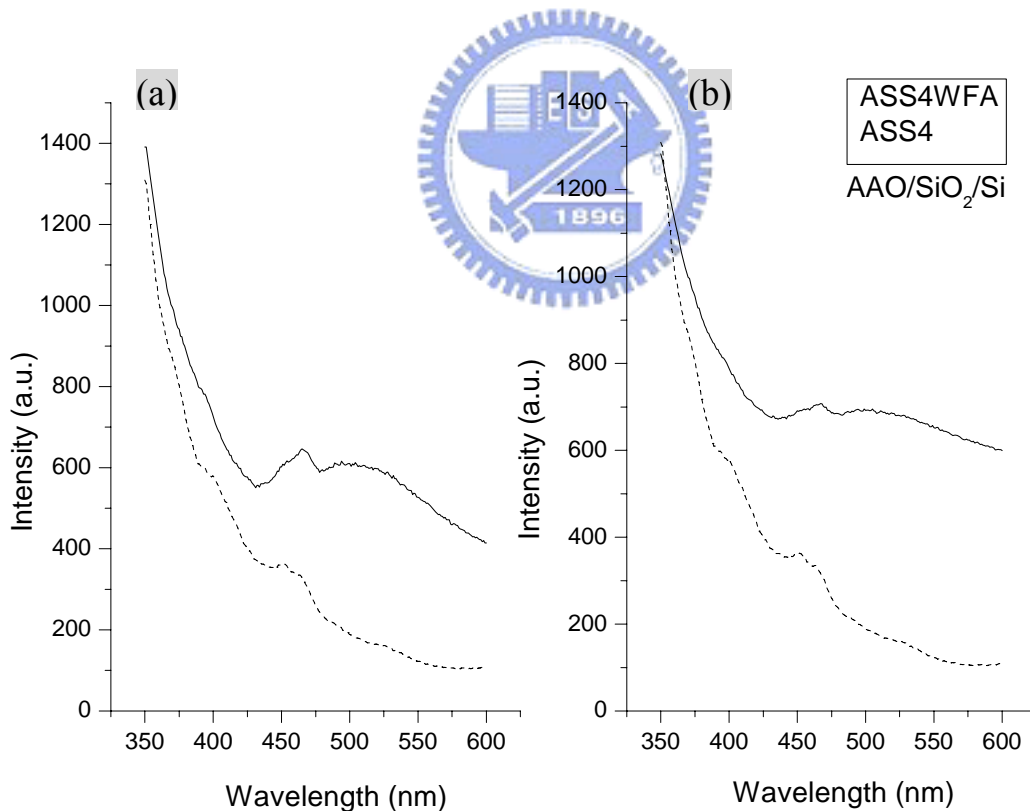


Fig. 3.2-16: It reveals the with Xe lamp as an excitation source (320 nm) at room-temperature.

Chap. 3.2.5 Field Emission Analysis

First, we show a Fowler-Nordheim (F-N) function, which details were introduced at section ch 1.2.3, to analysis Field emission of our sample. The field emitting enhancement factor, β , exhibits the effect of field emission by quantification. Value of β is calculated by fitting the slop of $\ln(J/E^2)-1/E$ curve(name F-N plot). It illustrates at Fig. 3.2-17. We recommend the concept of operation region³⁷ for analysis further, which illustrates at FIG- 3.2-18. If the length is increased, the resistance property of NW would dominant the FE property early.

© F-N function fitting

1. Fowler-Nordheim (FN) equation:

$$J = (A\beta^2 E^2 / \Phi) \exp(-B\Phi^{3/2} / \beta E)$$

$$A : 1.56 \times 10^{-10} (AV^{-2}eV) ; B : 6.83 \times 10^3 (VeV^{-3/2} \mu m^{-1})$$

2. The field emitting enhancement factor, β : (slop is fitted in FN plot)

$$\text{Slope} = B\Phi^{3/2}d/\beta \rightarrow \beta = B\Phi^{3/2}/S$$

© Operation region

1. Off region
2. Turn-on (Active) region
3. Saturation region

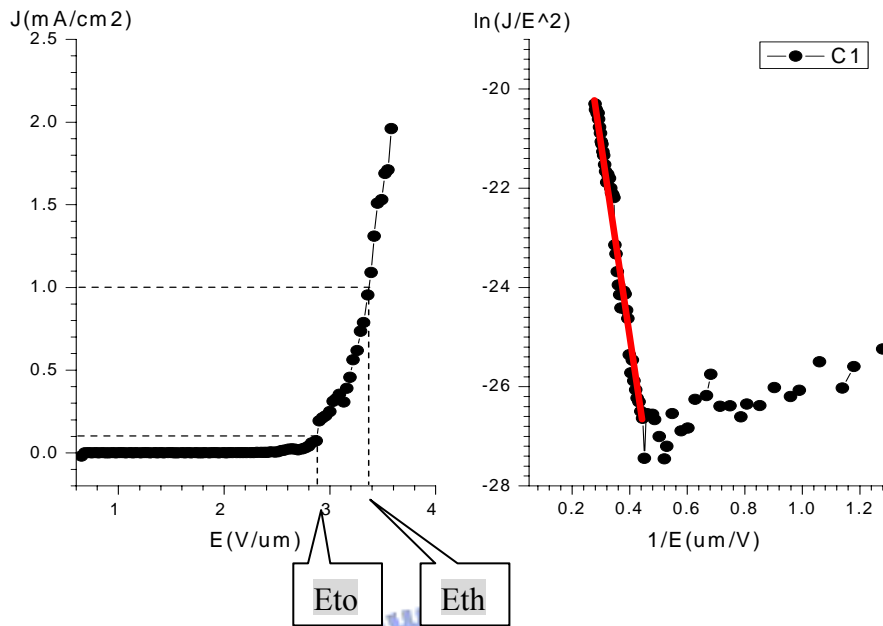


Fig. 3.2-17: Field emitting J-E curve and $\ln(J/E^2)-1/E$ curve.

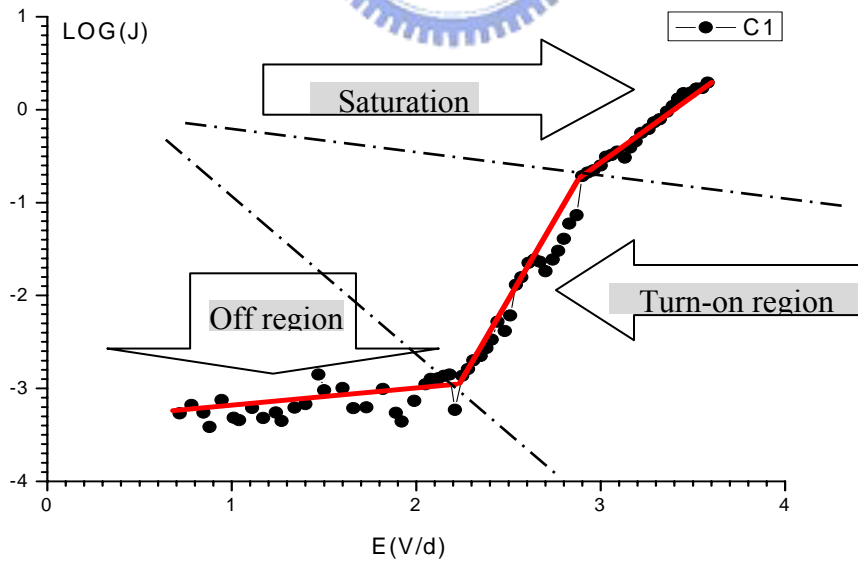


Fig. 3.2-18: It illustrates operation region of field emission.

Following, we show some results and discuss characteristic of filed emission. Further, we utilize characteristic of AAO to control the structure of ZnO NWs and study the effect of aspect ratio.

First, the flower-liked (nanosheet) ZnO structure shows at Fig. 3.2-19; it also exhibits characteristic of filed emission, and it's effect is better than NWs in the same scale actually²⁰. The major cause is the screen effect due to higher number density of NWs.

By comparing with Fig. 3.2-20 and Fig. 3.2-21, we observe the better value of β which becomes 2800 from 1600 and the higher current density which is enhanced one order. The photoenhanced field emission characteristic under 30W incandescent lamp irradiation is demonstrated the influence of the illumination on the field emission.

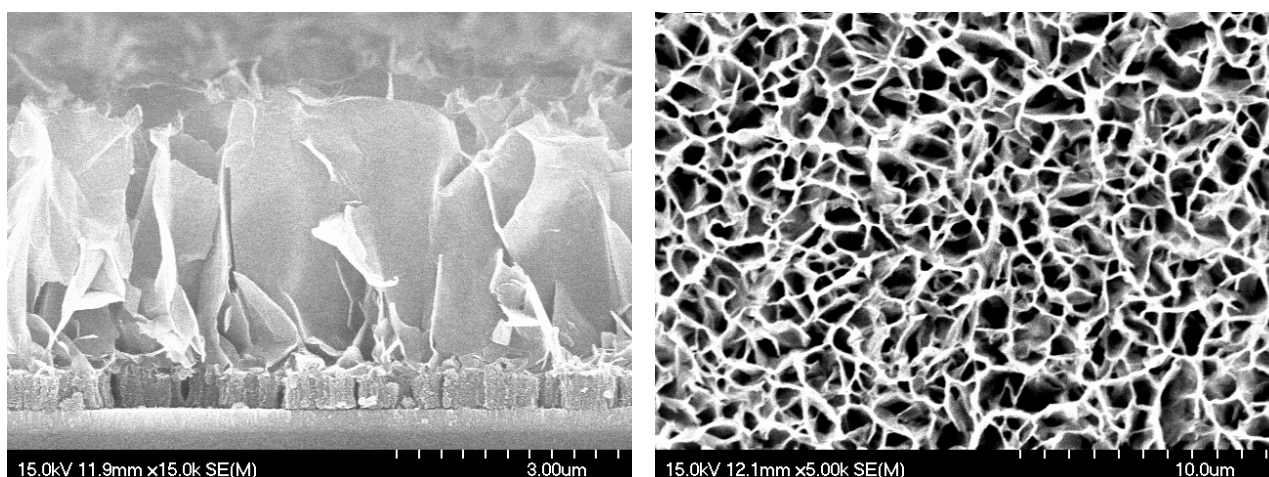
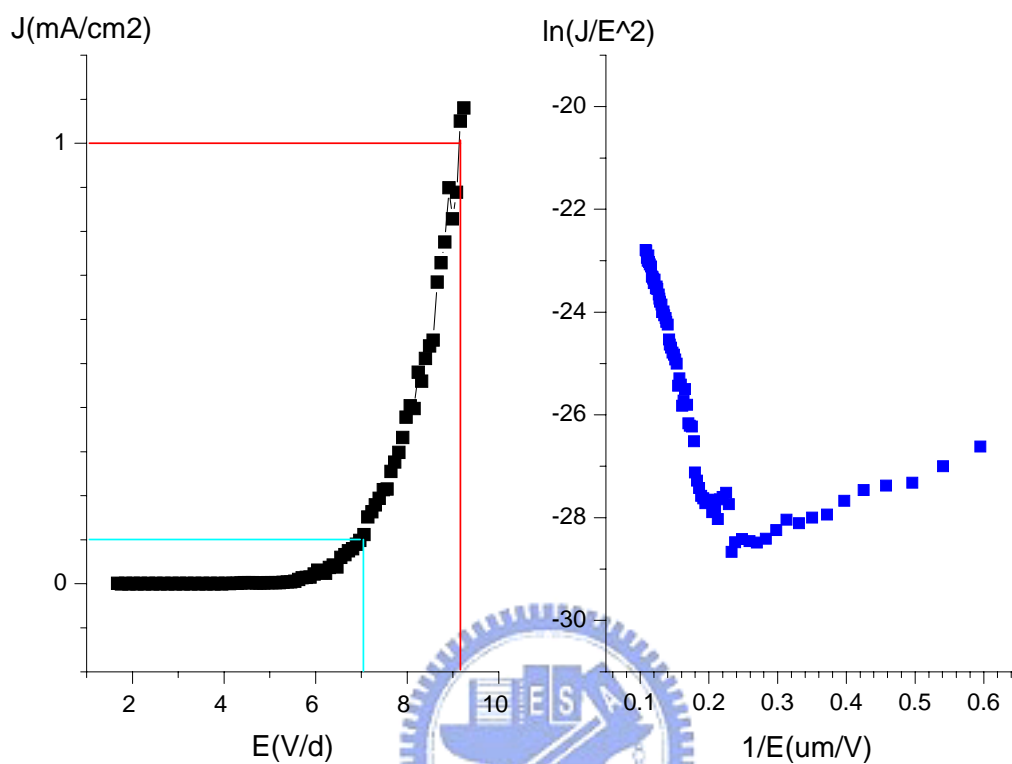


Fig. 3.2-19: The SEM images reveals the morphology of sample B2. It was AAO full of ZnO by hydrothermal in 2.5 hrs at 95°C

Characteristics of 1D ZnO Nanowires Array Grown by AAO Assistance

C-W Chang



electrode-A(cm ²)	0.00709
thickness(um)	500
D(um)	619
d=D-THICK(um)	119
Slope	5.20E+01
W-zno(eV)	5.37
W-zno ^{1.5} (eV ^{1.5})	12.444041
emitting factor- β	1630

Fig. 3.2-20: It shows field emission J-E curve and F-N plot of sample B2. The table shows the detail data.

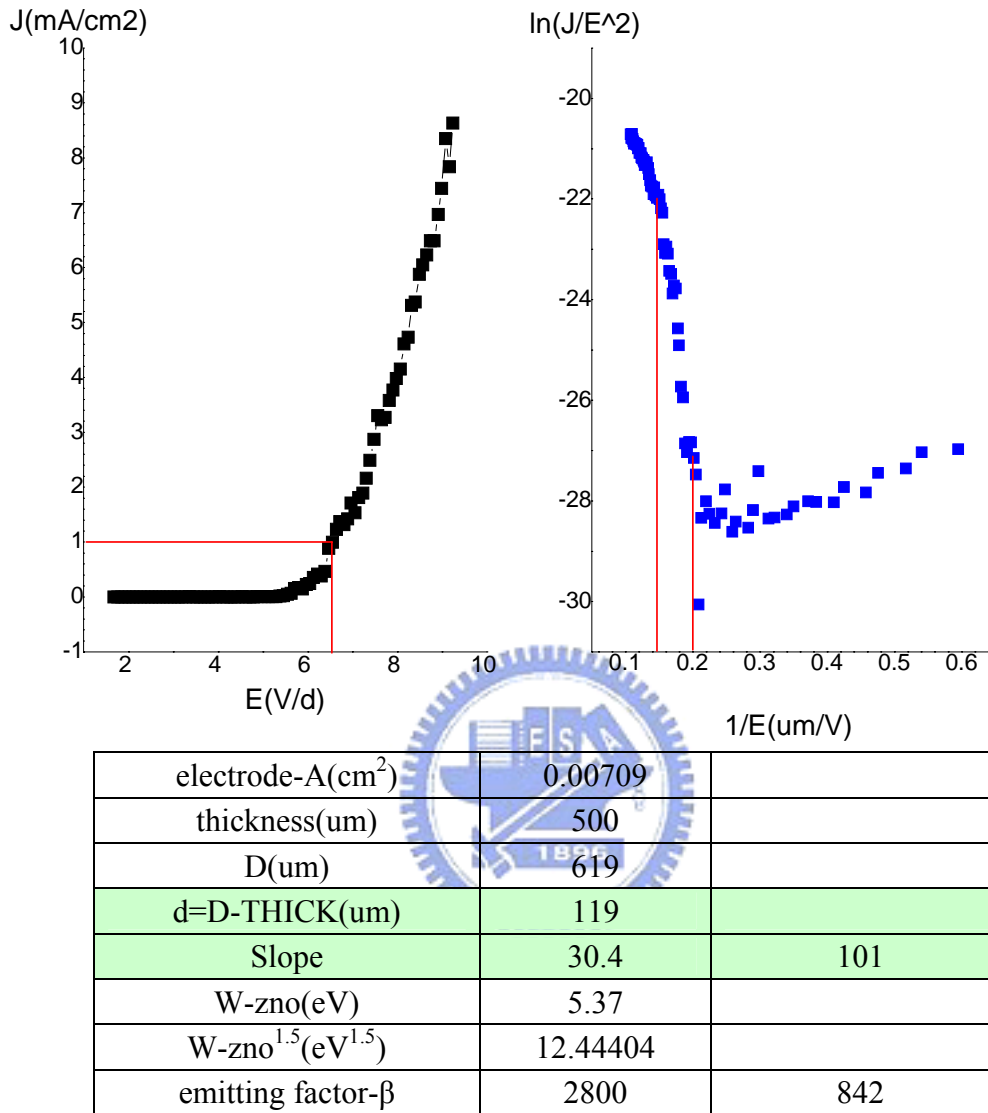


Fig. 3.2-21: It shows field emission J-E curve and F-N plot of sample B2 under a 30W lamp. The table shows the detail data. It indicates the photo-enhanced field emission characteristic.

Furthermore, we discuss the effects of annealing on field emission property. At Fig. 3.2-22, the SEM images reveals the morphology of sample C1; clearly, it indicates the length of ZnO NW is about 500nm, and Fig. 3.2-23 reveals that it exhibits better field emission property than flower-liked ZnO. The causes maybe are better crystallization, morphology and high aspect ratio.

Through by comparing with Fig. 3.2-24, we observe the better value of β which becomes 3660 from 2200. We suggest the cause is the better crystallization due to annealing treatment. By the way, we didn't observe the photo-enhanced effect²⁰ at this sample, thus we suggest the flower-liked ZnO was disappeared result in unable to receive energy from photon.

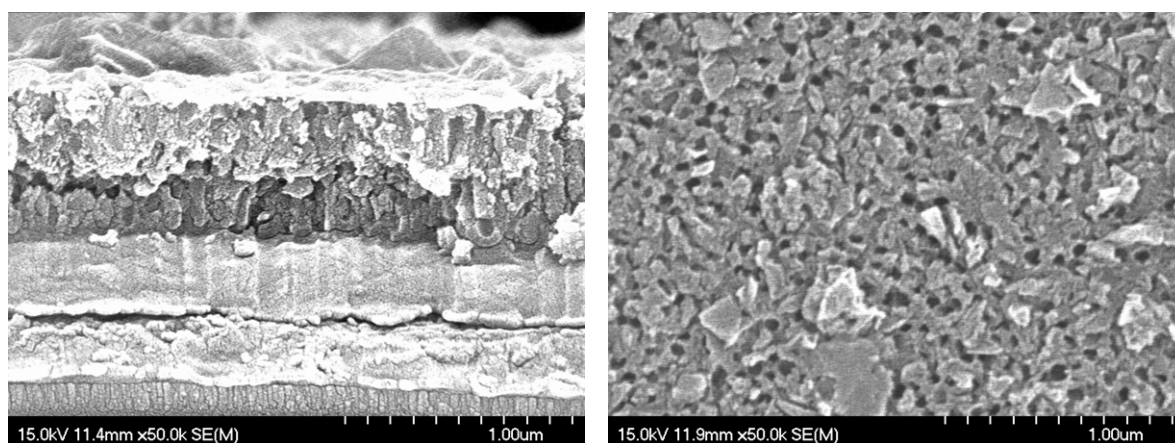
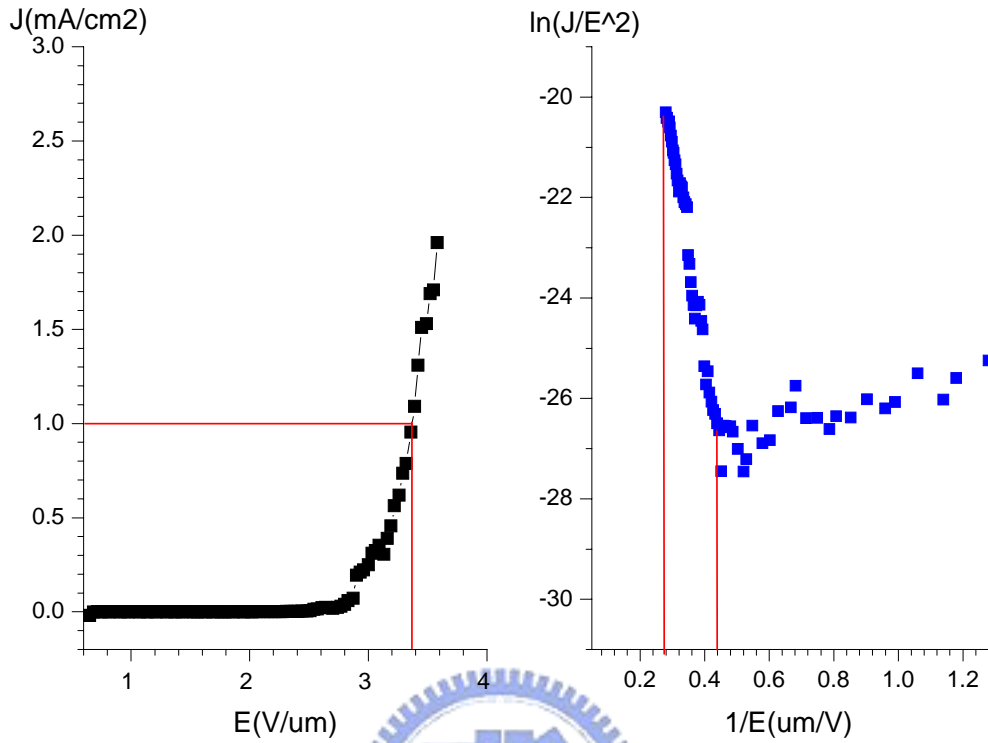


Fig. 3.2-22: The SEM images reveals the morphology of sample C1. It was AAO full of ZnO by hydrothermal in 2.5 hrs at 95°C and removed the surplus ZnO on the AAO surface. And length/diameter is 500-600/70-80nm.

Characteristics of 1D ZnO Nanowires Array Grown by AAO Assistance

C-W Chang

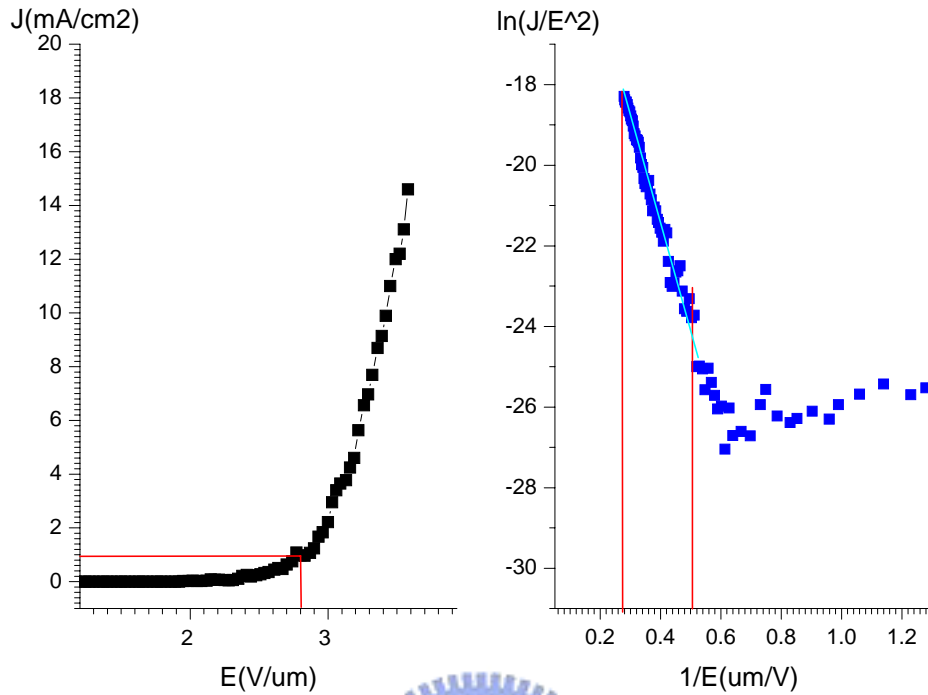


electrode-A(cm ²)	0.00709
thickness(um)	501
D(um)	808
d=D-THICK(um)	307
Slope	38.6
W-zno(eV)	5.37
W-zno ^{1.5} (eV ^{1.5})	12.44404
emitting factor-β	2200
length/diameter	550-600/70-80nm
Aspect ratio	6.875-8.57
E _{turn on} (1uA/ cm ²)	~2.4(V/um)
E _{threshold} (1mA/cm ²)	~3.38(V/um)

Fig. 3.2-23: It shows field emission J-E curve and F-N plot of sample C2. The table shows the detail data.

Characteristics of 1D ZnO Nanowires Array Grown by AAO Assistance

C-W Chang



electrode-A(cm ²)	0.00709
Thickness(μm)	501
D(μm)	808
d=D-THICK(μm)	307
Slope	23.2
W-zno(eV)	5.37
W-zno ^{1.5} (eV ^{1.5})	12.44404086
emitting factor-β	3.66E+03
length/diameter	550-600/70-80nm
Aspect ratio	6.875-8.57
E _{turn on} (1μA/cm ²)	~1.93(V/μm)
E _{threshold} (1mA/cm ²)	~2.84(V/μm)

Fig. 3.2-24: It shows field emission J-E curve and F-N plot of sample C2 which was improved by annealing (with 400°C at 2hrs). The table shows the detail data.

Characteristics of 1D ZnO Nanowires Array Grown by AAO Assistance

C-W Chang

At TAB-3.2-1, we compare the FE properties with different reports including CNT with AAO, ZnO by VLS, ZnO with or without AAO by hydrothermal method. Of course, the FE properties of CNT formed by VLS are better, which due to better crystallization and high aspect ratio. We observe that the values of β are match with the same aspect ratio of NW by hydrothermal method, but the turn on field and threshold field are higher. It major cause by the bottom layer under AAO.

Kind	CNT with AAO (2001) ³⁸	CNT with AAO (2003)	CNT with AAO (2004) ³	ZnO NW on Si (2004) ¹²	ZnO on PET(2005) ²⁰		ZnO with AAO
					Flower-like	NWs	
Growth method	VLS 900°C	VLS 900°C	VLS 650°C	VLS 750-950°C	Hydrothermal 80~90°C		
Length Diameter	500~*um 70~80	? 70	900~1um 80			500 50	600 60~80
Aspect ratio	8~10		11~12			10	8~10
emitting factor- β	AL5200 ALNB3360	5600 980	Ascut5800 Cut2580	Cu 7180 Au 4700 3810	4503	3340	3410
$E_{\text{turn on}}$ (1uA/cm ²)	1.9-2.1 (V/um)	2.8	Ascut2.15 Cut2.84	0.83 at 25 uA/cm ²	1.1	1.6	1.9-2.0
$E_{\text{threshold}}$ (1mA/cm ²)		7.2		8.5 at 1.5 mA/cm ²	1.6	2.1	2.7-2.8
Number density (tips/cm ²)			10 ⁷ ~10 ⁸			1.2x10 ⁹	~10 ¹⁰
P.S.	Normally $\beta_{\text{CNT}}=800-1900$, $\beta_{\text{ZnO}}=\sim 900$ at 2002 Number density=10 ⁹ ~10 ¹² tips/cm ²						

Tab. 3.2-1: Comparison with other studies.

Besides, at the above F-N plots, we observed the turning point at the field emission region. We suggest it was a phenomenon called switching effect³⁹, which the principle meaning is the conducting channel was not uniformly distributed through out the whole NWs, some emission channel may have low thresholds. When some channel switch on first, the heat effect can promote emission from the surround elements. However the applied voltage keeps increasing, some channels may fail due to the excessive current. Consequently, we observed the different effect of FE in a sample when the filed increasing.

Fig. 3.2-25, it reveals field emission property of the higher aspect ratio. The length/diameter is 1600/70-80nm, and the aspect ratio is about 20. The only different of sample C2 and Ass6.4 is the length ZnO. So, we sure the values of β increase to 5890 due to increase the aspect ration.

According to above results, we believed the better FE property due to increase the aspect ration. The aspect ratio was composed by length and diameter; we would study the effect by adjusting length or diameter. Further, we would study the limited value of β whether exist or not.

Following, we show the results classed by two directions; one is different aspect ratio fixed the diameter, and another one is fixed the length.

Etch J-E curves and data of EF property, which are classed by different aspect ratio fixed the diameter, are showed at Fig. 3.2-26 and Tab. 3.2-2. We observe the value of β and the aspect ratio are in proportion, the tendency generally slows down which shows at Fig. 3.2-27. Moreover, the active region becomes small when the length is increased; it shows at

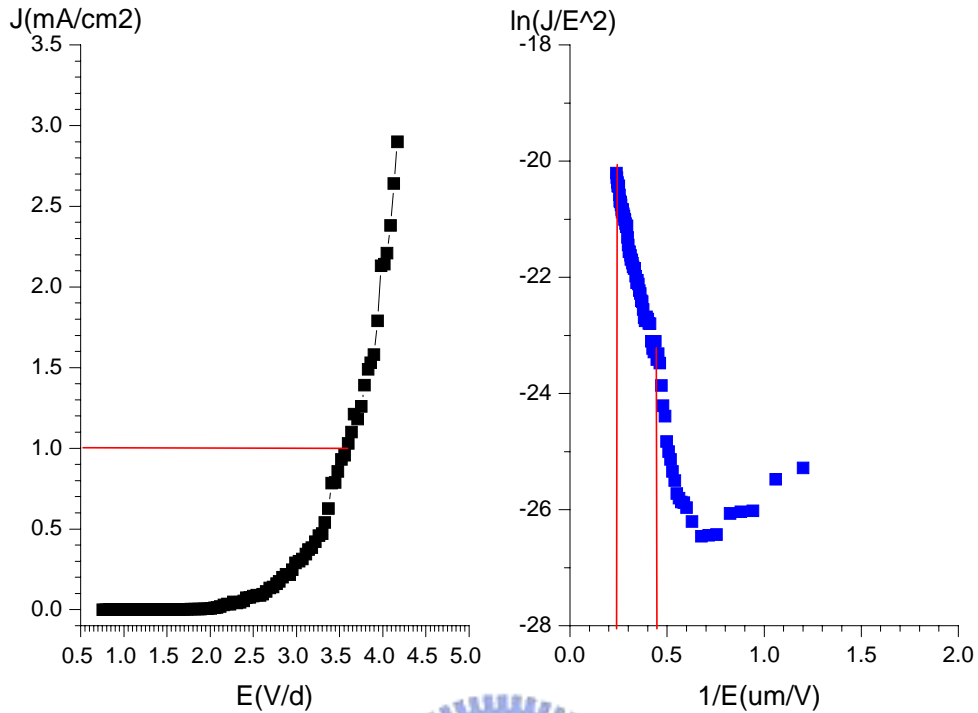
Fig. 3.2-28 and Fig. 3.2-29. The main cause is that longer length urges the resistance dominate the FE property early.

At Fig. 3.2-30 and Fig. 3.2-31, they show the FE property is enhanced by decreased diameter in the same length. The main cause is the screen effect reduced by decreased diameter. However, the structure become fragile when the diameter decreased, and it is not strong enough to endure many times of electric measurement.

Fig. 3.2-32 shows the tendency of the FE- β versus Different aspect ratio. Although the tendency is in proportion, we can observe that it generally slows down. When the aspect ratio is increased, there are some physical limitation will more perceptible, such as screen effect and resistance. Consequently, we believe that the maximum of β exists; namely, the infinite value of β is impossible existence.

Characteristics of 1D ZnO Nanowires Array Grown by AAO Assistance

C-W Chang



electrode-A(cm ²)	0.01
thickness(um)	501.00
D(um)	765.00
d=D-THICK(um)	264.00
Slope	14.43
W-zno(eV)	5.37
W-zno ^{1.5} (eV ^{1.5})	12.44
emitting factor- β	5890
length/diameter	1600/70-80nm
Aspect ratio	~20
E _{turn on} (1uA/ cm ²)	~2.05 (V/um)
E _{threshold} (1mA/cm ²)	~3.6(V/um)

Fig. 3.2-25: It shows field emission J-E curve and F-N plot of sample ASS6.4. The table shows the detail data. And length/diameter is 1600/70-80nm.

Characteristics of 1D ZnO Nanowires Array Grown by AAO Assistance

C-W Chang

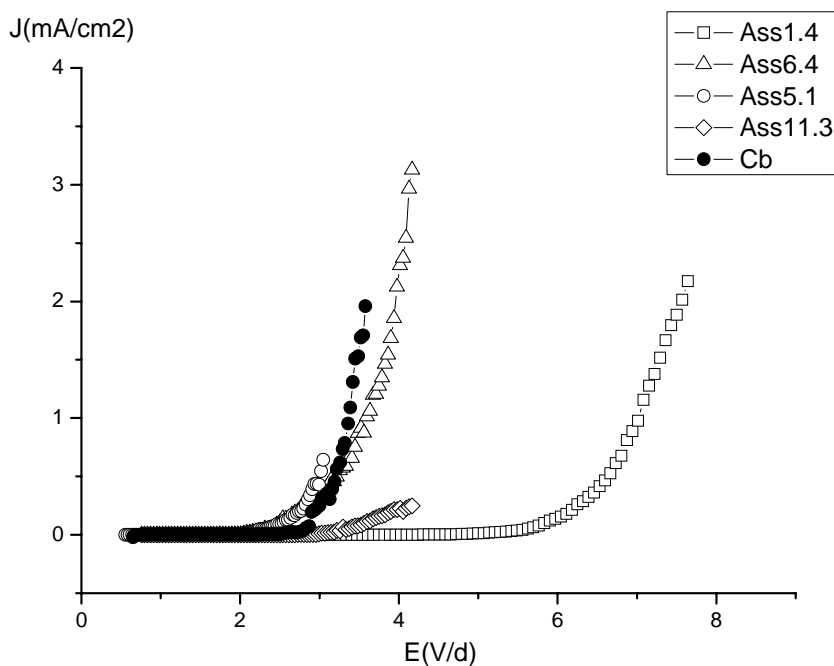


Fig. 3.2-26: It shows field emission J-E curves of different aspect ratio and fixed the diameter.



	L (um)	D (nm)	Aspect ratio	Eto (at 1uA/ cm2)	Eth (at 1mA/cm2)	β	R	Active region
Ass1.4	0.5	80	6.25	4.9	7.04	1600		2.2
Cb	0.6	80	7.5	2.04	3.38	2200		1.0
Ass11.3	1	80	12.5	1.8/1.9	x	3400		0.9
Ass5.1	1.2	80	15	1.6/1.7	x	44-4800		0.6
Ass6.4	1.6	80	20	1.51	3.59	5200		0.5
Ass10.3	2	80	25	1.27?	x	x		x

Tab. 3.2-2: It shows the details data of different aspect ratio fixed the diameter.

Characteristics of 1D ZnO Nanowires Array Grown by AAO Assistance

C-W Chang

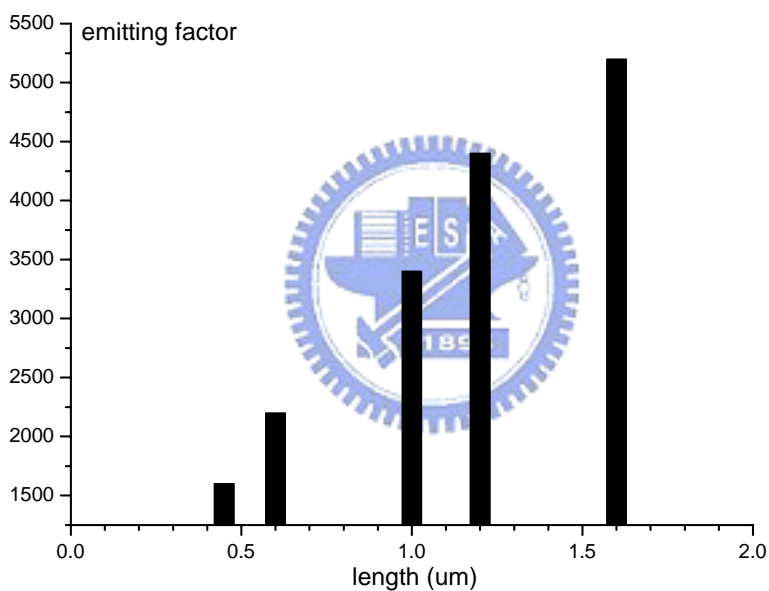
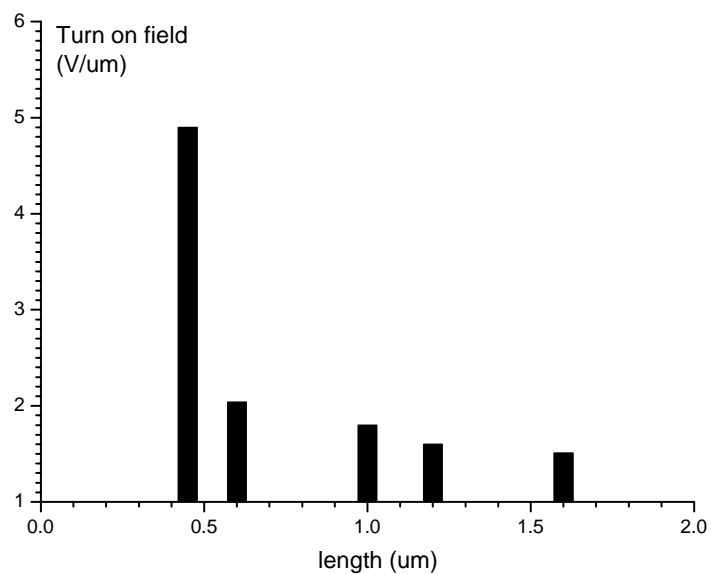


Fig. 3.2-27: (a) Turn on field versus NW length, and (b) FE- β versus Different NW length.

Characteristics of 1D ZnO Nanowires Array Grown by AAO Assistance

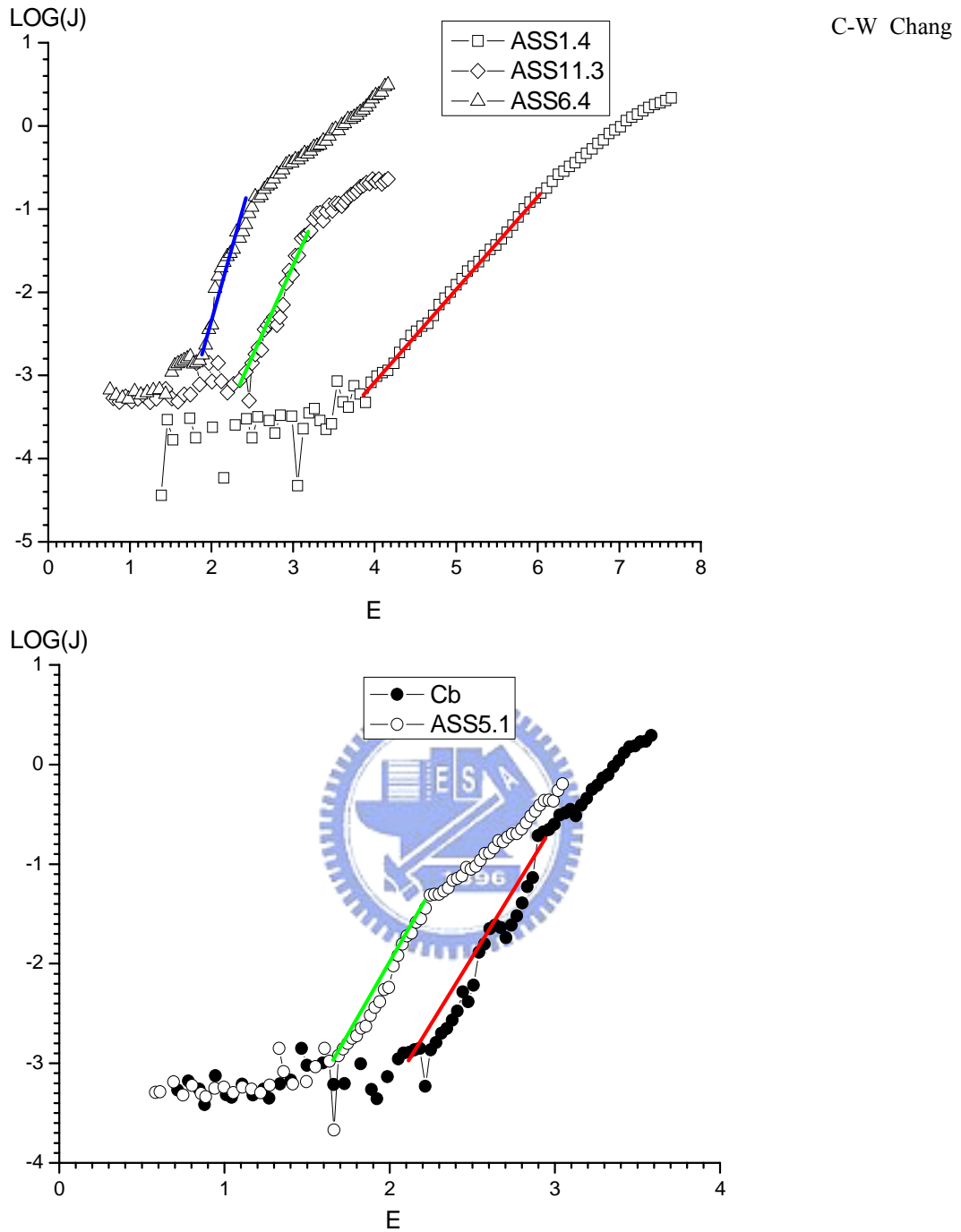
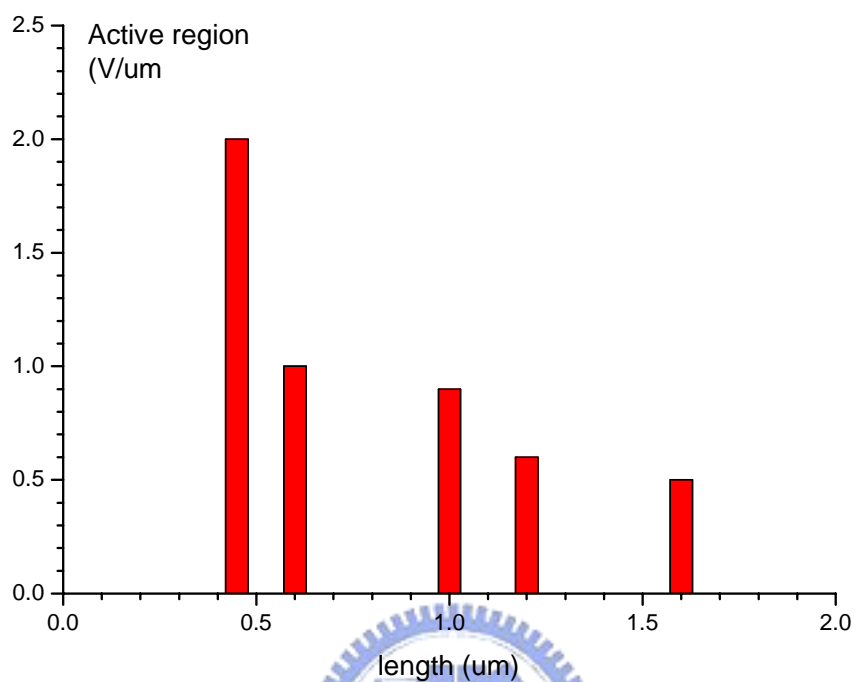


Fig. 3.2-28: Active region for Different NW length (fixed diameter=80nm).Length (um):ASS1.4=0.5, ASS11.3=1, ASS6.4=1.6, Cb=0.6, ASS5.1=1.2.

Characteristics of 1D ZnO Nanowires Array Grown by AAO Assistance

C-W Chang



	Length (um)	Diameter (nm)	Aspect ratio	Active region
Ass1.4	0.5	80	6.25	2.2
Cb	0.6	80	7.5	1.0
Ass11.3	1	80	12.5	0.9
Ass5.1	1.2	80	15	0.6
Ass6.4	1.6	80	20	0.5
Ass10.3	2	80	25	

Fig. 3.2-29: Active region for Different NW length fixed the diameter.

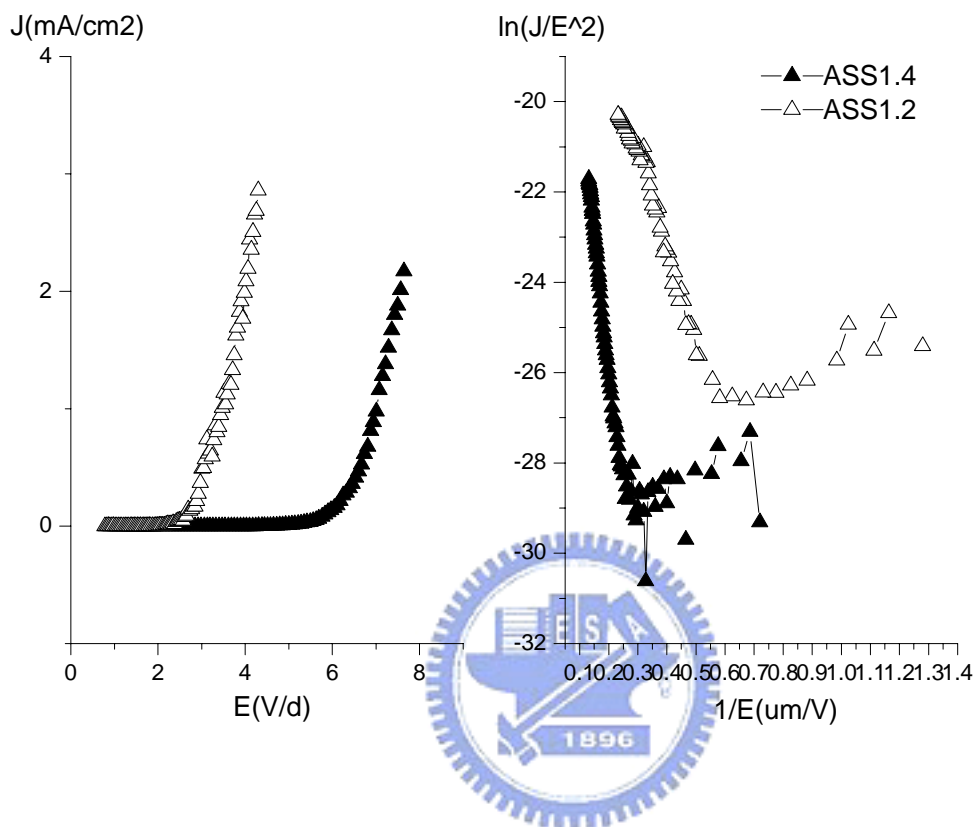


Fig. 3.2-30: FE for Different NW diameter fixed length ($L=500\text{nm}$). Diameter (nm):
 ASS1.4 = 80, ASS1.2 = 30.

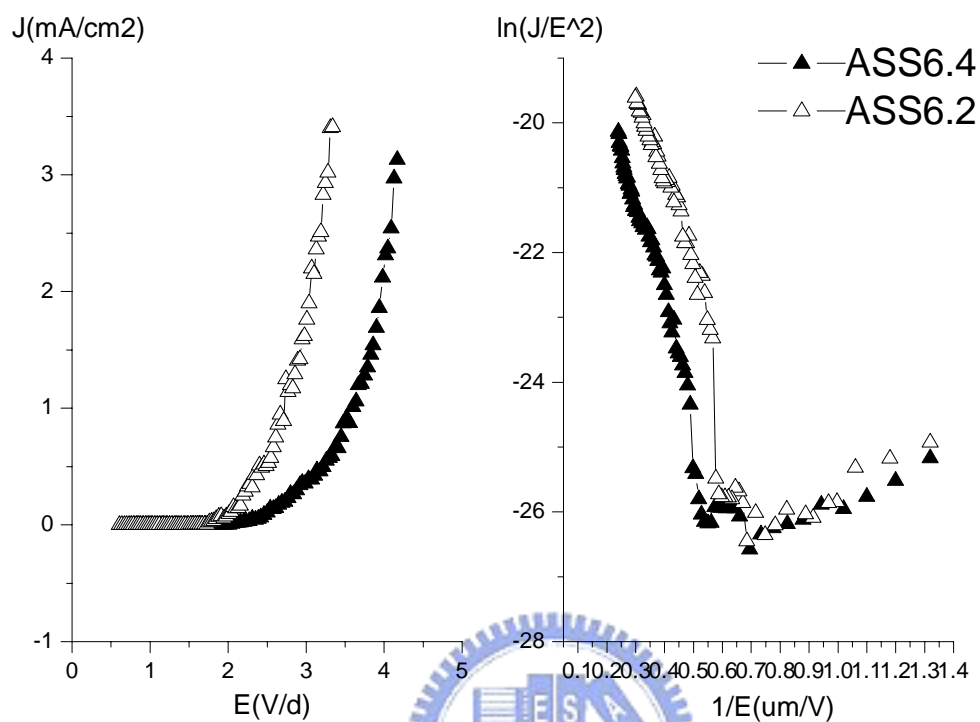
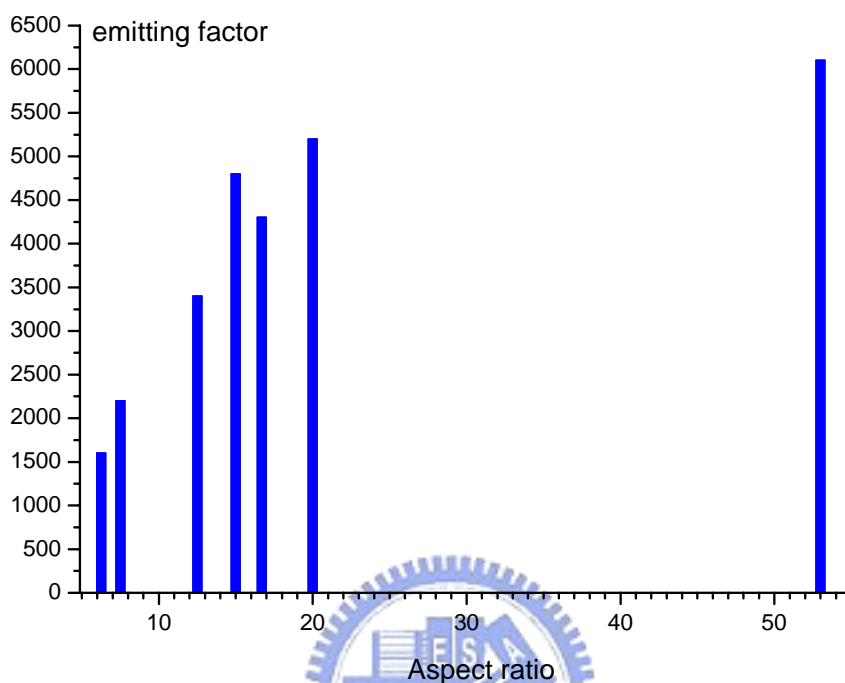


Fig. 3.2-31: FE for Different NW diameter fixed length ($L=1600\text{nm}$). Diameter (nm):
 ASS6.4 = 80; ASS6.2 = 30

Characteristics of 1D ZnO Nanowires Array Grown by AAO Assistance

C-W Chang



	Length (um)	Diameter (nm)	Aspect ratio	β
Ass1.2	0.5	30	16.7	4300
Ass1.4	0.5	80	6.25	1600
Cb	0.6	80	7.5	2200
Ass5.1	1.2	80	15	4800
Ass6.2	1.6	30	53	6100
Ass6.4	1.6	80	20	5200
Ass11.3	1	80	12.5	3400

Fig. 3.2-32: FE- β versus Different aspect ratio.

Chap. 3.3 Capacitance

Fig. 3.3-1 reveals the structure of capacitance; (c) shows the partial area of top electrode. We defined three kinds size of top electrode. Image (d) illustrates the measurement method. After measurement of C-V, we observe that the leakage current was large and capacitance was not good enough; therefore, we suggest the causes are surface remained ZnO residual and bad quality of AAO (dielectric).

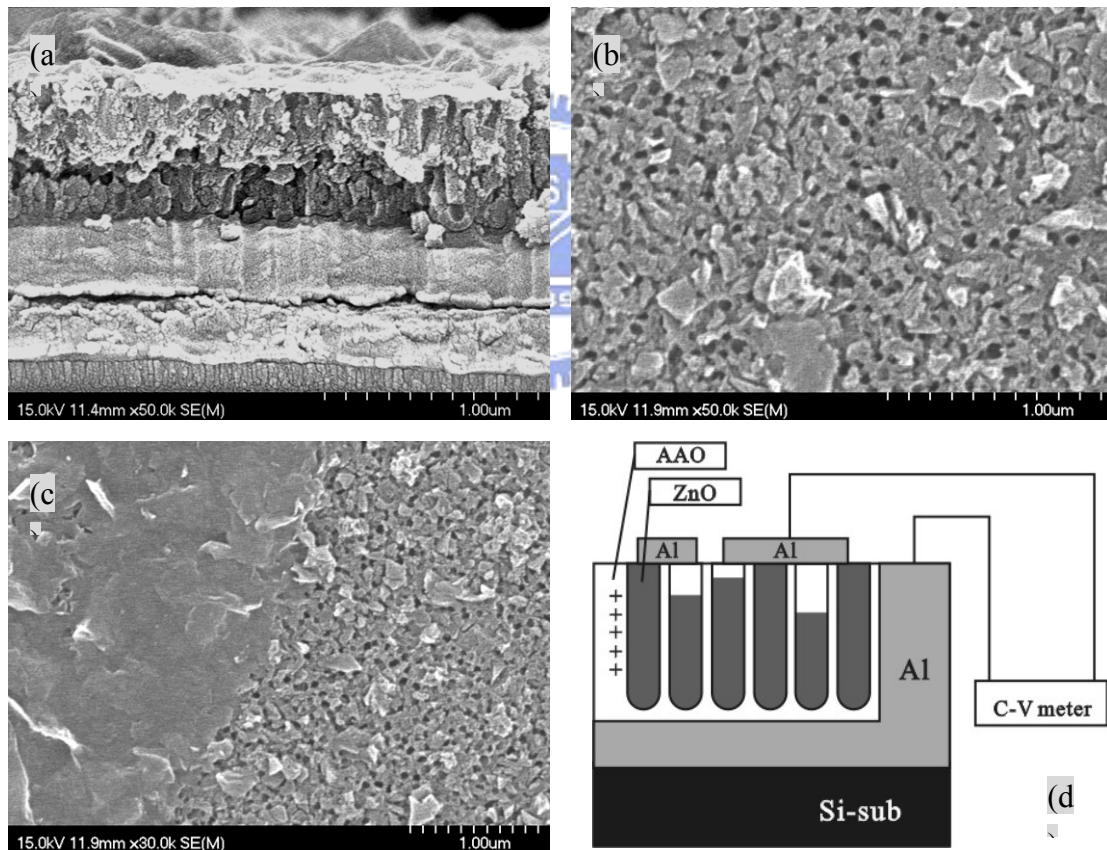


Fig. 3.3-1: SEM images of cross-section view (a), top-view(b)(c). (d) was illustration of capacitance measurement. (a) reveals the AAO full ZnO. (b) reveals few ZnO residues on the surface. The partial circle in the image (c) was the top electrode.

Chapter 4 Conclusions

In summary, well-aligned and vertical-grown ZnO nanowires, controlled to achieve required geometric structure by high ordered AAO assistance, are successfully fabricated on Si-substrate by a hydrothermal route at 95°C for 2 hrs. Beside the optical property, we focused on the properties of field emission. In this study, we demonstrated that the FE characteristics significantly depend on the aspect ratio of ZnO NW; we observed the relation between aspect ratio and the field emitting enhancement factor β is in proportion. For example, β is enhanced to 6100 when the aspect ratio is 53. However, we believe the infinite β does not exist. Due to the previous tendency gradually become smooth with the increasing aspect ratio.

Moreover, we introduced some concepts to investigate the nanostructures by the material analyses and the electrical measurements. There are some faults been observed and some improvements recommended.

First, about the turn on field, the higher turn on field is caused by the high resistive AAO bottom, as we know. We suggest some method to further improve: 1. to decrease the bottom thickness. 2. to remove bottom. At the end of second anodization, the voltage from high to low dropped gradually within a period, which a thinner bottom layer might be obtained. If the removal of the bottom was achieved, additional processes to fabricate the AAO mask are necessary to pattern our sample. By this way, the surface uniformity of the mask is difficulty to be synthesized. If the

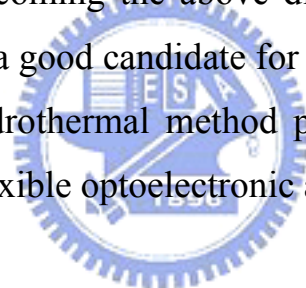
Characteristics of 1D ZnO Nanowires Array Grown by AAO Assistance

C-W Chang

question of bottom could be solved, we are going to obtain a vertical and high ordered ZnO array after removing AAO template, which could exhibit better property of field emission.

Second, about the crystalline of ZnO, the conventional hydrothermal method employed the seed layer where single crystal ZnO was formed. Consequently, we could deposit the seed material on the bottom of AAO pores although the AAO bottom existed. Besides, it could employ both seed layer and mask to growth single crystal ZnO NWs.

We could fabricate the required geometry structure of ZnO NWs at low temperature by overcoming the above difficulties. ZnO NWs array grow so vertical that it is a good candidate for the future flat panel display applications, and the hydrothermal method provides a low temperature process for fabricating flexible optoelectronic and field emission devices.



References

- ¹ Po-Lin Chen, Jun-Kai Chang, Cheng-Tzu Kau, and Fu-Ming Pan *Appl. Phys. Lett* 86, 123111 2005
- ² Kyung-Han Jung, Jong-won Yoon, Naoto Koshizaki and Young-Soo Kwon *Jpn. J. Appl. Phys.* 44, 7A 5300 2005
- ³ Soo-Hwan Jeong and Kun-Hong Lee *Jpn. J. Appl. Phys* 8B, L1106 2004
- ⁴ Q. B.Wu, S. Ren, S. Z. Deng, J. Chen, and N. S. Xu *J. Vac. Sci. Technol.* B22(3), 1282 2004
- ⁵ H. O. Le and S. J. Chua, Y. W. Koh and K. P. Loh, Z. Chen, C. V. Thompson and E. A. Fitzgerald *Appl. Phys. Lett* 87, 101908 2005
- ⁶ Y. F. Mei, Z. M. Li, R. M. Chu, and Z. K. Tang, G. G. Siu, Ricky K. Y. Fu, and Paul K. Chu, W. W. Wu and K. W. Cheah *Appl. Phys. Lett* 86, 021111 2005
- ⁷ Y. B. Tang, H. T. Cong, Z.G. Zhao, and H. M. Cheng *Appl. Phys. Lett* 86, 153104 2005
- ⁸ Bingqiang Cao, Weiping Cai, Yue Li, Fengqiang Sun and Lide Zhang *Nanotechnology* 16 1734 2005
- ⁹ Chi-Liang Kuo, Tz-Jun Kuo, and Michael H. Huang *J. Appl. Chem. B* 2005, 109 20115
- ¹⁰ Hideki Masuda and Masahiro Satoh *Jpn. J. Appl. Phys.* 35 L126 1996
- ¹¹ Seung Min Park and Chang Hyun Bae, Woosung Nam, Sung Chan Park, and Jeong Sook Ha *Appl. Phys. Lett* 86 023104 2005

- ¹² Seu Yi Li, and Pang Lin, Chia Ying Lee, and Tseng Yuen Tseng *J. Appl. Phys.* 95, 3711 2004
- ¹³ S. Iijima, *Nature (london)* 354,56 1991
- ¹⁴ C. H. Liu, W. C. Yiu, F. C. K. Au, J. X. Ding, C. S. Lee and S. T. Lee *Appl. Phys. Lett* 83, 3168 2003
- ¹⁵ Shingo Hirano, Nobuo Takeuchi, Shu Shimada, and Kyosuke Masuya, Makoto Kuwabara, *J. Appl. Phys.* 98, 094305 2005
- ¹⁶ Xu C X, Sun X W, Yuen C, Chen B J, Yu S F and Dong Z L *Appl. Phys. Lett.* 86 011118 2005
- ¹⁷ Fujihara S, Suzuki A and Kimura T 2003 94 2411
- ¹⁸ Chia Ying Lee, Seu Yi Li, Pang Lin, and Tseng Yuen Tseng, *J. Appl. Phys.* 99, 024303 2006
- ¹⁹ Huang M H, feick H, Yan H, Kind H, Weber E, Russo R and Yang P 2001 *Science* 292 1897
- ²⁰ Chia Ying Lee, Seu Yi Li, Pang Lin, and Tseng Yuen Tseng, *Journal of Nanoscience and Nanotechnology*, 5, 1088-1094 2005
- ²¹ Chia Ying Lee, Tseng Yuen Tseng, Seu Yi Li, Pang Lin *Nanotechnology*, 17 83 2006
- ²² In Taek Han, Ha Jin Kim, Young-Jun Park, Naesung Lee, Jae Eun Jang, Jung Woo Kim, Jae Eun Jung, and Jong Min Kim *Appl. Phys. Lett.* 81, 2070 2002
- ²³ Y. W. Heo, Y. K. Kwon, Y. Li, S. J. Pearton, and D. P. Norton, *Appl. Phys. Lett.* 84, 3474 2004

- ²⁴ Y. K. Kwon, Y. Li, Y. W. Heo, M. Jones, P. H. Holloway, D. P. Norton, Z. V. Park, and S. Li, *Appl. Phys. Lett.* 84, 2685 2004.
- ²⁵ Lisheng Wang, Xiaozhong Zhang, Songqing Zhou, Yueliang Zhou, Junjie Qi *Appl. Phys. Lett.* 86, 024108 2005
- ²⁶ Illy B, Shollock B A, macManus-Driscoll J L and Ryan M P 2005 *nanotechnology* 16 320
- ²⁷ J. B. Cui, C. P. Daghljan, U. J. Gibson, R. Pusche, P. Geithner, and L. Ley *J. Appl. Phys* 97, 044315 2005
- ²⁸ Hui Zhang, Deren Yang, Xiangyang Ma, and Duanlin Que *J. Phys. Chem. B* 109, 17055 2005
- ²⁹ O. Jessensky, F. Müller, and U. Gösele, *Appl. Phys. Lett.* 72,1173 1998
- ³⁰ K. Ebihara, H. Takahashi, and M. Nagayama, *J. Met. Finish. Soc. Jpn.* **34**, 548 1983
- ³¹ A. P. Li, F. Müller, A. Birner, K. Nielsch, and U. Gösele, *Appl. Phys. Lett.* 84 6023 1998
- ³² V. Pokalyakin and S. Tereshin, A. Varfolomeev and D. Zaretsky, A. Baranov, A. Banerjee, Y. Wang, S. Ramanathan, and S. Bandyopadhyay, *J. Appl. Phys* 97, 124306 2005
- ³³ N. Kouklin and S. Bandyopadhyay, S. Tereshin, A. Varfolomeev, and D. Zaretsky, *Appl. Phys. Lett.* 76, 460 2000
- ³⁴ Y. F. Mei, G. G. Siu, Rickly K.Y. Fu, P. Chen, X. L. Wu, T. F. Hung, and Paul K. Chu, Y. Yang. *J. Appl. Phys.* 97, 034305 2005
- ³⁵ J. Wang, G. Du, Y. Zhang, B. Zhao, X. Yang, and D. Liu, *J. Cryst. Growth* 263,

Characteristics of 1D ZnO Nanowires Array Grown by AAO Assistance

C-W Chang

269 2004

36 K. Vanheusden, W. L. Warren, C. H. Seager, D. R. Tallant, J. A. Voigt, and B. E. Gnade, *J. Appl. Phys.* 79, 7983 1996

37 Jean-Marc Bonard, Christian Klinke, Kenneth A. Dean, Bernard F. Coll, *PHYSICAL REVIEW B* 67, 115406 2003

³⁸ Soo-Hwan Jeong, Hee-Young Hwang, and Kun-Hpng Lee *Appl. Phys. Lett.* 78, 2052 2001

³⁹ Kehui Wu, X. R. Wang, S. Liu, E. G. Wang, *JOURNAL OF APPLIED PHYSICS* 90,4810 2001

